

Flexible and Robust Control of Heavy Duty  
Diesel Engine Airpath Using Data Driven  
Disturbance Observers and GPR Models

by

Volkan Aran

**Submitted to**  
**the Graduate School of Engineering and Natural Sciences**  
**in partial fulfillment of**  
**the requirements for the degree of**  
**Doctor of Philosophy**

**SABANCI UNIVERSITY**

July, 2019

Flexible and Robust Control of Heavy-Duty Diesel Engine Airpath Using Data  
Driven Disturbance Observers and GPR Models

Volkan Aran

APPROVED BY

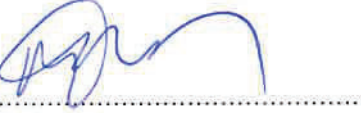
Prof. Dr. Mustafa Ünel  
(Thesis Supervisor)



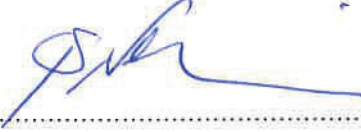
Assoc. Prof. Dr. Kemalettin Erbatur



Assist. Prof. Dr. Meltem Elitaş



Prof. Dr. Şeref Naci Engin



Prof. Dr. Metin Gökaşan



DATE OF APPROVAL: 12/7/2019

© Volkan Aran 2019  
All Rights Reserved

# Flexible and Robust Control of Heavy Duty Diesel Engine Airpath Using Data Driven Disturbance Observers and GPR Models

Volkan Aran

ME, Ph.D. Thesis, 2019

Thesis Supervisor: Prof. Dr. Mustafa Ünel

**Keywords:** Diesel Engine, Airpath Control, Disturbance Observer, Gaussian Process Regression, Sliding Model Control, Model Based Control, WHTC

## Abstract

Diesel engine airpath control is crucial for modern engine development due to increasingly stringent emission regulations. This thesis aims to develop and validate a flexible and robust control approach to this problem for specifically heavy-duty engines. It focuses on estimation and control algorithms that are implementable to the current and next generation commercial electronic control units (ECU). To this end, targeting the control units in service, a data driven disturbance observer (DOB) is developed and applied for mass air flow (MAF) and manifold absolute pressure (MAP) tracking control via exhaust gas recirculation (EGR) valve and variable geometry turbine (VGT) vane. Its performance benefits are demonstrated on the physical engine model for concept evaluation. The proposed DOB integrated with a discrete-time sliding mode controller is applied to the serial level engine control unit. Real engine performance is validated with the legal emission test cycle (WHTC - World Harmonized Transient Cycle) for heavy-duty engines and comparison with a commercially available controller is performed, and far better tracking results are obtained. Further studies are conducted in order to utilize capabilities of the next generation control units. Gaussian process regression (GPR) models are popular in automotive industry especially for emissions modeling but have not found widespread applications in airpath control yet. This thesis presents a GPR modeling of diesel engine airpath components as well as controller designs and their applications based on the developed models. Proposed GPR based feedforward and feedback controllers are validated with available physical engine models and the results have been very promising.

# Veriye Dayalı Bozucu Gözlemcileri ve GPR Modelleri Kullanarak Esnek ve Gürbüz Dizel Motor Havayolu Kontrolü

Volkan Aran

ME, Doktora Tezi, 2019

Tez Danışmanı: Prof. Dr. Mustafa Ünel

**Anahtar kelimeler:** Dizel Motor, Havayolu Kontrolü, Bozucu Gözlemcisi, Gaussyen Proses Regresyon, Kayar Kipli Kontrol, Model Bazlı Kontrol, WHTC

## Özet

Dizel motor geliştirme sürecinde hava yolu kontrolü, gün geçtikçe sıkılaştıkça emisyon kuralları nedeniyle, önemlidir. Bu tezde, özellikle ağır vasıta araçların dizel motorları için, esnek ve gürbüz bir kontrol çözümü geliştirilmesi ve doğrulanması amaçlanmaktadır. Halihazırda kullanılan ve gelecekte kullanılması düşünülen kontrol üniteleri üzerinde uygulanabilir algoritmaların geliştirilmesi hedeflenmiştir. Bu amaçla, halihazırdaki kontrol üniteleri için, veriye dayalı bozucu gözlemcisi geliştirilmiş ve kütle hava debisinin (MAF) ve manifold mutlak basıncının (MAP) egzoz gaz geri dönüş valfi (EGR) ve değişken geometrili türbin vanası (VGT) vasıtasıyla takip kontrolünde uygulanmıştır. Önerilen kontrol yapısının kavramsal değerlendirilmesi fiziksel motor modeli üzerinde yapılmıştır. Önerilen bozucu gözlemcisi gerçek motor ve seri üretim seviyesi kontrol ünitesi üzerinde uygulanmıştır. Gerçek motorda başarımlı doğrulanması yasal motor homologasyon testi (WHTC) üzerinde yapılmış, ticari kontrolcü ile karşılaştırılmış ve muadile göre üstün takip başarımlı gözlemlenmiştir. Gelecekte kullanılması planlanan elektronik kontrol ünitelerinin kabiliyetlerinden yararlanmak için çalışma ilerletilmiş ve genişletilmiştir. Gaussyen proses regresyon (GPR) modelleri otomotiv endüstrisinde özellikle emisyon modellenmesinde yaygın olmasına rağmen hava yolu kontrolünde geniş bir uygulamaları yoktur. Bu çalışma GPR modelleri ile havayolu birleşenlerinin modellenmesini, bu modellere dayalı kontrolcü tasarımlarını ve uygulanmasını sunmaktadır. Önerilen GPR yöntemine dayalı kontrolcüler mevcut olan fiziksel havayolu modelleri üzerinde doğrulanmıştır ve ümit verici sonuçlar elde edilmiştir.

*Dedicated to the memory of my father, Ali, who always supported my curiosity.*

# *Acknowledgements*

Foremost, I would like to extend my sincere gratitude and appreciation to my thesis advisor Prof. Dr. Mustafa Ünel for his academic guidance and continuous support throughout my studies. He supported and guided me with his patience, motivation and immense wisdom. I have been extremely lucky to have a supervisor who cared so much about my study and who was detail oriented. Without his guidance and continuous feedback, this Ph.D. would not have been achievable.

I would like to thank the rest of my thesis committee: Assoc. Prof. Kemalettin Erbatur, Asst. Prof. Meltem Elitaş, Prof. Dr. Şeref Naci Engin, and Prof. Dr. Metin Gökaşan, for their insightful comments and questions.

I am grateful to Gökhan Alcan for his continuous help and collaboration. I am also in debted to my labmates Diyar Khalis Bilal, Emre Yılmaz, Talha Boz and Sanem Evren Han for their kindness and support.

The idea of initiating a project on the diesel engine airpath control as my Ph.D. topic is first supported and proposed by Kazi Adil and Ozan Nalcioğlu at Ford OTOSAN in 2014. I would like to acknowledge their motivation for starting a Ph.D. study. I gratefully acknowledge the financial support provided by Tübitak under TEYDEB grant 3150371.

I am also grateful to Dr. Bülent Ünver for his support on physical engine model and valuable technical discussions. I would also like to extend my gratitude to my colleagues, Çetin Gürel, Metin Yılmaz and Kerem Köprübaşı for fruitful discussions on experiment design and implementation activities. Special thanks to old teammates Emre Tekin and Mehmet Mutluergil for their valuable support on embedded software implementations.

I am deeply indebted to my wife, Serap, for her patience and support during all the years. Without her support, I would not have kept it together. As a result of pursuing a Ph.D., along with a professional life, my available time for my family was limited. I would also like to extend my deepest gratitude to my mother, Mükerrerem, and my brother, Gökhan, for their valuable support and patience.

# Contents

<b>Abstract</b>	<b>iii</b>
<b>Özet</b>	<b>iv</b>
<b>Acknowledgements</b>	<b>vi</b>
<b>Contents</b>	<b>vii</b>
<b>List of Figures</b>	<b>xi</b>
<b>List of Tables</b>	<b>xv</b>
<b>1 Introduction</b>	<b>1</b>
1.1 Motivation . . . . .	3
1.2 Contributions of the thesis . . . . .	4
1.3 Outline of the thesis . . . . .	5
1.4 Publications . . . . .	5
<b>2 Diesel Engine Airpath Background and Literature Survey</b>	<b>7</b>
2.1 Diesel Engine Airpath . . . . .	8

---

2.1.1	Diesel Engine Basics . . . . .	8
2.1.2	Diesel Engine Airpath Components . . . . .	12
2.2	Literature Survey . . . . .	13
2.2.1	Output Selection . . . . .	13
2.2.2	Modeling and Estimation . . . . .	16
2.2.3	Control Algorithm Selection . . . . .	22
<b>3</b>	<b>Identification of Diesel Engine Airpath</b>	<b>33</b>
3.1	Inputs/Outputs and Candidate Model Set for Diesel Engine Airpath	34
3.2	Design of Experiments for Diesel Engine Airpath . . . . .	36
3.2.1	Generic Design of Experiment Criteria for Identification . . .	37
3.2.2	Proposed Experiment Design and Application . . . . .	38
3.3	Model Evaluation Criterion . . . . .	41
<b>4</b>	<b>Data Driven Disturbance Observer</b>	<b>42</b>
4.1	Disturbance Observer Overview . . . . .	42
4.2	Data Driven Disturbance Observer Design . . . . .	45
<b>5</b>	<b>Gaussian Process Regression Modeling of Airpath</b>	<b>48</b>
5.1	Gaussian Process Regression (GPR) . . . . .	52
5.2	Overall GPR Dynamic Model for Diesel Engine Airpath . . . . .	55
<b>6</b>	<b>Flexible and Robust Airpath Control</b>	<b>59</b>
6.1	Data Driven Disturbance Observer Based Diesel Engine Airpath Robust Control . . . . .	60
6.2	GPR Modeling Based Diesel Engine Airpath Robust Control . . . . .	64
6.2.1	GPR Feedforward Control . . . . .	64

---

6.2.2	GPR Feedback Control . . . . .	68
6.2.2.1	GPR Based PI Control . . . . .	69
6.2.2.2	GPR Feedforward and Saturated Integral Control .	69
6.2.2.3	GPR Based Sliding Mode Control . . . . .	69
<b>7</b>	<b>Results and Discussions</b>	<b>72</b>
7.1	Engine ECU Implementation . . . . .	72
7.2	Engine Simulation Environments . . . . .	73
7.2.1	OTOSAN Engine Model . . . . .	73
7.2.2	Linkoping Engine Model . . . . .	74
7.3	Engine Testing . . . . .	75
7.4	Identification Results . . . . .	76
7.4.1	OTOSAN Engine Model Implementation . . . . .	77
7.4.2	Real Engine Implementation . . . . .	78
7.5	GPR Modeling Results . . . . .	82
7.5.1	OTOSAN Engine Model . . . . .	82
7.5.1.1	Airpath Components . . . . .	82
7.5.1.2	Feedforward . . . . .	84
7.5.2	Linkoping Engine Model . . . . .	86
7.5.2.1	Airpath Components . . . . .	87
7.5.2.2	Feedforward . . . . .	90
7.6	Disturbance Observer Based Control Results . . . . .	91
7.6.1	OTOSAN Engine Model Implementation . . . . .	91
7.6.2	Real Engine Implementation . . . . .	93

---

7.7	GPR Based Control Results and Discussions . . . . .	98
7.7.1	GPR Feedforward with Discrete Time Sliding Mode Control	98
7.7.2	GPR PI Control . . . . .	101
7.7.3	GPR-FF Saturated Integral Control . . . . .	103
7.7.4	GPR Based Sliding Mode Control . . . . .	104
<b>8</b>	<b>Conclusions</b>	<b>105</b>
	<b>Bibliography</b>	<b>108</b>

# List of Figures

1.1	Heavy Duty Vehicle and Engine . . . . .	2
1.2	Implementation Environments . . . . .	4
2.1	Ideal Constant Pressure Cycle . . . . .	9
2.2	NOx-Soot Formation Characteristics adapted from [5]. . . . .	10
2.3	A cooled EGR application scheme . . . . .	11
2.4	Common airpath components and a sample layout . . . . .	12
3.1	Generic System Identification Process adapted from [54] . . . . .	34
3.2	A diesel engine dynamometer airpath system flowchart . . . . .	38
3.3	A sample WHTC speed and torque frequencies . . . . .	39
3.4	DoE Input Signals, Coverage and Frequencies . . . . .	40
3.5	Calibration Dependent Airpath Identification Process . . . . .	40
4.1	Conceptual Diagram of Original DOB Scheme from [68] . . . . .	43
4.2	Conceptual Diagram of Designed DOB Scheme . . . . .	45
5.1	Diesel Engine Airpath Elements . . . . .	49
6.1	Implementation Hardware and Control Solutions Diagram . . . . .	59
6.2	DOB Signal Flow for EGR and VGT implementation . . . . .	61

6.3 Overall Control Scheme with Data Driven Disturbance Observer, Airpath Outer Loop Controller (DTSMC) and Trajectory Generator . . . . .	64
6.4 Engine Mapping Region . . . . .	66
6.5 Three mapping boost values . . . . .	66
6.6 A sample training data selection bin . . . . .	67
7.1 OTOSAN Engine Model Block Diagram . . . . .	74
7.2 Ecotorq E6 engine and aftertreatment system . . . . .	75
7.3 Test Setup . . . . .	76
7.4 EGR Model inputs and output . . . . .	77
7.5 Training (Top) and Validation (Bottom) Results . . . . .	77
7.6 MAF training test overall . . . . .	78
7.7 MAF validation test overall . . . . .	78
7.8 MAP training test overall . . . . .	79
7.9 MAP validation test overall . . . . .	79
7.10 MAF model contributions . . . . .	80
7.11 MAP model contributions . . . . .	81
7.12 Feedforward and inverse model comparison for EGR . . . . .	81
7.13 Feedforward and inverse model comparison for VGT . . . . .	82
7.14 $W_{xi}$ validation plot $R^2 = 0.95$ . . . . .	83
7.15 $W_{ie}$ validation plot $R^2 = 0.97$ . . . . .	83
7.16 $W_{xt}$ validation plot $R^2 = 0.98$ . . . . .	83
7.17 $P_t$ validation plot $R^2 = 0.99$ . . . . .	84
7.18 $P_c$ validation plot $R^2 = 0.98$ . . . . .	84

---

7.19	Validation Fit Results for VGT with 95% validation confidence regions	85
7.20	Validation Fit Results for EGR with 95% validation confidence regions	85
7.21	EGR Model Error vs. Pressure Difference on the EGR Line . . . . .	86
7.22	Manifold absolute pressure vs. time simulation result with LiEM . . .	86
7.23	MAF modeling results . . . . .	87
7.24	Throttle flow modeling results . . . . .	88
7.25	Compressor power modeling results . . . . .	88
7.26	MAP modeling results . . . . .	89
7.27	Compressor outlet pressure modeling results . . . . .	89
7.28	Exhaust manifold temperature modeling results . . . . .	90
7.29	Inverse throttle model results . . . . .	90
7.30	Inverse WG model results . . . . .	91
7.31	MAF control result for 20% to 80% load step test . . . . .	92
7.32	Sinusoidal disturbance vs. DOB output . . . . .	92
7.33	Pulse array disturbance vs. DOB output . . . . .	93
7.34	The step test - sinusoidal disturbance and DOB inactive . . . . .	93
7.35	The step test - sinusoidal disturbance and DOB active . . . . .	94
7.36	The step test - pulse disturbance and DOB inactive . . . . .	94
7.37	The step test - pulse disturbance and DOB active . . . . .	94
7.38	Proposed MAF controller performance on WHTC . . . . .	95
7.39	Commercial MAF controller performance on WHTC . . . . .	95
7.40	Proposed MAP controller performance on WHTC . . . . .	96
7.41	Commercial MAP controller performance on WHTC . . . . .	96
7.42	Proposed controller for EGR valve actuation on WHTC . . . . .	97

---

7.43	Commercial controller for EGR valve actuation on WHTC . . . . .	97
7.44	MAP tracking with look-up FF + PID on a WHTC section . . . . .	98
7.45	MAF tracking with look-up FF + PID on a WHTC section . . . . .	99
7.46	Actuator efforts with look-up FF + PID on a WHTC section . . . . .	99
7.47	MAP tracking with GPR FF + DTSMC on a WHTC section . . . . .	100
7.48	MAF tracking with GPR FF + DTSMC on a WHTC section . . . . .	100
7.49	Actuator efforts with GPR FF + DTSMC on a WHTC section . . . . .	100
7.50	MAF (left), MAP (middle) tracking and actuator positions (right) at a selected transient section of WHTC . . . . .	102
7.51	MAF (left), MAP (middle) tracking and actuator positions (right) at another selected transient section of WHTC . . . . .	102
7.52	Compressor outlet pressure and MAP step responses of GPR FF+sat(I)	103
7.53	Compressor outlet pressure and MAP step responses of GPR based SMC . . . . .	104
7.54	Compressor outlet pressure and MAP step responses of GPR based SMC . . . . .	104

# List of Tables

7.1	MAF & MAP Control Performance Metrics . . . . .	98
7.2	MAF & MAP Control Performance Metrics . . . . .	101
7.3	MAF & MAP Control Performance Metrics for GPR-PI and GPR- FF +DTSMC . . . . .	103

# Chapter 1

## Introduction

Diesel engines are the most dominant powerplants for commercial land and marine vehicles. Its applications range from mining (Fig. 1.1) to transportation and power generation. Main well-known drawback of the diesel engine is its combustion by products, namely emissions. Stringent emission regulations of the diesel engines created the need for better engine out emission control. Diesel engine emission control can be examined under two titles: Air path and Fuel path. Air path control consists of mainly regulating the following three actuators: throttle valve, exhaust gas recirculation valve, variable geometry turbine vane or waste gate. Transient control of diesel engine air path is focused on transient emissions and torque build up. One of the most important exhaust emission gases is Nitrous Oxide. Exhaust gas recirculation (EGR) system is the major Nitrogen Oxide (NOx) reduction system for engine out emissions [1].

Emerging electrical engine and battery technologies are challenging the diesel engine. Hybridization and aftertreatment technologies require different actuators and system layouts. Thus, any control structure should be flexible to these upcoming physical hardware changes. Software validation and testing for embedded systems is a major time consuming task and its economical impact is significant. These costs can be reduced with a flexible architecture which encompasses modeling and control library elements that can be used for different engine configurations. Airpath control problem of vehicles is a setpoint tracking problem under dynamic



FIGURE 1.1: Heavy Duty Vehicle and Engine

disturbances. Due to engine speed and torque variations with respect to varying requests from the driver and dynamic conditions of the road itself, boundary conditions and setpoints of the control problem are variable. Additionally, commercial vehicles require around 1 million kilometers service life. Serial production of hundreds of parts creates a variability from engine to engine. Robustness to the part variances and aging of the components is required for mobile vehicle applications. These concerns defined general overview of the problem and airpath control system should be flexible to the hardware changes and robust to the sudden changes in the boundary conditions as well as part to part variance and aging of the components to some extent. A flexible and robust control system is being sought for heavy duty diesel engine air path problem.

This study aims to create a controller architecture for heavy duty diesel engine air path which will be flexible to the hardware changes and robust to the defined variations.

## 1.1 Motivation

Automotive grade sensor applications require accuracy, reliability, durability and cost effectiveness. It is not always easy to meet these expectations with solely hardware based solutions. So, modeling of static and dynamic relations of the airpath parameters is a common approach. Diesel engine airpath control requires modeling of certain parameters due to control or diagnostic requirements of the engine. These models should be implementable to the serial level electronic control units. Simplified parametric physical or empirical models are the common approach for the problem. These models are uniquely tailored to certain hardware architectures (e.g. pressure sensor placed throttle upstream or downstream means totally different model equations). Creating a new software component and adapting the rest of the algorithm are costly and time consuming. However, using same components with different parameter values requires significantly less amount of validation effort. Therefore, independence from such hardware changes is one of the driving factors for this study.

Data-driven, machine learning or black-box modeling approaches are inherently independent of corresponding physical system configurations. However, accurate data-driven modeling requires higher computational power in terms of both memory and runtime with respect to the simplified physical models. Automotive engine electric control units are being enhanced but still most of the current hardware has limits for machine learning type model implementations. This thesis aims to develop implementable models and control approaches for available control hardware on Ford-OTOSAN Ecotorq engines. There are two types of control units that are considered: current Bosch EDC17 and prospective MED1 generation as shown in Fig. 1.2. These constraints are dealt with two different approaches to the problem: A flexible and implementable to current generation ECU method and a detailed modeling that utilizes next generation hardware capabilities.

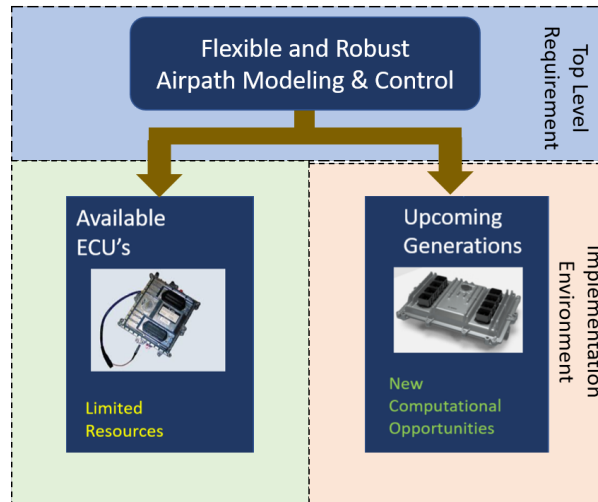


FIGURE 1.2: Implementation Environments

## 1.2 Contributions of the thesis

Contributions of the thesis can be highlighted as follows:

- Identification of Diesel Engine Airpath: Exciting speed and fuel quantity channels with chirp signals, MAF and MAP outputs are estimated using nonlinear finite impulse response (NFIR) models.
- Data driven disturbance observer for Diesel Engine Airpath: A novel disturbance observer based on system identification is developed and applied on real engine.
- GPR based modeling structure for Airpath: A flexible modeling structure for diesel engine airpath is developed. Its feasibility and performance are demonstrated with real engine data and simulations.
- Data driven disturbance observer based robust control for the Diesel Engine Airpath: A discrete-time sliding mode controller combined with a data driven disturbance observer is utilized for the robust control of the airpath.
- Gaussian process feedforward modeling for Diesel Engine Airpath: Feed-forward terms for the airpath controller are modelled via Gaussian Process

Regression (GPR) and its benefit in the overall control is demonstrated on validated engine model.

- GPR based sliding mode controller synthesis: A novel sliding mode controller whose equivalent control part is estimated based on the GPR airpath model is developed and its performance advantages are demonstrated.

### 1.3 Outline of the thesis

Basic knowledge on the diesel engines are presented before the literature survey in Chapter 2. A short system identification summary and implementation on the diesel engine airpath is explained in Chapter 3. Data driven disturbance observer and disturbance observer basics are presented in Chapter 4. Physical component models and Gaussian process regression models for overall diesel engine airpath are provided in Chapter 5. Proposed DOB and GPR based controllers are developed in Chapter 6. Simulation and experimental results related to airpath identification, modeling and control are presented and discussed in Chapter 7. Finally, the thesis is concluded with several remarks in Chapter 8 and possible future directions are indicated.

### 1.4 Publications

- V. Aran, M. Unel, “Gaussian process regression feedforward controller for diesel engine airpath”, *International Journal of Automotive Technology* 19 (4), 635-642, 2018
- V. Aran, M. Unel, “Data driven disturbance observer design and control for diesel engine airpath”, *11th Asian Control Conference (ASCC 2017)*, Gold Coast, Australia, 2017

- 
- V. Aran, M. Unel, “Feedforward mapping for engine control”, *42nd Annual Conference of the IEEE Industrial Electronics Society (IECON 2016)*, Florence, Italy, 2016
  - G. Alcan, M. Unel, V. Aran, M. Yilmaz, C. Gurel, K. Koprubasi, “Predicting NOx emissions in diesel engines via sigmoid NARX models using a new experiment design for combustion identification”, *Measurement*, Vol. 137, Pages 71-81, 2019
  - G. Alcan, M. Unel, V. Aran, M. Yilmaz, C. Gurel, K. Koprubasi, “Diesel engine NOx emission modeling using a new experiment design and reduced set of regressors”, *IFAC-PapersOnLine*, Vol. 51, Issue 15, Pages 168-173, 2018
  - T. Boz, M. Unel, V. Aran, M. Yilmaz, C. Gurel, C. Bayburtlu, K. Koprubasi, “Diesel engine NOx emission modeling with airpath input channels”, *41st Annual Conference of the IEEE Industrial Electronics Society (IECON 2015)*, Yokohama, Japan, 2015
  - V. Aran, M. Unel, “Diesel Engine Airpath Controller via Data Driven Disturbance Observer”, Journal Paper (**under review**)
  - V. Aran, M. Unel, “GPR Based Flexible and Robust Airpath Control”, Journal Paper (**under preparation**)

# Chapter 2

## Diesel Engine Airpath

### Background and Literature

#### Survey

An engine is a machine that uses energy from steam or liquid fuel to create motion. First type of them appeared as steam engines. They burn fuel outside the “engine” and heat up the water and use steam pressure to create desired motion. That idea triggered the well-known industrial age. Later, steam engines were replaced with internal combustion engines (ICE) in transportation area due to better fuel efficiency and relatively light weight of the internal combustion engines. However, steam engines are still used primarily in power generation and some marine propulsion applications. Internal combustion engines, unlike their steam counterparts, utilize combustion pressure to create the motion directly. Spark ignition (SI) engine is the first type of them and invented by Nikolaus Otto in 1876. This engine opened the way to the practical automobiles as we know. However, another German engineer had been searching “ideal heat-driven machine” [2] and compression ignition (CI) engine was invented by Rudolf Diesel in 1892. Now the engine and its standard fuel are both called “Diesel”. Although it is mechanically more complex, superior fuel efficiency of diesel engine granted its dominance in the commercial vehicles. Diesel exhaust is classified as probably carcinogenic to

humans in 1988 by United Nations International Agency for Research Cancer [3]. Following this result, governments set successively stringent emission regulations for diesel engines. Simultaneously, the classification was updated as carcinogenic to humans in 2012. Thus, currently vehicle emission control technologies and its audition mechanism are critical. Electric motors with increasingly efficient battery technologies are threatening existence of diesel in the transportation but fuel efficient and cost effective emission reduction technologies may elongate its life.

## 2.1 Diesel Engine Airpath

Background information for the diesel engine domain is presented in two main subsections. First, general diesel engine information and role of airpath in the general engine operation is presented. Then, specific airpath components are introduced.

### 2.1.1 Diesel Engine Basics

In order to explain the role of airpath in the engine operation, ideal thermodynamic cycle and emission formation basics are presented in this subsection. All heat engines follow a similar pattern; namely, compress, combust and expand. In this thesis, four-stroke diesel engine is the focus. These four strokes are intake, compression, expansion and exhaust. Since all these events occur in the same cylinder but at different times (or crank angles) it is called reciprocating engine. These set of events are called a cycle. An ideal constant pressure cycle for a typical turbocharged engine is depicted in Fig. 2.1. In the cycle graph on the right, ideal intake pressure  $P_i$ , ideal exhaust pressure  $P_x$ , maximum cylinder pressure  $P_{max}$ , atmospheric pressure  $P_a$ , cylinder volume at crank angle zero (i.e. top dead center)  $V_{min}$ , cylinder volume at crank angle  $180^\circ$   $V_{max}$  are shown. The air trapped in the  $V_{max}$  is compressed to  $V_{min}$ , as a result  $P_i$  reaches to the  $P_{max}$  in the process between 1-3. An ideal combustion of injected fuel in a constant pressure is assumed between 3-4. Pressurized gases in the cylinder is expanded to  $V_{min}$  in

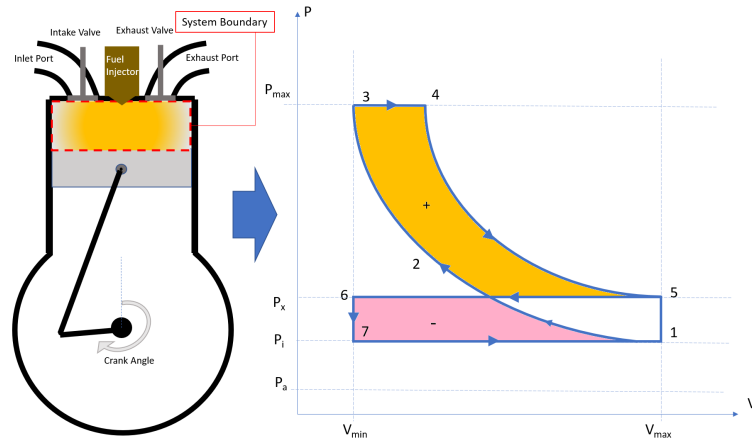


FIGURE 2.1: Ideal Constant Pressure Cycle

order to deliver torque to the crank in 4-5. Exhaust gases are emitted out in 5-6 via exhaust port. Intake port opened and cylinder is filled with air during 6-1. The work in such a cycle can be calculated as

$$Work = \oint P \partial V \quad (2.1)$$

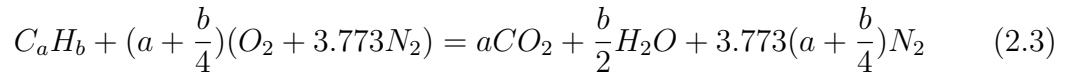
and similar to [1], the described ideal cycle work is expressed as

$$Work = P_i(V_{max} - V_{min}) \frac{Q^*}{c_v T_i (\gamma - 1)} \left( \frac{r_c}{r_c - 1} \right) \eta_{f,i} - (V_{max} - V_{min})(P_x - P_i) \quad (2.2)$$

where  $T_i$  is the intake temperature,  $r_c = \frac{V_{max}}{V_{min}}$  is compression ratio,  $Q^*$  is the heat generated by combustion of the injected fuel and  $\eta_{f,i}$  is the indicated fuel conversion efficiency. Increased intake pressure  $P_i$ , results in increased engine output work. Therefore, for a given engine volume and pressure ratio, increasing charge air to the cylinder, hence increasing the inlet pressure, is desired. This functionality is assigned to the superchargers or turbochargers which are additional engine components outside the cylinder.

Creating mechanical work is main aim of the engine but this should be done under certain emission constraints for the modern onroad diesel engines. Diesel engine emission control technologies can be categorized under two headlines: Combustion control and after combustion treatments (i.e. aftertreatment technologies).

First one focuses on conditioning in cylinder thermodynamic and chemical properties. For a general hydrocarbon, which is defined as  $C_aH_b$ , the ideal complete combustion equation [1] is expressed as



where there is just enough amount of the oxygen to convert all reactants to oxidized products. This fuel/oxygen ratio defines *stoichiometric* (theoretical) proportions. The stoichiometric air fuel ratio  $[\frac{A}{F}]_s$  is calculated from (2.3) as

$$[\frac{A}{F}]_s = \frac{34.56(4 + \frac{b}{a})}{12.011 + 1.008\frac{b}{a}} \quad (2.4)$$

Two defined major cancerogenic diesel emission types are nitrogen oxides  $NO_x$  and soot. Formation of these two are characteristically closely related with combustion temperature and fuel/air equivalence ratio ( $[\frac{A}{F}]_s^{-1}$ ). The exact numbers changes with respect to the engine piston and injector design as well as internal flow characteristics (such as swirl and tumble) but general formation trends are similar to the characteristic depicted in Fig. 2.2 where increasing concentration of the emission is represented with darker shades.

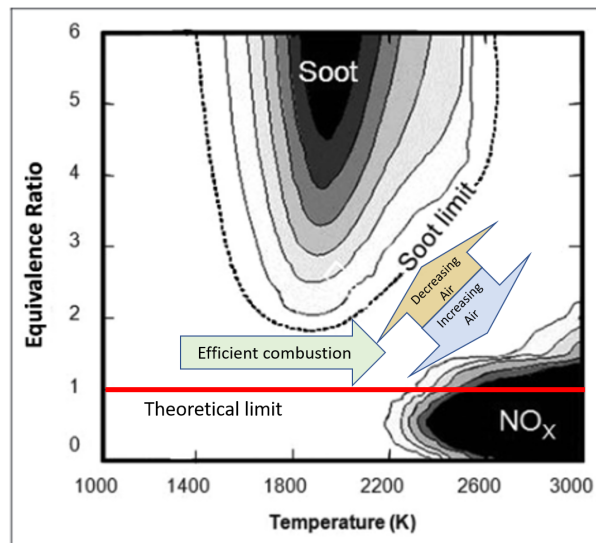


FIGURE 2.2:  $NO_x$ -Soot Formation Characteristics adapted from [5].

Overcharging of the cylinder in order to increase produced work and decreasing the excess air is desirable for an efficient engine operation as explained above. This dilemma is solved with exhaust gas recirculation (EGR). Exhaust gas recirculation is implemented via connecting exhaust line to the intake line and in order to control the flow rate on the line, a valve is introduced as depicted in Fig. 2.3.

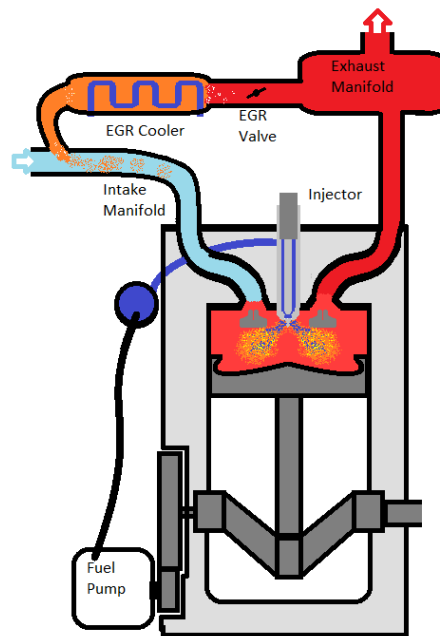


FIGURE 2.3: A cooled EGR application scheme

EGR allows increasing the mass flow in the intake manifold therefore increasing the intake pressure while keeping oxygen concentration of the intake flow under control. For a stoichiometric combustion there is no oxygen in the exhaust gas and mixing exhaust with fresh air decreases the total oxygen concentration. Another property of exhaust is that its heat capacity is higher than that of the fresh air. The mixture has higher heat capacity and less oxygen concentration with respect to same amount of fresh air. Remembering the behaviour depicted in Fig. 2.2, EGR is both decreasing the combustion temperature and increasing the equivalence ratio; therefore an effective measure against NO<sub>x</sub> formation. But apparently it has a soot penalty. This discussion leads to complex combustion optimization questions and this is beyond the scope of this thesis.

Other airpath components will be discussed in detail in the following subsection and they are mainly either manipulating inlet manifold pressure or changing inlet manifold oxygen concentration.

### 2.1.2 Diesel Engine Airpath Components

A typical modern diesel engine has configuration depicted in Fig. 2.4. Different configurations are possible but main elements of the heavy duty diesel engines are presented here.

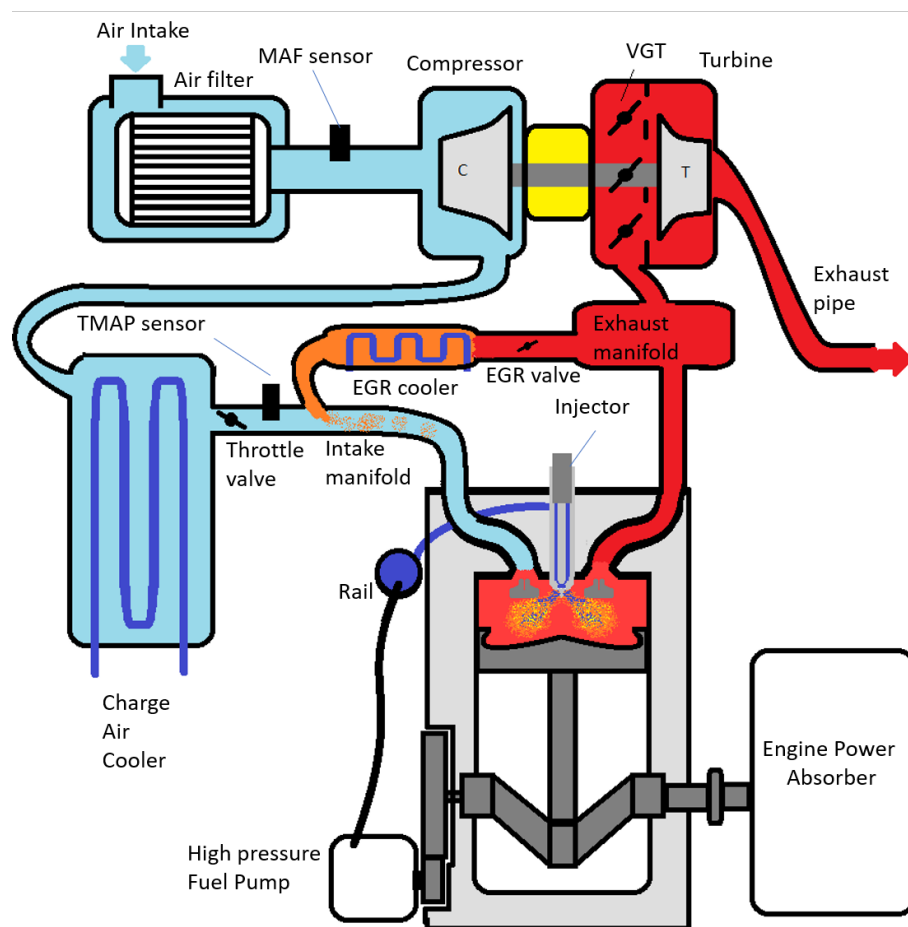


FIGURE 2.4: Common airpath components and a sample layout

The air from ambient is filtered through a generally paper filter to eliminate ingestion of dust and particles to the compressor. Typically a mass air flow (MAF) sensor is placed just after air filter (where flow is uniform) and it also provides temperature output. Compressors of the automotive turbochargers are radial machines

and their power is provided via turbines through a shaft on bearings. Temperature of the compressed air increases and since the engine block is a constant volume pump increased intake gas temperature reduces total mass flow rate. So compressed air is cooled as well as EGR. A throttle is placed just after the charge air cooler and it is used for low air flow requirements of certain operation modes. Since they are affected by soot deposits of the exhaust gases, boosted air pressure (a.k.a. manifold absolute pressure MAP) and temperature are measured after the charge air cooler and before the EGR mixing point. Inlet and exit flow through cylinders are regulated via intake and exhaust valves. Generally, they are controlled by mechanical means but there are also variable valve timing actuator applications. Combustion products are fed to the exhaust manifold and their kinetic energy is harnessed in the turbines and this is regulated via variable nozzles (or wastegates). Finally, turbine out gasses are fed to the aftertreatment systems for further emission reduction.

## **2.2 Literature Survey**

Airpath control literature for diesel engines is presented here from output selection, modeling and estimation and control algorithm selection point of views. These are general diesel engine control papers; however, their findings are evaluated from heavy duty diesel engine point of view.

### **2.2.1 Output Selection**

Main airpath components of the diesel engine, turbocharger and EGR, are introduced in order to increase power density and specific fuel consumption while decreasing exhaust emissions. An airpath control system is used by a performance and emission (P&E) calibration engineer who is responsible for tuning the engine parameters in order to meet legal emission limits and vehicle performance targets. From calibration engineer point of view selection of output parameters are important. The main aims of the P&E calibration engineer can be boiled down to

the control of particulate matter emissions (PM), Nitro Oxide compounds (NO<sub>x</sub>) emissions and specific fuel consumption (SFC). Output selection and related sensor layouts are dependent to the various criteria; namely, packaging of hardware, type of applications, emission level, sensor technology, airpath and aftertreatment control, diagnostics, calibration complexity, lifetime targets etc. In the literature, the evaluations of the outputs are naturally from the academic point of view. On the other hand, from the industrial point of view this problem is more complex. First academic literature will be presented. In their leading research Nieuwstadt et.al. [20] showed that setpoint and output selection is more important for achieving engine performance and emission outputs than the control algorithm. However, these results are based on European driving cycle which is nearly steady test cycle and recent emission cycles like WHTC (World harmonized transient cycle) for heavy duty diesel engines have mainly composed of transient operation points. Later, output selection problem is widely argued in the context of model predictive control. [90].

Common selection for outputs are compressor mass flow (MAF) and intake manifold absolute pressure (MAP), since these two parameters are directly measurable and combustion related. A challenge with this type of output selection with model predictive control is discussed in [88]. The problem is that if MAF setpoint is unfeasible than MAP setpoint tracking becomes poor. Extensions of this problem are discussed in [90]. This paper is dedicated to output selection for Model Predictive Controller (MPC) in diesel engines. It is stated that only case-specific solutions to the unfeasible MAF setpoint problem are presented so far. In the paper it is shown that MAF and MAP control is inferior in terms of keeping EGR rate intake manifold lambda (or intake manifold oxygen concentration) at the desired values. On the other hand, motion planning approach [89] proposes solving EGR-VGT coupling and unreachable desired value problems via model based constraints on setpoint trajectories.

Although MAF and MAP are combustion related parameters, there are other measurable or calculable physical parameters which have direct relations to the combustion outputs. Exhaust oxygen concentration is selected in [7]. Exhaust

oxygen sensors (UEGO) are slow but strongly affected by EGR rate. NO<sub>x</sub> reduction with the use of UEGO instead of MAF is reported but setting a constant lambda resulted in change of combustion parameters. NO<sub>x</sub> reduction is resulted not only from the controller but also (mainly) combustion input setpoint changes. Extensive analysis of UEGO sensor is not presented. However, performance results in terms of emission have been found comparable with commercial controller. Similar selections are done in [25]. Air to fuel ratio and burned gas fraction parameters are selected in this work. But measured parameters are MAF and MAP. Oxygen concentration parameters are modelled. The problem is stated as emission reduction and because of direct relation with emissions, Air to fuel ratio (AFR) and burned gas fraction (F1) are calculated and selected as output variables.

EGR-fraction (or EGR-rate) is another direct alternative for MAF. It is used in [14] with MAP for the purpose of reduction of computational complexity faced in model predictive control. Aiming minimization of the pumping work and emission control, EGR-rate and intake manifold lambda are selected as outputs in [32]. It is stated that for pumping work minimization, using EGR-rate and lambda instead of MAF and MAP provides direct information. However, in their recent study [90] EGR-rate and P3-MAP (P3: exhaust manifold pressure) are selected as outputs while using lambda as a constraint in model predictive control with pumping loss minimization objective besides emission control objectives. Same sensor replacement of MAF sensor with P3 sensor was also proposed previously [90] for cost reduction purpose.

Direct emission control approach is becoming applicable with the new developments in sensor technology. This is important because of its expected superior emission robustness with respect to the other feedbacks or models. Recent work in [46] has focused on the control of EGR and VGT in addition to the swirl valve and start of injection angle with NO<sub>x</sub> and PM feedback. Industrial NO<sub>x</sub> sensor and emission laboratory level PM sensor are used. Aim of the research is to show possibility of direct emission control in real engine. Significant reduction in calibration complexity is reported. In another work [11] for air path control of heavy duty diesel engines compatible with Euro 6 emission standards, Engine out NO<sub>x</sub>

(specific NO<sub>x</sub>), lambda and pressure difference between exhaust and intake manifolds are selected as controlled outputs. This selection is also aimed to robustly maintain engine out emissions in the legal monitoring levels during lifetime of the engine. However, it should be noted that the complex and increased number of sensor application means increased costs and emission robustness problems with aging of the sensor.

## **2.2.2 Modeling and Estimation**

Modern diesel engine airpath is generally composed of a snorkel, air filter, compressor, charge air cooler, throttle valve, egr mixer, intake manifold (sometimes with variable swirl valve), engine block (variable valve timing can be added for specific variants), exhaust manifold, turbine, aftertreatment system and the connection pipe routing for all. For this work, system boundary is taken between compressor inlet and turbine outlet. The focus will be on control oriented models.

Continuum fluid dynamics are represented with Navier-Stokes equations. In most general form it is a set of Partial Differential Equations (PDE). If the flow is accepted as incompressible, equation becomes Differential Algebraic Equation (DAE). Under the one dimensional flow assumption resulting motion can be represented by an Ordinary Differential Equation (ODE). Models with these latter two types of equations are compared for diesel engine air system modeling in the thesis [37]. Application of the flow and pressure models to the real world engines showed that the models have steady state deviations. Five papers are published from the thesis and they are related with model augmentation from different perspectives; namely, ODE model based EKF, Simultaneous estimation and mapping of the bias, DAE based EKF and comparison of DAE and ODE estimators. Observability analysis for the suggested methods are presented. Diesel engine airpath states of intake manifold pressure, exhaust manifold pressure, turbine speed, compressor mass airflow, volumetric efficiency are selected. All the related validation tests are done in real world dynamometers with engines from the SCANIA. Comparison of DAE and ODE estimators showed that for the same accuracy models, DAE based

approach needs less computational effort in terms of step length. ODE models are found hard to implement to the current truck ECU's.

Core of diesel engine airpath is turbocharger and EGR. Their interaction can be identified with intake manifold and exhaust manifold pressure states. Application of intake manifold pressure sensor is common but exhaust manifold sensor is not preferred due to implementation difficulties. Exhaust manifold pressure estimation is presented for diesel engine airpath in [36]. This modeling approach differs from other literature with the consideration of turbine speed in the exhaust manifold pressure estimation. A modified Newton-Raphson method is used. Modification is done for predefined number of iterations and same calculation load for each time step. Validation and comparison with orifice based equation model is done in simulation with higher fidelity models. Simulation results showed superior performance of the proposed method over orifice model.

Two different in cylinder modeling based exhaust manifold pressure estimation methods are compared in [34]. Although the research is spark ignition engine oriented, airpath is still the same. One of the two proposed exhaust manifold estimators is based on energy conservation during the gas exchange process in an assumed ideal cycle. Second method is based on exhaust manifold pressure effect on in cylinder residual exhaust gas effect. This effect will be less with increased compression ratio (as in the diesel engines). Dynamometer step tests are used for comparison and verification. Energy based method was found more robust and residual gas method is over sensitive to the air mass errors.

Another truck engine model with gas flow observer design is presented in the thesis [39]. The study aims to improve a prior MAF estimator and extend a prior diesel engine airpath model. This study includes modeling of airpath with exhaust brake (this is a heavy duty specific actuator). First noise characterization and modeling with respect to the turbine speed is tried and the presented approach is failed. In order to avoid computational burden of model linearization Constant Gain Extended Kalman Filter is used instead of Extended Kalman Filter.

Using Kalman Filters to improve airpath model accuracy is shown by [9]. Based on the results of the [37], DAE models are used in the thesis. Both Unscented Kalman Filter and Extended Kalman Filter methods are used to predict lambda, EGR fraction, MAF, intake and exhaust manifold pressures. UKF is tried in order to see benefits of a gradient independent approach. Real engine tests showed that EKF and UKF have similar accuracies but different computational characteristics. Maximum stable time step for UKF is smaller than EKF and UKF needs more computational load. EKF is further improved to adapt covariance matrices (Q and R) with respect to the operating point. The reported MAF estimation is suggested for MAF sensor replacement in case of a sensor failure.

A sensitivity analysis for simplified mean value physical models for the diesel engine is presented in [35]. The study aims to design a model based diagnosis system for diesel engine. EKF, sliding mode, open loop model and high gain observers are compared in the thesis. For the diagnosis tests, sliding mode and adapted open loop model observer are selected because of their superior model parameter uncertainty robustness. Since sliding mode observer needs 5 times faster simulation in comparison to the open loop model, open loop model is suggested for ECU implementation. The experiments for the validation and parametrization are done on heavy duty diesel engines.

In the leading study [40], problems with diesel engine mean value models and control are shown and remarks on plant characteristics are presented. MIMO identification linear models of EGR and VGT to MAP and MAF showed right half plane zeros in the transfer functions from EGR valve position to MAF and MAP; thus the later famous non-minimum phase behaviour of the EGR line is explained. Also relative gain array analysis showed that for a decentralized control architecture EGR valve should be selected for controlling flow and VGT for the MAP; but for another operating point the opposite is desirable (sign reversal property of airpath). Physical intuitions behind the phenomena are also explained.

Simple mean value engine model for complete diesel engine airpath simulation inside ECU is presented in [44]. The model lacks EGR line only turbocharger is

added to the modeling structure. Parameter tuning is done with physical values and error minimization optimization from real world driving data. Simulations are unstable over 8ms time steps and this may be problem in a ECU application (Generally 10, 20, 100ms tasks are used). Real world truck engine data is used for validation.

Linear parameter varying model implementation on the diesel engine airpath is presented by [47]. Linear models are previously shown to be successful at simulating engine behaviour for limited engine operation region. Performance of the modelled states, namely airflow and intake exhaust pressures is measured with variance-accounted-for (VAF) criteria. Each output is modelled via MISO subsystem model. The physical understanding of the systems are used in subsystem identifications. VGT is excited with pseudo-random binary sequence (PRBS) signals; and EGR, fuel quantity, engine speed input signal types are white noise in the parameter identification experiments for the models. Model is validated with transient engine tests. Hammerstein model is used for benchmark. This model is used in  $H_\infty$  control in [48].

Complete mean value physical modeling for the diesel engine airpath is presented in [49]. This model aims to both simulation and analysis besides control. ODE based model structures are used for airpath submodels. Model has states of intake and exhaust manifold pressures, oxygen mass fractions of both manifolds, turbocharger speed, and actuator dynamics. The study also includes torque output besides modelled outputs of manifold pressures, compressor flow and turbine speed. Model parameter identification tests are EGR and VGT position steps at different operation regions. ODE based model structure are used for flow models. Model validation is done with engine tests. The model is reported to have essential properties of the system (e.g. non-minimum phase behaviour in the channel EGR to MAP). The model Matlab software is downloadable from <http://www.fs.isy.liu.se/Software>.

Real gas dynamics behaviour is known to be represented as PDEs. In his dissertation [43], Stockar presented a novel solution for PDE's through solving decoupled

set of ODE's. A crank angle resolution (i.e. engine rotation frequency pulsations are taken into account) modeling for engine is also presented as implementation. Presented model can predict the pressure wave propagations inside the tubes. Level of complexity is different from other mentioned literature. This approach is alternative for current 1-D modeling of engine. Model is tuned with higher fidelity 1-D gas dynamics models (i.e. GT-Power engine models). For the validation, 1-D gas dynamics model and the proposed model are compared with real engine results. Proposed method has similar performance with 1-D gas dynamics models. For the assesment of computational complexity, further investiagations are needed since only proof of concept is presented. This type of modeling is interesting from airpath control point of view when variable valve timing is the case in a high speed engine.

Compressor is one of the key elements of the diesel engine airpath. It is also in the center of the turbocharger hardware protection efforts in a real world diesel engine. Presented compressor model [41] with surge choke regions is beneficial from hardware protection point of view. Method is based on an algorithm determining turbocharger map in the engine test bench including surge and choke regions. A surge control algorithm is also presented. In order to model real world scenarios, correction characteristics with changing ambient temperature and pressure is also investigated. Benefits of extra throttle between sequential turbocharger system is shown. Experimental data for tuning and validation of the study is collected on a GM SI engine.

Experiment design is a key point of modeling or finding model parameters. Optimal experiment design for airpath model is studied in[45]. Speed, injected fuel quantity, EGR valve position, VGT position and swirl valve position are defined as manipulative inputs and MAF and MAP are the model outputs. Swirl valve is left outside in the experiment design since it has only open and close positions for predetermined conditions. Focus of the paper is to estimate five model parameters namely, intake and exhaust manifold volumes, turbocharger efficiencies, and time constants for EGR, VGT, and turbocharger. Based on a nonlinear ODE diesel

engine airpath model, optimal experiment design problem is defined with the E-criterion ( $\max[\lambda_{\min}(F)]$  where  $F$  is the Fischer information matrix). Total cycle time is 20 s and frequency resolution is 0.05 Hz. Maximum designed frequencies for the input signals are EGR valve  $< 10Hz$ , VGT  $< 5Hz$ , engine speed  $< 2Hz$ , and fuel quantity  $< 4Hz$ . Multisine signals are used. Design optimization of input signals are done with three different strategies: RMS, frequency and RMS with varying ranges with respect to the frequencies. Design optimization is performed for four different operating points. Results of three strategies with white noise inputs showed that frequency optimization has best results for the E-criterion. Tuned model performance is shown for validation of the modeling.

Gaussian process regression (GPR) has gained popularity in dynamical systems modeling and estimation in the last decade. An up-to-date GPR related dynamic systems literature can be found in [56]. One of the most useful recent updates of the system identification theory is accepted as “kernel methods” which are implemented as Gaussian process models [57]. In this study, GPR estimations for linear time invariant and stable systems are presented. It is stated that such methods improve the estimation accuracy significantly. A new concept called numerical Gaussian process (GP) is discussed in [58]. This new definition of GP aims to model physical processes that are described by partial differential equations via GPR method. This method utilized physical knowledge in the model construction but it has a cubic computational complexity with respect to the size of the training set. Another dynamical system modeling study which is based on GPR is presented in [59]. Rotorcraft dynamics GPR-NARX model is constructed for the estimation of pitch, roll and yaw rates. It is compared with the previous physical law based modeling software and shown that the GPR-NARX approach has better estimation performance. Similarly, robotic motion modeling is popular in the literature and a recent example can be found in [60]. This study utilized GPR for modeling human motions in 6D. Resulting model accuracies are found significantly better than the state-of-the-art methods. There is also an automotive specific modeling software for specifically emissions modeling based on GPR methods [61]. This is one of the best emission modeling tools in the industry.

### 2.2.3 Control Algorithm Selection

PI(D) based industrial control algorithms are common. With the variations in the application, PID control is one of the standard methods in the airpath control literature ([20], [25], [8], [21], [32], [13], [23]) besides increasingly popular model predictive control ([88], [12], [26], [27], [18], [90], [19], [14]). Other control methods such as: Sliding Mode Control ([30], [29], [33], [6]),  $H-\infty$  control ([17], [87]), LQG-LTR [7], Adaptive Control [24] and Control Lyapunov Functions [86] are also found in the airpath control literature with lower frequency. Setpoint selection and controller architecture interactions are reported to be remained unexplored [25]. Latter the discussion is done only in the model predictive control (MPC) context [90].

Aiming the objective comparison of control methods on diesel engine airpath, PI control schemes are implemented in order to compare output and sensor architecture selection benefits [20]. This paper includes 4 different PI controllers and one Lyapunov based controller. Differences between PI controls are their feedback sensors and control outputs. Controller performances are evaluated via resultant feedgas emissions (i.e. NO<sub>x</sub>, HC, CO, PM) on European drive cycle dynamometer tests. But the results of the work were inconclusive in terms of control algorithm comparison between Lyapunov, Rank one PI and PI, since the used drive cycle was mainly steady and tuning of each one of the controller was not in the same maturity. It was reported that change of setpoints is dominant over change of controller for the tested conditions.

Although measured variables are commonly intake manifold sensor and mass air-flow sensor outputs for commercial diesel engines with EGR and VGT, performance variables are selected as intake burned gas fraction (F1) and air to fuel ratio (AFR) in [25]. Nonlinear plant is modelled with respect to the engine speed, fuel quantity, EGR and VGT positions using steady state models. System is linearized around certain operating points of speed and MAF. Robust control problem is defined for a linear controller. Fuel quantity and speed disturbance effects are taken as inputs to the setpoint generation only. Resulting system is found rank deficient

for the optimized values of the selected performance outputs. LQG control for linearized plant around one operating point is presented. The design is aimed to solve the plant singularity and setpoint generation errors by applying singular value decomposition of the plant DC gain matrix. Dynamometer fuel step test results showed faster responses in AFR and slower responses in F1 .

Transient performance of airpath has gained more importance with introduction of new combustion concepts like Homogeneous Charge Compressed Ignition (HCCI) and new emission regulations. Another side of the solution for the problems related with the setpoint trajectories are presented in [8] [89]. The implementation is done in HCCI engine and this type of engines are known to have critical combustion characteristics which needs precise control of the transients of the airpath. Feedforward motion planning and control has inputs of intake airflow and EGR flow. Feedforward controller also takes constraints into account in this trajectory generation stage. In the second stage, control for realizing flow trajectories via EGR and VGT position is done with separate SISO PI controls on EGR and VGT. Luenberger type EGR flow observer is used to estimate EGR flow on the valve. PI control loops acted on normalized areas of the valves. ECE cycle transient dynamometer experimental results are presented for performance validation.

Optimum control for emission and performance is the main objective for most of the engine control applications. VGT position control based on a neural network which is trained with explicit optimization results for the best SFC and NO<sub>x</sub> is presented in [21]. This control is replacement of open-loop position control maps with a neural network (NN). The output of NN model, optimum VGT positions for maximum power and minimum emissions are directly sent to the actuator. Comparison with a commercial controller is presented with dynamometer measurements. Stability and robustness of the proposed method are not discussed.

Another relatively simpler (in terms of calculation effort) online optimum control is presented in [32]. Control problem is formulated as SISO EGR and VGT controls for EGR-rate and lambda outputs. Pumping loss minimization, turbocharger overspeed protection, desired value limitation control objectives are handled with

additional feedback loops (total 4 PIDs). In addition to the airpath regulation via EGR and VGT, engine torque control using airpath outputs is proposed. Also an automatic tuning method with least squares regression is realized on ETC simulations. In order to calibrate trade off between EGR errors and boost building up, weighting factors to the objective function of the automatic controller tuning are added. Finally, ETC dynamometer tests to compare the proposed controller with current production regulator (Scania) showed pumping loss decrease when lambda and EGR rates for the both controllers are the same.

Airpath control literature is dominated by model based control approaches. Application of directly data-driven techniques such as Virtual Reference Feedback Tuning (VRFT)[13] is rare. This novel method aims to identify controller parameters (i.e. PI gains) directly from a training data. An optimum prefilter to the data and extended instrumental variables with variance weighting are the contributions to the standard VRFT method. In order to validate the proposed strategy of MIMO VRFT method, diesel engine airpath control problem of MAF, MAP tracking is selected as the case. Valve position PRBS signals are used for identification of the system. Comparison of MIMO VRFT results with SISO VRFT showed that MIMO design has expectedly better decoupling and better overall tracking performance. Compared to the model based design method, proposed technique is shown to be preferable if modeling errors are expected as in the simplified diesel engine airpath models.

Model uncertainty problem of the diesel engine airpath is treated with Qualitative Feedback Theory (QFT) and MIMO PID structure in [23]. System is modelled using 15 points selected (i.e. operating points are based on speed and fuel quantity) in the NEDC region with EGT and VGT step tests. For the selected 15 operating points variation in the first order delayed model parameters of MIMO system is accepted as plant model parameter uncertainty. The controller design is based on QFT framework. Since the resulting system becomes ill-conditioned for decentralized control, a static forward path decoupler is designed. Dynamometer step test showed dramatic difference in the step responses between controllers with and without decoupler.

Although industrial implementation of model predictive control is not as common as PID control, it is very popular in the recent airpath control literature. In a leading application paper of model predictive control for diesel engine airpath[88], constrained optimal control using multilinear model is presented. Local models are identified with 4 inputs (i.e. EGR and VGT setpoints, Speed and Fuel). Input signals are created based on the idea of fixing an operating point for each region and superposing stochastic deviations which have a system compatible frequency. Explicit model predictive control is proposed for online application. Actuator position limitations are regarded as constraints. Model states are estimated using a Kalman filter. Region switching behaviour is tested and smooth behaviour is observed at dynamometer. FTP and NEDC tests showed superior tracking performance and better resultant emission output of proposed control over production ECU control of the selected engine. Controller robustness against environmental conditions is seen as a risk.

Online optimization is proposed in [12] for diesel engine mode predictive control. Their unique online active set strategy is extended for nonlinear system and applied to the diesel engine airpath. Model identification of the work is similar to the model of the [88] with difference of second order local model structure instead of first order system with delay. A smaller region, that consists of two local models, is considered. Authors have developed online quadratic programming for linear models and this work adds multi model switching therefore, variation in the related matrices (e.g. Hessian and constraint matrices). Nonlinear optimization problem is handled via solving a varying quadratic program (QP). The complete algorithm for diesel engine airpath is implemented on the dSPACE Autobox to run with 50ms sampling time. Implemented algorithm used control horizon of 0.25s and prediction horizon of 5s. Real engine tests showed that QP iterations are around at most 10 and all of the calculations are finished in one sampling time. MAF and MAP tracking performances of the controller were fast but there were oscillations in the steady region. Aim was the realization of the online model predictive control on the real engine. Although it is not implemented on the real engine ECU and

the local models were limited with two regions, realizability of the algorithm is presented.

Practical implementation on current real world engine hardware is focus of the model predictive control study of [26]. Piecewise affine models are used for the given model predictive control framework. General derivation and application of model predictive control for diesel engine airpath is discussed. Explicit optimization method is followed in order to reduce calculation time burden (with the cost of increasing memory consumption [27]). The paper is focused on satisfying constraints under steady state disturbances. The algorithm is implemented on real engine ECU. Actuator position limitations and engine out NO<sub>x</sub> emission constraints are imposed. By facilitation of a soft constraint, actuator position aggressiveness is calibrated. Results of different tuning are presented and result of constraint violations under steady state disturbance showed that NO<sub>x</sub> constraint is highly affecting the actuator stability. Model uncertainty is discussed as cause of measured instabilities with constraints. Later a more generic discussion on model predictive controller for diesel engine airpaths with results in two stage turbocharger engines are presented in a book chapter [27]. Latter work includes transient cycle tracking results of the controller in the first paper. Trade-offs of ECU memory and computation time are compared for explicit and implicit model predictive controllers. Model predictive controllers are found powerful as an airpath controller because of MIMO controller behaviour (i.e. Handling with VGT EGR coupled dynamics), ability to impose hardware limitations and compatibility with higher level constraints such as emissions. Its problematic sides are weakness to the model uncertainty and computational complexity.

Stability problems are reported for MPCs in the previous works. Considering dead time as one of the sources of instability for the system, [18] added a state observer for compensating dead time. They used 6th order state space model for MAF and MAP with respect to the EGR and VGT positions and included a Pade approximation for the dead time. Simulation of the proposed explicit MPC algorithm showed effectiveness of the dead time compensation. Shown responses are also notable from transient surge and smoke avoidance points of view. The algorithm

is implemented on rapid prototyping ECU of a diesel engine and tuning of the horizon depths (i.e. Control horizon and prediction horizon), dead time compensation effects and transient set point tracking are investigated experimentally. Results of the horizon tuning confirmed the computational applicability of algorithm to the real world engine. Similar to the simulation results, experimental results showed the improvement gained by the dead time compensation at transient setpoint tracking. At the end, implemented controller's transient performance is compared with the reference engine PID controller. Better overall tracking errors are reported in the tested transient cycle. It is reported to have drastic improvements on certain sections of the test.

Output selection effects on MPC is discussed in [90]. Two candidate sets were MAP, MAF and EGR fraction(rate) (xegr), pumping loss (pmep). Implicit MPCs are designed for both control outputs with an additional integral action for EGR rate. Minimization of the changes in the control signal is added to the cost function to avoid oscillations. This publication also includes an extensive set of constraints on model predictive control with respect to the previous MPC airpath literature. Pumping loss minimization is one of them. Authors have a previous work for pumping loss minimization with air control in which the controller is PID and they compared results with this work [32]. The solver described in [12] is used in the study. Only simulation results are presented for comparison and evaluation of the performances. Two simulations are performed to see the modeling error effect: additional 10% modeling error in EGR and VGT areas and with a baseline model. For the presented model and problem formulations, overall ETC simulation performance of MPC xegr, pmep control has 6% lower average pumping losses with respect to the previous PID design and 3% better average xegr tracking performance. Although MPC controller results are still better, the difference between PID and MPC xegr, pmep controller error averages decreased in the 10% modelling error simulation and xegr and pmep performance differences become 3% and 1%, respectively. Proposed MAF, MAP MPC has the worst results in terms of xegr and pmep for both simulations with a dramatic difference. Real engine implementation for the MPC xegr, pmep controller is found feasible with a need

of total 1.7 MB memory and comparable run times with a reference implemented MPC algorithm.

Linearization of nonlinear models or using local multi-linear models simultaneously is common in the MPC airpath literature. Nonlinear model predictive control was accepted as infeasible to implement on diesel engine control before the work of [19]. Based on the Nonlinear Model Predictive Control NMPC scheme of [4] an online NMPC controller for diesel engine airpath with a generic NMPC approach is presented. For the stability discussion of the method reader is directed to the [4]. The method is model independent and a particular sequential quadratic programming routine is used in the solver. The open loop stable characteristic of diesel engine airpath is utilized to reduce complexity of the optimization problem. Simulations and experiments showed that there exist unstable valve position results due to the impossible set points of MAF and MAP (i.e. achieving both of the targets are not possible at the same time and resultant valve positions are chattering around the closest of the two). Calibration parameters of weighting for MAF and MAP errors are shown as tunability characteristics of the method in the simulations. Overall experimental NEDC tracking performance showed maximum 5% MAP overshoot. When it is compared with other MPC approaches, computational efficiency and nonlinear model usage ability are important. Previously reported weakness of the MPC was the performance problems due to the model inaccuracies. This approach overcomes the model complexity barrier of the MPC.

In order to decrease the effects of the disturbances (i.e. measured disturbances of engine speed and fuel quantity) on the control, rate based tube MPC is proposed by [14] for the diesel engine airpath. It is noted that, because of the physical limitations, rates of the speed and quantity are limited with respect to the absolute values. Rate based modeling uses state increments (so-called rates) instead of absolute state values. The tube-mpc scheme is first introduced by Mayne in 2005 [28]. Basic idea is to limit state trajectories into a tube by introducing relevant constraints to the optimization. Approximate algorithm is implemented on real engine and in simulation for computational simplicity. NEDC test simulations and steady state tests showed that controllers can track the setpoints while honoring

the constraints. Promised robustness advantage of the controller is not analyzed or tested. Costs of the approximations in terms of the accuracy and the performance are not discussed and left for the future work.

An initial Sliding Mode Control (SMC) design to the diesel engine airpath was focused on VGT only [30]. EGR flow is accepted as an external input. Reduced order models are used for constructing the regular form and the actuator dynamics are included in the control design. Compressor flow observer is used for calculating equivalent control and controller performance is shown in the simulation step tests.

An example of SMC MIMO airpath control design can be found in [29]. Regular form could not be found for MIMO model of EGR and VGT. Same observer in a previous paper [30] is used for the compressor flow. Because of sensitivity of the model inversion on EGR valve to the manifold pressure ratio, simulated performance of the controller on EGR flow has more overshoots and undershoots than compressor flow. Coupled effects caused non-monotonic flow and EGR position responses in the step tests.

Motivated by Low Temperature Combustion (LTC) modes in the diesel engine, [33] designed another set of MIMO SMC for intake manifold fresh air fraction (F1), MAP and MAF, exhaust manifold pressure and compressor outlet pressure control outputs. Throttle valve is added to the conventional control input set of EGR and VGT. In addition to the two sliding mode controller design for different combustion modes, an intermediate state and a supervisory controller is designed and their stabilities are proven in the text. Since LTC modes require low intake flow, this mode requires a controller for EGR and Throttle valves. Due to the MAF sensor noise issues, exhaust manifold AFR sensor is used for calculation of the system output F1. An interesting trick for unstable characteristics of the throttle equation around pressure ratio of one is increasing VGT position. Normal combustion mode controller calculates EGR, VGT and throttle vane positions. Switching of the controllers are regulated via supervisory controller. Experimental results showed the known trade off between tracking performance and chatter tendency of the SMC on EGR position control. Stable and smooth controller switching is achieved

in the tests. Robustness against speed and quantity disturbances are shown via step tests.

Another diesel engine airpath controller output set of exhaust manifold and intake manifold pressures are selected in [6]. In order to reduce the chatter of SMC and improve disturbance rejection characteristics Super Twisting method and Extended State Observer are implemented with SMC. This is a kind of disturbance observer based sliding mode controller. Controller performance is evaluated via engine simulation. Disturbance rejection performances of the traditional SMC and designed SMC are compared and higher chattering effects are seen in the traditional one. Also the proposed controller was found better in nominal performance recovery after disturbances.

The work in [17] contributes to the airpath control problem by using Linear Parameter Varying (LPV) models and  $H_\infty$  loop shaping control design. For stability unlike other model based approaches, their controller can be calibrated with respect to the operating points while keeping the robustness guarantees. The quasi-LPV airpath model is tuned for NEDC region. For the study, experimental NEDC data showed that exhaust manifold pressure is mostly higher than intake manifold pressure and the model is neglected reverse flow on the EGR line. The quasi-LPV loop shaping controller is designed with the help of MATLAB Linear Matrix Inequalities toolbox. In the real engine implementation, controller matrices are calculated in the ECU sample time of 16ms. A part of the NEDC is used for validation. Compared with ECU controller, LPV controller showed better transient performance on MAF with nearly similar MAP results. In order to achieve such behaviour, a gain-scheduled post compensator is introduced. The implementation drawback of the method is calculation of the controller matrices at each time step. Robustness with respect to the speed and torque is shown but other hardware or model related disturbances such as wear on compressor or sensor drifts are not tested. Uncertainty parametrization is important in terms of stability and robustness of the  $H_\infty$  loopshaping controller [17]. Different uncertainty parametrizations (i.e. coprime factor uncertainty, additive uncertainty,

parametric state space uncertainty) are compared for diesel engine airpath control.

One of the leading research for exhaust gas oxygen (EGO) sensor based airpath control is provided in [7]. In this work, control is limited to the EGR valve position command output. Their design is based on keeping actual exhaust lambda constant. Assuming dynamic range of the input is limited, the Linear Quadratic Gaussian (LQG) method with Linear Transfer Recovery (LTR) is implemented. The designed controller is tested on a real 2 liter diesel engine at FTP cycle. Results showed comparable emission performance with commercial controller in terms of NO<sub>x</sub>+HC and PM. Dynamic performance improvement in comparison to the commercial MAF controller is not observed. Especially boost dynamic performance becomes poor. Also airpath is reported to have non-minimum phase [32] and nonlinear behaviours which challenges the LQG-LTR design.

Dynamic feedback linearisation (DFL) control design is selected by [24] for heavy duty diesel engine airpath control. Uncertainty analysis showed that feedback linearized system lacks robustness. In order to have a stable system with low outer loop gains, adaptive parameter estimation is utilized. Online parameter estimation for identifying third order model is based on a T-S Fuzzy algorithm. Algorithm performance is tested on SIL system in real time. DFL and adapted DFL results are compared on AFR and EGR rate output trajectory tracking control. Adaptation resulted in lower tracking error on low transients but aggressive maneuvers caused inferior tracking performance.

Aiming the robust control for the diesel engine airpath, domination redesign of the Sontag's formula with Control Lyapunov Function (CLF) is implemented in [86]. Robustness property is defined in gain and phase margins. Dynamometer step tests showed tracking performance of the controller. However, robustness to the model or sensor errors are not shown with tests.

Gaussian process adaptive control is an emerging approach. This approach is shown to be providing smoother transients than previous Model Reference Adaptive Control (MRAC) approaches [50]. Gaussian process online estimation is being

computationally effective and promising for the embedded applications [51]. Another adaptive and *cautious* (caution term is used for regularization of control signal with respect to the model uncertainty) is presented in [62]. GPR based computed-torque control is proposed for the robot arm control problem in [63]. Stochastic boundedness of the sample path is guaranteed in the study. GPR-NMPC method is applied for autonomous miniature race cars in [64]. Track is learned after each lap and its performance is improved significantly after the first lap. According to GP bibliography presented in [56], GPR application on diesel engine airpath control first appeared in [70].

# Chapter 3

## Identification of Diesel Engine Airpath

Identification of the dynamical system between EGR and VGT inputs and MAF and MAP outputs is the main focus of this chapter. Ford OTOSAN Ecotorq engine with configuration depicted in Fig. 2.4 is the target system for the identification study. Theoretical system identification summary, design of experiment for the diesel engine airpath system and related model details will be presented. This chapter aims to develop the base model structure which will be used for the data driven observer in the subsequent chapter. The process of system identification as Ljung defines [54] composed of three main elements: data, candidate model set and candidate model evaluation criterium. Another critical information input to the process is prior knowledge about the targeted system. Their interactions and a basic flow chart of the system identification is depicted in Fig. 3.1. Specific utilization of a priori knowledge for the diesel engine airpath on each steps and related details are presented in the following sections.

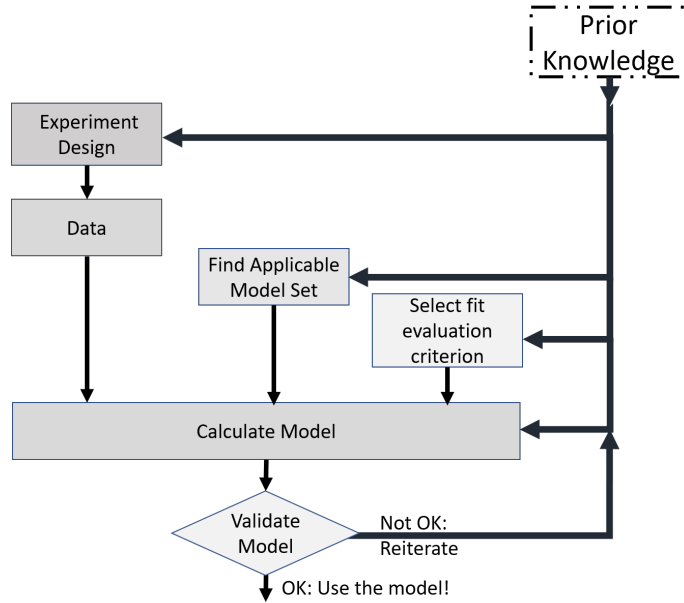


FIGURE 3.1: Generic System Identification Process adapted from [54]

### 3.1 Inputs/Outputs and Candidate Model Set for Diesel Engine Airpath

The diesel engine airpath system dynamics model in [86] is one of the most popular models for airpath control systems design in the literature and used in [17] and [6]. Following this model, system dynamics can be written as follows.

$$\dot{P}_i = G_1(P_i) + F_1(P_i, P_c, P_x, Ar_{EGR}) \quad (3.1)$$

$$\dot{P}_x = G_2(P_i, W_f) + F_2(P_i, P_c, P_x, Ar_{EGR}) \quad (3.2)$$

$$\dot{P}_c = G_3(P_c) + F_3(P_x, Ar_{VGT}) \quad (3.3)$$

$$W_{ci} = F_4(P_i, P_c) \quad (3.4)$$

where  $P_i$  is MAP,  $P_c$  is compressor power,  $P_x$  is exhaust manifold pressure,  $Ar_{EGR}$  is EGR Valve area,  $Ar_{VGT}$  is turbine inlet vane area,  $W_{ci}$  is MAF,  $G_j$  ( $j = 1, 2, 3$ ) are linear and  $F_k$  ( $k = 1, 2, 3, 4$ ) are nonlinear mappings. There are two types of EGR valves, namely, poppet type and butterfly type. Their position to area relations are different and the first one is used for light duty vehicles while the latter

is common in heavy duty engines. Neglecting shaft diameter, a typical area to valve position relation of a butterfly type valve is given as

$$Ar(\theta) = \frac{\pi D^2}{4} \left(1 - \frac{\cos(\theta)}{\cos(\theta_0)}\right) \quad (3.5)$$

where  $\theta$  is the valve position angle measured from vertical axis in the clockwise direction,  $D$  is the throttle plate diameter and  $\theta_0$  is the valve position angle in the fully closed position. There is also internal dynamics of the actuator and actuator position controller but this is out of the scope of this section. These effects will be taken into account in Chapter 6. In this study, we assumed an NFIR (Nonlinear Finite Impulse Response) system which is separable into linear and nonlinear parts and identified these two parts separately.

Based on prior information which is obtained from the physical model ((3.1)-(3.5)), controlled outputs MAF ( $W_{ci}$ ) and MAP ( $P_i$ ) are identified with inputs  $P_i$ ,  $P_x$ ,  $P_c$ ,  $\theta_{EGR}$  and  $P_c$ ,  $P_x$ ,  $\theta_{VGT}$ , respectively. A generic NFIR model with one layer sigmoid network nonlinearity is used for representation of both MAP and MAF outputs as MISO models; i.e.

$$\hat{y}(k) = L^T(X(k-1) - \bar{X}) + \delta + \sum_{i=1}^{m_s} \left( a_i \frac{1}{1 + e^{-(X(k-1) - \bar{X})^T Q b_i - c_i}} \right) \quad (3.6)$$

where  $X \in R^N$  is the regressor vector,  $\bar{X} \in R^N$  mean regressor vector,  $L \in R^N$  is a vector of linear subspace parameters,  $\delta$  is a scalar output offset,  $Q \in R^{N \times N}$  is a matrix of nonlinear subspace parameters,  $b_i \in R^N$  is dilation and  $c_i$  is a scalar translations parameter and  $m_s$  is the number of sigmoid elements. Summation is from one to the number of sigmoid units. For the MAF output modeling, the regressor vector  $X_{MAF}$  is defined as

$$\begin{aligned} X_{MAF}(k-1) \triangleq & [P_i(k-1) P_i(k-2) \dots P_i(k-n_1) \dots \\ & P_x(k-1) P_x(k-2) \dots P_x(k-n_2) \dots \\ & P_c(k-1) P_c(k-2) \dots P_c(k-n_3) \dots \\ & \theta_{EGR}(k-1) \theta_{EGR}(k-2) \dots \theta_{EGR}(k-n_4)] \end{aligned} \quad (3.7)$$

where  $n_1 + n_2 + n_3 + n_4 = N$ . Similarly, for the MAP output modeling, the regressor vector  $X_{MAP}$  can be introduced as

$$\begin{aligned} X_{MAP}(k-1) \triangleq [ & P_c(k-1) P_c(k-2) \dots P_c(k-n_1) \dots \\ & P_x(k-1) P_x(k-2) \dots P_x(k-n_2) \dots \\ & \theta_{VGT}(k-1) \theta_{VGT}(k-2) \dots \theta_{VGT}(k-n_3)] \end{aligned} \quad (3.8)$$

where  $n_1 + n_2 + n_3 = N$ . Linear and nonlinear parts of the identified system can be written as

$$\hat{y}(k) = G_{id}X(k-1) - G_{id}\bar{X} + \delta + \sum_{i=1}^{m_s} \left( a_i \frac{1}{1 + e^{-(X(k-1) - \bar{X})Qb_i - c_i}} \right) \quad (3.9)$$

where  $G_{id} \in R^{1 \times N}$  represents identified linear part of the MAF or MAP output. The model set is composed of the models of the form (3.9) and the goal of the identification process is determining parameters of the best fitting model to the data.

## 3.2 Design of Experiments for Diesel Engine Airpath

Experiments are the source of the data. An experiment should be designed such that output data is maximum informative. Design of experiment includes determining inputs signals, their time and frequency domain characteristics, sampling ratios and presampling filters [55]. Design problem is defined as determining optimum values for these parameters with respect to selected design criteria while respecting the system constraints. Design criteria are generated for the assesment of the maximum *informative* or *better* experiment.

### 3.2.1 Generic Design of Experiment Criteria for Identification

A data set is defined as *informative* if it can discriminate the best model from candidate model set with respect to the evaluation criterion. A general advice is selecting input and output set such that the output prediction is sensitive to the important parameters of the intended application. This can be defined as (in)validation power of the data as well. System shall represented all its characteristics in the output signal when the ideal input design is applied. This also can be stated as minimum model output covariance is sought for candidate model sets with designed input data.

An open loop system identification is required to identify the best fitting model from the candidate model set described in the previous subsection. Candidate model has both linear and nonlinear parts. The bias and variance of the estimate are dependent to the input spectrum but not to the signal waveform for linear open loop identification and periodic signals has persistency advantages.

High correlation between input channels in the experiment design creates an ambiguity in terms of contribution of each input channel to the output. Pairwise correlation between input channels can be measured with Pearson factor which is calculated as

$$p(x, y) = \frac{\sum_{i=1}^n (x_i - \bar{x})(y_i - \bar{y})}{\sqrt{\sum_{i=1}^n (x_i - \bar{x})^2} \sqrt{\sum_{i=1}^n (y_i - \bar{y})^2}} \quad (3.10)$$

for  $n$  element  $x$  and  $y$  arrays. Since the covariance matrix of the candidate model set outputs is inversely proportional to the input power [54], maximum input power for the designed inputs are sought. This property is measured with crest factor and defined as

$$C_r^2 = \frac{\max_t u^2(k)}{\lim_{N \rightarrow \infty} \frac{1}{N} \sum_{k=1}^N u^2(k)} \quad (3.11)$$

where  $u$  is the input signal of  $N$  samples. Minimum value of the crest factor is the better and the minimum value is 1. Binary type of signals are advantageous in this metric. However, it should be noted that binary type signals do not cover a wide amplitude range and this weakens their validation capability against nonlinear models.

### 3.2.2 Proposed Experiment Design and Application

Engine control system has two external inputs in general. They are acceleration pedal position and engine speed. Based on given pedal position and engine speed pre-calibrated desired values for all sub-components are calculated. Identification tests are conducted at engine dynamometers and this test platform allows simulation of various kinds of the load scenarios, i.e. road conditions in terms of speed and load. A dynamometer airpath system flowchart is depicted in Fig. 3.2.

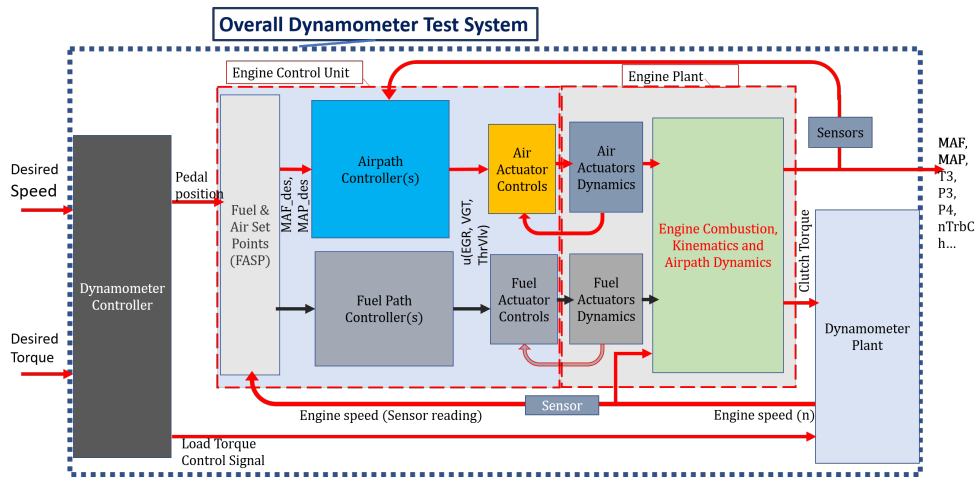


FIGURE 3.2: A diesel engine dynamometer airpath system flowchart

Experiment is designed for dynamometer and certain calibration sets. A calibration set means certain fixed fuel and air setpoints and controller parameters. Besides physical engine behavior, these parameters define prior probabilities of the inputs and outputs. Airpath control aims to follow desired flow and pressure setpoints so that a control oriented model with fixed calibration parameters increases accuracy of the model. However, this approach requires repeating the tests

again after changes in the calibration and this is found acceptable since the test is simple and rather short, and does not require extensive set of instruments. Thus, manipulated inputs for the experiment are selected as engine speed and torque but the regressors defined in (3.7) and (3.8) are used as model inputs.

Chirp signals which are periodic signals with varying frequencies are popular in the nonlinear dynamic system identification due to their persistent excitation capabilities. Besides, they have a good amplitude space coverage. Chirp signals are selected as input signal waveform and they are defined as

$$y = A \sin(2\pi(f(t))) \quad (3.12)$$

$$f(t) = f_o + kt \quad (3.13)$$

$$k = \frac{f_{max} - f_o}{T} \quad (3.14)$$

where minimum frequency is  $f_o$ , maximum frequency is  $f_{max}$ , duration between maximum and minimum frequencies is  $T$  and the frequency slope or the chirp ratio is  $k$ . Frequency coverage is one of the most important properties of a good experiment design. Target cycle for the engine modeling is called World Harmonized Transient Cycle. It is generated to represent typical heavy duty vehicle behaviour in the dynamometer environment. A sample Fast Fourier Transform results are depicted in Fig. 3.3. Its maximum and minimum frequencies can be taken as 0.05Hz and 5Hz since WHTC is defined in 10Hz.

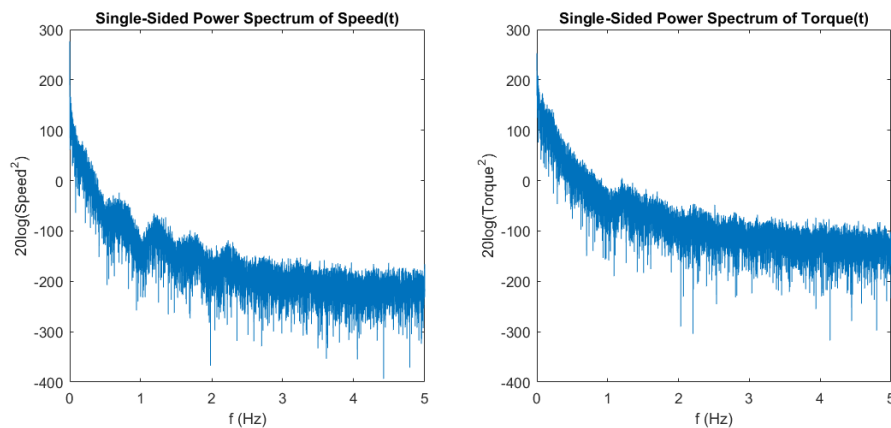


FIGURE 3.3: A sample WHTC speed and torque frequencies

Frequency coverage and crest factor minimization were discussed but input correlation and amplitude coverage are also important. In order to minimize input correlation frequencies, ramps of each channel are selected as inverse. Time domain, signal coverage and frequency vs time plots are depicted in Fig. 3.4.

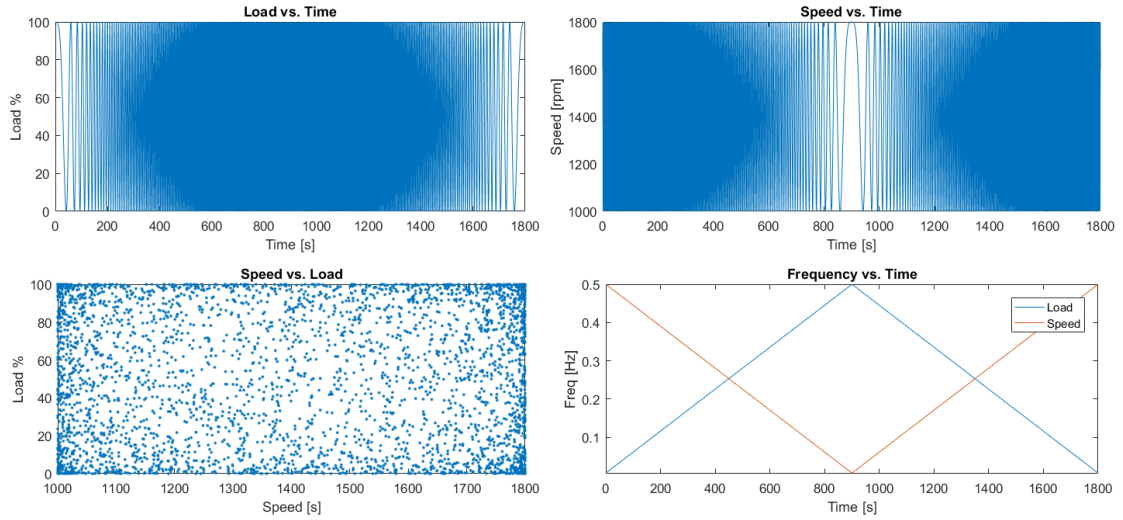


FIGURE 3.4: DoE Input Signals, Coverage and Frequencies

Designed inputs signals has a Pearson coefficient value of  $p(\text{Speed}, \text{Load}) = 0.03$ . These inputs are applied to the dynamometer controller and resulting model inputs are recorded and used for respective models as shown in Fig. 3.5

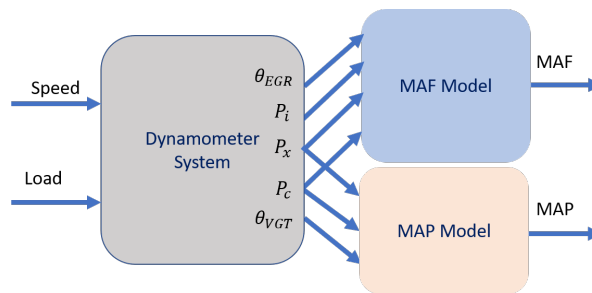


FIGURE 3.5: Calibration Dependent Airpath Identification Process

Finally, a half hour test cycle is designed and it can be run in any phase of the engine development project without any prior preparation such as hardware limitation or DoE boundary checks.

### 3.3 Model Evaluation Criterion

Candidate models are compared with their validation test cycle performance. Validation test cycle is selected as WHTC. A common performance metric is the normalized root mean square error (*nrmse*) fitness value, which is defined as

$$nrmse\ fitness = 100 \times \left(1 - \frac{\|y - \hat{y}\|}{\|y - \bar{y}\|}\right) \quad (3.15)$$

where  $y$  is the real value,  $\hat{y}$  is the estimated value and  $\bar{y}$  is the average value of the output. Best model in the candidate set is evaluated with the highest fit value in the WHTC data.

# Chapter 4

## Data Driven Disturbance Observer

This section focuses on disturbance observer design for limited capability engine control units. Next chapter revisits the problem with a higher fidelity estimation structure but with more complex calculations. As stated in Section 1.1, this thesis has two target electronic control units. Disturbance observer based control approach is designed for commercially available control units.

### 4.1 Disturbance Observer Overview

Real world control engineering problems generally require certain robustness measures against external disturbances to the system as well as parameter variations and uncertainties of the system. Robust feedback control approaches are developed in order to deal with these problems. The most popular approach is proportional integral derivative (PID) control and certain disturbance attenuation characteristics are gained from the integral term. Online model estimation techniques are developed in order to overcome model uncertainties and tuning control parameters with respect to these models are main ideas of adaptive control. Robust control techniques have focused on worst case scenarios of model uncertainties and

control ability to cope with these uncertainties is researched. Sliding mode control is popular for its external disturbance rejection capabilities and suppression of parameter uncertainty effects. High frequency switching nature of this approach is both its source of robustness and actuator chatter risk. Internal model control is another approach with practical popularity due to its intuitive nature and simple application philosophy. These approaches are categorized as passive antidisturbance control (PADC) methods [66]. These feedback driven disturbance rejection methods have a general trade off between control tracking performance and disturbance rejection capability. Rising share of the integral part of PID control increases tendency to overshoot or undershoot; fast identification or gain regularization of adaptive controllers makes system less reliable; overconservative design of robust controllers deteriorate system nominal response; chatter alleviation remedies for sliding mode control weakens the disturbance rejection capabilities; and high dimensional internal model control requires sophisticated matrix inversions. Active antidisturbance control (AADC) methods are feedforward approaches and they depend on estimation or measurement of the disturbance [66]. Traditional feedforward control and disturbance modeling or estimation methods aim to compensate disturbances without compromising the nominal performance.

Original disturbance observer concept is proposed by Ohnishi [67]. This was a frequency domain development based on the single input single output system depicted in Fig. 4.1 where  $d(s)$  denotes external input disturbance,  $n(s)$  is the measurement uncertainty and  $G_n(s)$  is the estimated nominal plant. Ohnishi's disturbance observer aims to estimate measurement uncertainties and input disturbances as a lumped disturbance  $\hat{d}_l$ .

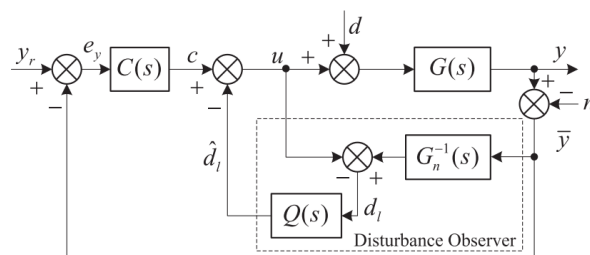


FIGURE 4.1: Conceptual Diagram of Original DOB Scheme from [68]

The lumped, total disturbance on the input and the input can be represented as

$$d_l(s) = \bar{y}(s)G_n^{-1}(s) - u(s) \quad (4.1)$$

$$u(s) = G^{-1}(s)y(s) - d(s) \quad (4.2)$$

By substituting (4.2) into (4.1), it follows that

$$d_l(s) = [G_n^{-1}(s)(y(s) - n(s))] - [G^{-1}(s)y(s) - d(s)] \quad (4.3)$$

Rearranging (4.3) one can obtain

$$d_l(s) = [G_n^{-1}(s) - G^{-1}(s)]y(s) - G_n^{-1}(s)n(s) + d(s) \quad (4.4)$$

where the first term represents inverse nominal model error contribution, the second term accounts for measurement uncertainty and the last term is the external input disturbance. Thus, Ohnishi's proposed disturbance observer scheme covers all the related uncertainties and disturbances but it is not effective to measurement uncertainties as shown below. However, implementation of the inverse plant is not generally feasible and a filter transfer function  $Q(s)$  is required. Estimated lumped disturbance  $\hat{d}_l$  is calculated as

$$\hat{d}_l(s) = Q(s)[(G_n^{-1}(s) - G^{-1}(s))y(s) - G_n^{-1}(s)n(s) + d(s)] \quad (4.5)$$

and when it is fed to the system, control input becomes

$$u(s) = c(s) - Q(s)[(G_n^{-1}(s) - G^{-1}(s))y(s) - G_n^{-1}(s)n(s) + d(s)] \quad (4.6)$$

For a frequency range that makes  $Q(s) \approx 1$ , (4.6) implies

$$y(s) = G(s)(c(s) - (G_n^{-1}(s) - G^{-1}(s))y(s) + G_n^{-1}(s)n(s) - d(s) + d(s)) \quad (4.7)$$

$$\implies y(s)G(s)G_n^{-1}(s) = c(s)G(s) + G(s)G_n^{-1}(s)n(s) \quad (4.8)$$

$$\implies y(s) = c(s)G_n(s) + n(s) \quad (4.9)$$

In (4.9), it is seen that the system is forced to behave like the nominal plant and input disturbance effect and model uncertainty are diminished; however output measurement uncertainty is still effective. Filter design and its effects on the performance and stability of the system are active research topics in the disturbance observer area and have a major effect on the disturbance observer performance. Although the disturbance observer is aimed to reject disturbances without any compromise, the filter  $Q$  limits disturbance attenuation capability of the disturbance observer.

## 4.2 Data Driven Disturbance Observer Design

Disturbance observer designs in the literature use nominal physical plant information. Original DOB scheme is proposed by Ohnishi et. al. [67] based on frequency domain analysis. In the classic DOB control structure, estimated disturbances are fed back to the control loop. Classic DOB design requires two main steps: finding a nominal inverse model ( $G_n^{-1}$ ) and applying the required filter ( $Q$ ) for causality. Further overview on disturbance observer methods can be found in [68]. In our approach, the disturbance rejection control is developed from time domain FIR system models which are obtained via system identification. This distinguishes our approach from other methods like state space based uncertainty and disturbance estimator (UDE) design in [69].

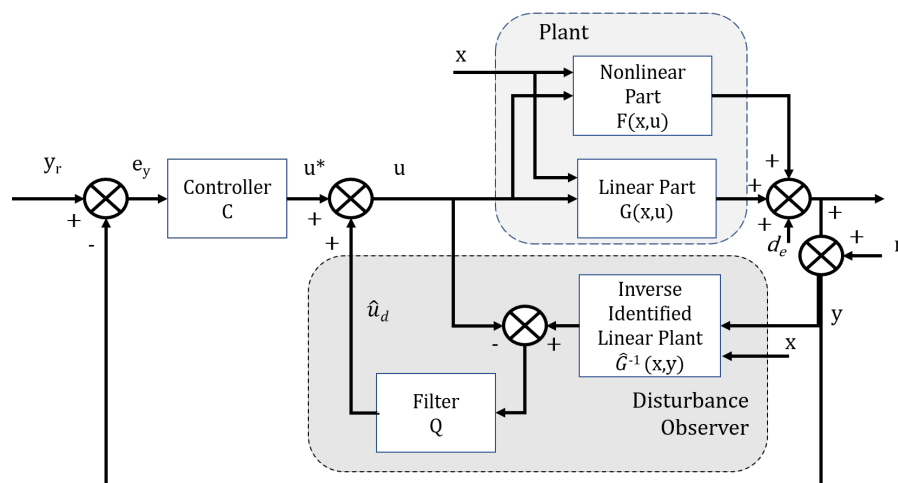


FIGURE 4.2: Conceptual Diagram of Designed DOB Scheme

It is assumed that the airpath system is separable into nonlinear and linear parts and nonlinear part is deliberately ignored, since it creates computational complexity for the aimed embedded application. Overall system with proposed DOB structure can be shown as in Fig. 4.2.

The output ( $y$ ) of a nonlinear separable system with nonlinearities  $F(x, u)$ , output disturbance ( $d_e$ ) and measurement uncertainties ( $n$ ) can be represented in terms of state  $x \in R^{N-1}$  in discrete-time as

$$y(k) = \hat{G}(x(k-1), u(k-1)) + \dots \\ \dots + \underbrace{\tilde{G}(x(k-1), u(k-1)) + F(x(k-1), u(k-1)) + d_e(k-1) + n(k-1)}_{\triangleq d(k-1)} \quad (4.10)$$

where  $\hat{G}$  is the estimated linear part of the system with the estimation error  $\tilde{G}$  and  $d$  is the total disturbance. Let the estimated nominal linear part be defined as  $G_{id} = [\hat{A} \ \hat{B}]$  with  $\hat{A} \in R^{1 \times (N-1)}$  and  $\hat{B} \in R$ . In light of (4.10), it follows that

$$y(k) = [\hat{A} \ \hat{B}] \begin{bmatrix} x(k-1) \\ u(k-1) \end{bmatrix} + d(k-1) \quad (4.11)$$

We assume existence of a disturbance compensation control such that  $\hat{B}u_d(k) = d(k)$  and it linearizes the nonlinear system as

$$y(k) = [\hat{A} \ \hat{B}] \begin{bmatrix} x(k-1) \\ u(k-1) + u_d(k-1) \end{bmatrix} \quad (4.12)$$

Rearranging (4.12), one obtains

$$u_d(k-1) = (y(k) - \hat{A}x(k-1))/\hat{B} - u(k-1) \quad (4.13)$$

In order to compute  $u_d(k)$  from (4.13), one needs previous control (i.e.  $u(k-1) = \theta_{EGR}(k-1)$ ), previous state and the current output. The equation can be written

in terms of current state and current control signal as follows:

$$u_d(k) - \Delta y(k)/\hat{B} = (y(k) - \hat{A}x(k)/\hat{B} - u(k)) \quad (4.14)$$

where  $\Delta y(k) \triangleq y(k+1) - y(k)$ . Similar to the literature [69], we assume that there exists a low-pass filter  $Q(s)$  with impulse response  $q(k)$  and the total disturbance  $d(k)$  is significant over the bandwidth of the filter. Applying  $Q$  filter to both sides of (4.14), one can write

$$\hat{u}_d(k) = ((y(k) - \hat{A}x(k))/\hat{B} - u(k)) \star q(k) \quad (4.15)$$

where  $\star$  denotes the convolution operator and the estimated disturbance compensation control is  $\hat{u}_d(k) = (u_d(k) - \Delta y(k)/\hat{B}) \star q(k)$ . Estimation error ( $e_{u_d}(k) = u_d(k) - \hat{u}_d(k)$ ) for the disturbance compensation control will be given as

$$e_{u_d}(k) = u_d(k) - (u_d(k) - \Delta y(k)/\hat{B}) \star q(k) \quad (4.16)$$

The estimation error can be diminished with an optimum filter design if the output and the disturbance signals have distinct frequency ranges.

# Chapter 5

## Gaussian Process Regression

### Modeling of Airpath

This chapter presents development of a data-driven flexible modeling for diesel engine airpath system for embedded model based control utilization. Turbine, compressor, engine block, exhaust gas recirculation (EGR) valve, variable geometry nozzle assembly (VNT or VGT) are main components of the airpath system. In this chapter, modeling will be presented for each component and at the end of the chapter, overall model of the system will be presented. This modeling approach aims to create a flexible framework for the airpath system that can be used with different hardware combinations without having a major change in the embedded software. Modern diesel engines have major components and typical layout in Fig 5.1. There are other engine architectures with combinations of the same elements such as two cascaded turbocharger or one additional EGR line which connects the compressor inlet to the turbine outlet. Also emerging technologies like electrically assisted turbochargers are becoming popular. This vibrant nature of the airpath architecture alternatives makes it more complex to develop model based control software for manufacturers. Although a data driven and flexible modeling structure is sought, a priori information based on physical modeling is crucial for the assesment of the model fitting to the system. Complex thermodynamics of the internal combustion engine manifests itself in the static relationships of the

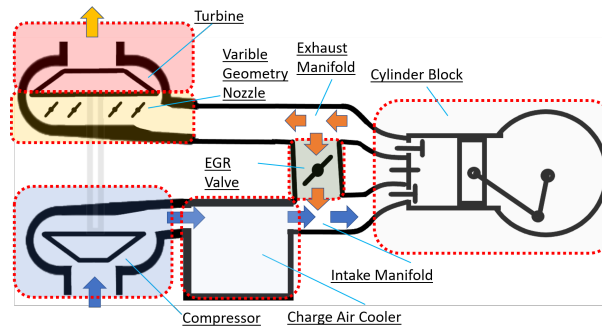


FIGURE 5.1: Diesel Engine Airpath Elements

engine. In this thesis, a mean value model is considered for the all components. The following discussion presents physical motivations behind the selected input variables of the respective component models and practical aspects of gathering the data.

Radial air compressors are one of the most complex aerodynamic machines. Its design and analysis process require both intensive finite element method simulations [78] and tests (related test standard SAE J1723) [77]. Final characteristics of a turbocharger compressor is represented via so called compressor map. A compressor map gives compressor speed, flow, pressure ratio and (generally) isentropic efficiency relations. This map includes boundaries of feasible operation (i.e. surge and choke lines) whose details can be found in [78]. Compressor map also includes isentropic efficiency and speed, flow, pressure ratio surfaces. It represents a 4-D surface and it is generally represented as two separate 3-D maps with (flow, pressure ratio, efficiency) and (flow, pressure ratio, speed) groups. One of the popular methods [79],[80] is using ellipse functions for approximating compressor efficiency and quadratic polynomials for volumetric flow functions. These approaches have accuracy problems in near boundary regions due to their simplified nature. In this study, it is assumed that compressor bench test data or engine dynamometer data are available. Compressor test is simulated with the compressor model in [80]. Inputs to the model are compressor inlet pressure  $P_{ci}$ , compressor outlet pressure  $P_i$ , compressor outlet mass flow rate  $W_{co}$  and compressor inlet temperature  $T_{ci}$ . Compressor outlet to inlet pressure ratio ( $PR = P_i/P_{ci}$ ) is used in the simulation. Similarly,  $P_{co}$  is modelled utilizing  $\omega$ ,  $P_{ci}$  and  $W_{co}$ , or  $W_{co}$  is modelled utilizing  $\omega$ ,

$P_{ci}$  and  $P_{co}$ .

Turbines are identified with a similar characterization process similar to compressors [77] and the resulting turbine map contains symmetrical information with the compressor map. By using related corrected coordinates [81], the turbine map represents a pressure ratio ( $PR_t = P_x/P_{xo}$ ) surface in terms of turbine outlet pressure  $P_{xo}$ , turbine inlet temperature  $T_x$ , turbine inlet mass flow  $W_{ti}$  and VGT vane position  $\theta_{VGT}$ . Therefore turbine inlet pressure  $P_x$  can be represented in terms of the following parameters.

$$P_x \approx P_{xo} f(P_{xo}, W_{ti}, T_x, \theta_{VGT}) \quad (5.1)$$

where  $P_{xo}$  is the turbine outlet pressure,  $W_{ti}$  is the turbine inlet flow,  $T_x$  is turbine exit temperature and  $\theta_{VGT}$  is the VGT vane position. A contemporary turbine power  $P_t$  model based on Euler turbine equation is derived in [82] as

$$P_t = \frac{2\pi}{15} \omega (W_{ti})^2 \frac{D_{t1}}{D_{t2}^2 - D_{tn}^2} \frac{RT_{xo}}{P_{xo}} \tan \theta_{VGT} \quad (5.2)$$

where  $P_{xo}, T_{xo}$  are the turbine outlet pressure and temperature,  $D_{t1}, D_{t2}, D_{tn}$  are the turbine wheel diameter, the turbine outer diameter and the turbine nut diameter, and  $\omega$  is the turbine shaft angular speed. But this model is limited with low turbine inlet Mach numbers with full energy recovery assumption. Also incidence angle effects, pulsation, secondary flows and loss factors are omitted in the derivation [81]. For wider range of applicability especially for high load cases model should include compressibility relations and this may lead to an iterative solution as seen in gas turbine performance models [83]. Thus data driven interpolation modeling is still required.

Unlike radial compressors, constant volume compressor with a piston and cylinder is simpler to model for its mass flow rate. However, an internal combustion engine piston and cylinder interaction is more complex than a standard air compressor due to dynamic external and internal variables. A mean value model deals with average values of an in cylinder event during one crank rotation. Basic airflow rate

to a four-stroke turbocharged engine flow through the inlet ports can be find as

$$W_{ie} = \eta_v \frac{P_i V_{cyl} N}{2 R_{gas} T_i} \quad (5.3)$$

where  $V_{cyl}$  is the displacement volume of the engine,  $\eta_v$  is the volumetric efficiency,  $N$  is the engine rotational speed,  $P_i$  is the intake manifold pressure,  $T_i$  is the intake manifold temperature and  $R_{gas}$  is the ideal gas constant. Volumetric efficiency is known to be related with the following factors [84]: air/fuel ratio, fuel type, fuel latent heat, mixture temperature, exhaust to intake manifold pressure ratio, compression ratio, engine speed, intake and exhaust manifold port design, intake and exhaust valve geometry, lift and timings. Fuel type and related fuel properties, geometries, timings, compression ratio are mostly fixed variables for an engine. In practice, efficiency values are determined with engine dynamometer tests. Considering (5.3) and volumetric efficiency dependencies stated in [84], we selected engine speed  $N$ , intake manifold pressure  $P_i$ , intake manifold temperature  $T_i$ , fuel flow rate  $W_f$  as inputs to the GPR flow rate model of the cylinder block. These data can be measured simultaneously with engine inlet flow (which can be measured via onboard mass airflow sensor while EGR line is blocked). Butterfly type EGR valves are used in the target Ecotorq engine. Butterfly valve modeling is studied in the literature [84], [85] focusing on throttle valves. Similarly, mass flow through a butterfly EGR valve can be calculated with the following equation if exhaust to inlet pressure ratio is less than the critical value ( $P_i/P_x < 0.528$ ).

$$W_{xi} = \frac{C_D A_{EGR} P_x}{\sqrt{R T_x}} \left(\frac{P_i}{P_x}\right)^{1/\gamma} \left(\frac{2\gamma}{\gamma-1} \left[1 - \left(\frac{P_i}{P_x}\right)^{(\gamma-1)/\gamma}\right]\right)^{1/2} \quad (5.4)$$

where  $C_D$  is discharge coefficient that is found experimentally,  $\gamma$  is the specific heat ratio of the exhasut gas,  $A_{th}$  is the geometric opening of the flow area. Since it changes with the area itself [85], it is practical to use effective area  $A_{eff} = C_D A_{EGR}$  as an empirical parameter. Characterization of flow depends on complex relation with the related design aspects; dominant inputs to the flow are  $P_x$ ,  $P_i$ ,  $A_{EGR}$ . These are used for the GPR modeling of the mass flow rate through the EGR valve  $W_{xi}$ .

## 5.1 Gaussian Process Regression (GPR)

Gaussian process regression (GPR) or Kriging (named after Daniel Krige a famous mining engineer) is a major engineering approach for geostatistics since 1951[91]. Its application is initiated as a spatial interpolation tool and found wider applications with increasing theoretical development in other engineering disciplines as well. Gaussian process regression (GPR) models are being used for online inverse modeling of the robotic systems [96]. In an automotive application, inner loop dynamics of the throttle valve is represented by nonlinear autoregressive with exogenous inputs (NARX) model whose nonlinear part is a GPR [93]. Diesel engine fuel systems dynamics are modelled with local gaussian process regression in [94] for offline model based calibration. Recently, an ECU supplier has introduced an advanced modeling unit in its ECU and online simulation of GPR models become practical for the automotive industry. This is a new capability for the powertrain control development and its application areas are expected to be broadening.

Gaussian process (GP) models are selected as a flexible modeling approach for all components due its non-parametric and data preserving nature. Gaussian process models store its training data in itself and learns the distribution (interpolation) characteristics between them. Other parametric machine learning approaches like neural networks do not store the training data and that creates a difficulty in their validations.

Well known Gaussian probability distribution is a specific form of a Gaussian process. A probability distribution characterizes random variables of scalars or vectors but the properties of functions are defined with a stochastic process. Informally, a function can be accepted as an infinitely long vector with input  $x$  to output  $f(x)$  couples. If one samples a finite number of points and searches for the properties of the function, then the same answer will be found with Gaussian process inference as if all points were considered [92].

Formally, each  $y$  observation is assumed to be a sample of underlying function  $f(x)$  with a Gaussian noise model as follows.

$$y = f(x) + N(0, \sigma_n^2) \quad (5.5)$$

where  $\sigma_n$  is the standard deviation of the measurement noise. Prior covariance on the noisy observations  $y_i$  and  $y_j$  is defined as

$$\text{cov}(y_i, y_j) = k(x_i, x_j) + \sigma^2 \delta_{ij} \quad (5.6)$$

Covariance function  $k(x_i, x_j)$  is defined over input samples  $x_i$  and  $x_j$ , and  $\delta_{ij}$  is the Kronecker delta function. Definition of  $k(x_i, x_j)$  for the squared exponential covariance term is given as

$$k(x_i, x_j) = \sigma_d e^{-0.5r^T r} \quad (5.7)$$

where  $\sigma_d$  is so-called horizontal scale parameter and  $r$  is a scaled input sample given by

$$r = \left[ \frac{x_{i1} - x_{j1}}{l_1} \quad \frac{x_{i2} - x_{j2}}{l_2} \quad \dots \quad \frac{x_{in} - x_{jn}}{l_n} \right]^T \quad (5.8)$$

where so-called length scale parameters  $l_j$  determine weights between input channels.

For an experiment of  $m$  samples, one can construct the following covariance matrix that will be used in subsequent analysis:

$$K(X, X) = \begin{bmatrix} k(x_1, x_1) & k(x_1, x_2) & \dots & k(x_1, x_m) \\ \vdots & \ddots & \vdots & \vdots \\ \vdots & \vdots & \vdots & \vdots \\ \vdots & \vdots & \vdots & k(x_m, x_m) \end{bmatrix} \quad (5.9)$$

The length scale  $l$  and the horizontal scale  $\sigma_d$  are the main parameters of the model and they are called hyperparameters. These parameters are found by maximum

likelihood estimation. Training values are used for finding hyperparameters and they are also embedded into the model through  $K$  matrix. The test values are denoted by  $x_*$ . The covariance vector between the test point and the training points is defined as

$$k_* = [k(x_*, x_1) \ k(x_*, x_2) \ \dots \ k(x_*, x_m)]^T \quad (5.10)$$

Predicted output  $y_*$  is then calculated as

$$y_* = k_*^T (K + I\sigma_n^2)^{-1} y \quad (5.11)$$

Since the term  $(K + I\sigma_n^2)^{-1}$  is fixed, an efficient form of (5.11) is given as

$$y_* = k_*^T \alpha \quad (5.12)$$

where  $\alpha \in R^m$  and  $\alpha = (K + I\sigma_n^2)^{-1} y$ .

Maximum likelihood optimization cost function is defined as

$$\log p(y|X) = -0.5^T \alpha - \text{trace}(\log(L)) - n/2 \log(2\pi) \quad (5.13)$$

where  $L$  is retrieved through the cholesky decomposition; i.e.

$$L = \text{cholesky}(K + I\sigma_n^2) \quad (5.14)$$

Overall training process can be summarized as follows. For given measurements of inputs  $X$ , output  $y$  and measurement noise  $\sigma_n$ , select a covariance function (e.g. squared exponential). Minimize expected variance (or maximize likelihood) on training points via varying the hyperparameters (parameters of the kernel or covariance function). After finding the optimum hyperparameters, one can estimate the output for any given input  $x_*$  via (5.11).

## 5.2 Overall GPR Dynamic Model for Diesel Engine Airpath

The following static equations define the engine airpath behaviour of the configuration depicted in Fig. 5.1. Nonlinear static relations are modelled as

$$W_{co} = G_0(\omega, P_{ci}, P_{co}) \quad (5.15)$$

$$W_{xi} = G_1(P_x, P_i, r_{EGRact}) \quad (5.16)$$

$$W_{ie} = G_2(N, P_i, T_i, W_f) \quad (5.17)$$

$$W_{xt} = G_3(P_x, P_{xo}, T_x, r_{VGTact}) \quad (5.18)$$

$$P_x = G_4(W_{co}, W_f, T_x, P_{xo}, \theta_{VGTact}) \quad (5.19)$$

$$T_t = G_5(W_{co}, W_f, P_x, P_{xo}, \theta_{VGTact}) \quad (5.20)$$

$$T_c = G_6(W_{co}, P_i, P_{ci}) \quad (5.21)$$

where  $G_i$ s are respective GPR functions. Applying the chain rule to (5.15), the following equation is obtained.

$$\dot{W}_{co} = G_0^{(\omega)} \dot{\omega} + G_0^{(P_{ci})} \dot{P}_{ci} + G_0^{(P_{co})} \dot{P}_{co} \quad (5.22)$$

where  $G^{(x)} = \frac{\partial G}{\partial x}$ . Actuator dynamics and charge air cooler volume dynamics are generally neglected in the literature [86], [87], [79]. For a control oriented model, similar to [86], temperatures, compressor inlet and turbine outlet pressures are assumed to be constant (i.e.  $\dot{T}_x = 0, \dot{T}_i = 0, \dot{P}_{ci} = 0, \dot{P}_{xo} = 0$ ).

Since mean value modeling is assumed for the engine cylinder, airpath dynamics does not include pulsation effects caused by inlet or exhaust valves of the cylinders. So, volume filling and emptying, actuator inner loop response and turbocharger acceleration and deceleration are remaining dynamics to be considered. Static relations are modelled with GPR and physical dynamic state equations are used as follows. Charge air cooler (intercooler), intake and exhaust manifolds are main volume elements of a typical diesel engine system. For a constant volume with

input flows  $W_{in}$  and output flows  $W_{out}$ , time derivative of the ideal gas law can be written as

$$\Sigma W_{in} - \Sigma W_{out} = \frac{\dot{P}V}{R T} \quad (5.23)$$

where the temperature is assumed to be constant, i.e.  $\dot{T} = 0$ . Similarly, the charge air cooler (CAC) pressure  $P_{co}$  can be calculated with

$$\dot{P}_{co} = \frac{RT_{co}}{V_{cac}}(W_{co} - W_{coo}) \quad (5.24)$$

where  $T_{co}$  is CAC temperature,  $V_{cac}$  is CAC volume,  $W_{co}$  is compressor outlet flow and  $W_{coo}$  is intercooler exit flow. Similar equations for intake and exhaust manifolds can be written as

$$\dot{P}_i = \frac{RT_i}{V_i}(W_{coo} + W_{xi} - W_{ie}) \quad (5.25)$$

$$\dot{P}_x = \frac{RT_x}{V_x}(W_{xe} - W_{xt} - W_{xi}) \quad (5.26)$$

where  $T_i, P_i, V_i$  and  $T_x, P_x, V_x$  are intake and exhaust manifold temperatures, pressures and volumes, respectively; and  $W_{xi}, W_{ie}, W_{xe}, W_{xt}$  are EGR, cylinder inlet, turbine inlet and cylinder outlet flows.

Automotive airpath actuators are generally DC motors with position feedback sensors. Pneumatic actuators with solenoid pressure control valves also exist. But for the highest emission standards with transient homologation cycles, electrical actuators became dominant. These motor drives are connected to the valves, vanes or gates via a spring loaded gear or linkage mechanism. In the scope of this work, position control of the actuators are not included but its response is assumed to be a first order dynamics as follows.

$$\dot{\theta}_{act} = \frac{1}{\tau}(\theta_{des} - \theta_{act}) \quad (5.27)$$

where  $\theta_{des}$  is the desired valve position,  $\theta_{act}$  is the measured valve position and  $\tau$  is the inner loop time constant. Typical expected values for  $\tau_\theta$  are 50 – 200ms.

Aside from gas dynamics, mechanically, turbocharger is simply a rigid rotating inertia. Its rotational can be written as

$$\dot{\omega} = \frac{1}{I\omega}(P_t - P_c(1 + c_f)) \quad (5.28)$$

where  $I$  is the total rotational inertia. Turbocharger spool up is generally the slowest of the presented dynamic processes.

In this study, intercooler volume dynamics is neglected ( $P_{co} = P_i$ ) but the actuator inner loop response is included. Overall system dynamics can be represented as

$$\dot{P}_i = \frac{RT_i}{V_i}(G_0 + G_1 - G_2) \quad (5.29)$$

$$\dot{P}_x = \frac{RT_x}{V_x}(W_f + G_2 - G_3 - G_1) \quad (5.30)$$

$$\dot{\omega} = \frac{1}{I}(G_5 - G_6 - c_f\omega) \quad (5.31)$$

$$\dot{W}_{co} = G_0^{(\omega)} \frac{1}{I}(G_5 - G_6 - c_f\omega) + G_0^{(P_i)} \frac{RT_i}{V_i}(G_0 + G_1 - G_2) \quad (5.32)$$

$$\dot{\theta}_{EGRact} = \frac{1}{\tau_{EGR}}(\theta_{EGRdes} - \theta_{EGRact}) \quad (5.33)$$

$$\dot{\theta}_{VGTact} = \frac{1}{\tau_{VGT}}(\theta_{VGTdes} - \theta_{VGTact}) \quad (5.34)$$

It should be noted that (5.32) is linearly dependent on (5.29) and (5.31) if  $G_0^{(\omega)}$  and  $G_0^{(P_i)}$  are constant. Recall that, inputs of GPR functions,  $G_i$ s, are given explicitly in (5.15)-(5.21). Therefore, (5.29)-(5.34) can be recast as

$$\dot{x} = F(x, d) + Bu \quad (5.35)$$

where the state vector  $x$ , the control input  $u$  and the measured disturbance vector  $d$  are defined as

$$x = [P_i \ P_x \ \omega \ W_{co} \ \theta_{EGRact} \ \theta_{VGTact}]^T \quad (5.36)$$

$$u = [\theta_{EGRdes} \ \theta_{VGTdes}]^T \quad (5.37)$$

$$d = [N \ W_f]^T \quad (5.38)$$

The measured disturbances are the engine speed ( $N$ ) provided by the sensor and the fuel mass flow rate ( $W_f$ ) controlled by the fuel path. The input matrix  $B$  is defined as

$$B = \begin{bmatrix} 0 & 0 \\ 0 & 0 \\ 0 & 0 \\ 0 & 0 \\ \frac{1}{\tau_{EGR}} & 0 \\ 0 & \frac{1}{\tau_{VGT}} \end{bmatrix} \quad (5.39)$$

This model is used for control system design in Chapter 6 and component model validation results are presented in Chapter 7.

# Chapter 6

## Flexible and Robust Airpath Control

Main focus of the airpath control is disturbance alleviation and different active disturbance control methods (i.e. disturbance observer and feedforward control) are developed in this thesis. Two different solution paths are followed in this study as depicted in Fig. 6.1.

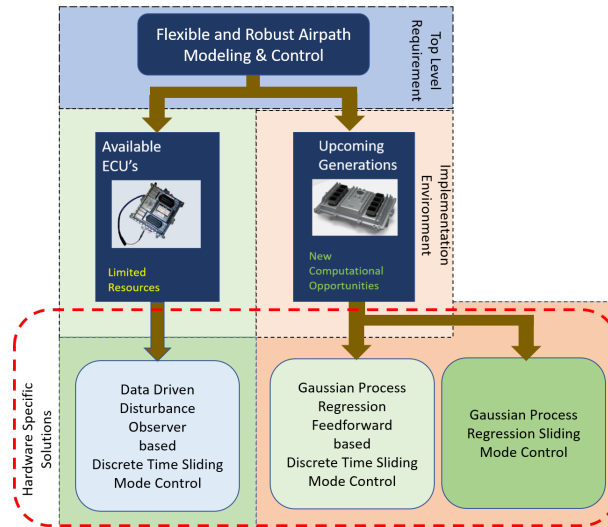


FIGURE 6.1: Implementation Hardware and Control Solutions Diagram

These approaches are tailored for two different target control platforms. Extensive modeling of the disturbances are not feasible with available engine control

units; so disturbance observer based solution is utilized for this type of target platforms. However, new generation control units with advanced features are being introduced and they made possible to use machine learning techniques in the embedded systems.

## 6.1 Data Driven Disturbance Observer Based Diesel Engine Airpath Robust Control

A general data driven disturbance observer design was presented in Chapter 4. Application details on MAF and MAP channels are presented in the following.

EGR and VGT controls are designed independently but their physical coupling is reflected to the control on the DOB design. In the light of (4.15), disturbance compensation control signals for EGR and VGT are calculated as

$$\hat{u}_{d(EGR)}(k) = ((MAF(k) - \hat{A}_{MAF}x_{MAF}(k))/\hat{B}_{MAF} - \theta_{EGRdes}(k)) \star q_{MAF}(k) \quad (6.1)$$

$$\hat{u}_{d(VGT)}(k) = ((MAP(k) - \hat{A}_{MAP}x_{MAP}(k))/\hat{B}_{MAP} - \theta_{VGTdes}(k)) \star q_{MAP}(k) \quad (6.2)$$

where  $\hat{A}_{MAF}$ ,  $\hat{A}_{MAP}$ ,  $\hat{B}_{MAF}$ ,  $\hat{B}_{MAP}$  are obtained via system identification. Recall that  $x_{MAF}$  and  $x_{MAP}$  are defined as

$$\begin{aligned} x_{MAF} \triangleq & [P_i(k-1) P_i(k-2) \dots P_i(k-n_1) \dots \\ & P_x(k-1) P_x(k-2) \dots P_x(k-n_2) \dots \\ & P_c(k-1) P_c(k-2) \dots P_c(k-n_3) \dots \\ & \theta_{EGR}(k-2) \theta_{EGR}(k-3) \dots \theta_{EGR}(k-n_4)] \end{aligned} \quad (6.3)$$

and

$$\begin{aligned}
 x_{MAP} \triangleq & [P_x(k-1) P_x(k-2) \dots P_x(k-n_1) \dots \\
 & P_c(k-1) P_c(k-2) \dots P_c(k-n_2) \dots \\
 & \theta_{VGT}(k-2) \theta_{VGT}(k-3) \dots \theta_{VGT}(k-n_3)]
 \end{aligned} \tag{6.4}$$

Overall disturbance control signal flow is depicted in Fig. 6.2. In the implemented engine configuration, there are sensors for MAP ( $P_i$ ), MAF ( $W_{ci}$ ) and valve positions  $\theta_{EGR}$   $\theta_{VGT}$ . Other inputs such as exhaust manifold pressure and compressor power are calculated with ECU built-in simple models.

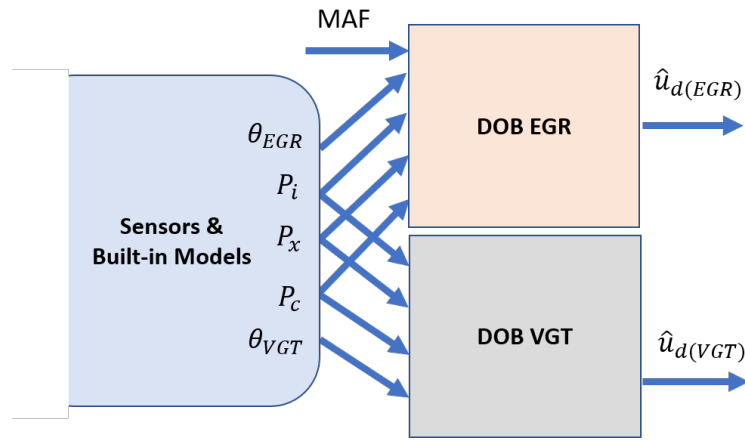


FIGURE 6.2: DOB Signal Flow for EGR and VGT implementation

In this study, a discrete-time sliding mode controller (DTSMC) in [95] is utilized. Noting that the airpath system given by (5.35) is affine in control, the error dynamics can be written as

$$\dot{\xi} = F(\xi) + B(\xi)u \tag{6.5}$$

where  $\xi$  is defined as  $\xi = [P_{id} - P_i \ P_{xd} - P_x \ P_{cd} - P_c]^T$ ,  $F$  and  $B$  are smooth nonlinear mappings, and  $u = [\theta_{EGR} \ \theta_{VGT}]$ . A sliding surface can be defined as

$$\sigma = G\xi \tag{6.6}$$

where  $G$  is a  $2 \times 3$  design matrix which makes  $GB$  invertible. The equivalent control is calculated by  $\dot{\sigma} = 0$ ; more specifically,

$$\dot{\sigma} = G\dot{\xi} = GF + GBu = 0 \Rightarrow u_{eq} = -(GB)^{-1}GF \quad (6.7)$$

Since we do not know  $F(\xi)$  and  $B(\xi)$  precisely,  $u_{eq}$  control obtained via (19) can not be used directly in sliding mode control. In light of (6.7), it follows that

$$\dot{\sigma} = GB(u - u_{eq}) \Rightarrow u - u_{eq} = (GB)^{-1}\dot{\sigma} \quad (6.8)$$

Selecting a Lyapunov function as  $V = 1/2\sigma^T\sigma \geq 0$  and taking its time derivative leads to

$$\dot{V} = \sigma^T\dot{\sigma} \quad (6.9)$$

$\dot{V}$  can be made negative definite with a  $D > 0$  by enforcing

$$\dot{\sigma} = -D\sigma \Rightarrow \dot{V} = -\sigma^TD\sigma \quad (6.10)$$

In light of (6.8) and (6.10), one obtains

$$-D\sigma = GB(u - u_{eq}) \Rightarrow u - u_{eq} = -(GB)^{-1}D\sigma \quad (6.11)$$

Computation of (6.8) and (6.11) at two different sample instants, i.e.  $t = kT$  and  $t = (k - 1)T$ , leads to

$$u(kT) - u_{eq}(kT) = (GB)^{-1}\dot{\sigma}(kT) \quad (6.12)$$

$$\begin{aligned} u((k - 1)T) - u_{eq}((k - 1)T) = \\ \dots - (GB)^{-1}D\sigma((k - 1)T) \end{aligned} \quad (6.13)$$

Continuity of equivalent control implies that

$$\lim_{\Delta \rightarrow 0} u_{eq}(t - \Delta) = u_{eq}(t) \quad (6.14)$$

Assuming  $T \approx \Delta$ ,

$$u_{eq}((k-1)T) = u_{eq}(kT) \quad (6.15)$$

Subtracting (6.13) from (6.12) by taking (6.12) into account and approximating  $\dot{\sigma}$  with Euler's backward difference, one obtains the following recursive control law

$$\begin{aligned} u(k) &= u(k-1) + \dots \\ &\dots + (GB)^{-1} \left( \frac{\sigma(k) + (TD-1)\sigma(k-1)}{T} \right) \end{aligned} \quad (6.16)$$

In applying this control to the system, the right hand side of (6.16) is usually saturated. However, since the control input  $u(k-1)$  can be observed with the valve position feedback sensor, (6.16) can be implemented as

$$\begin{aligned} u(k) &= u_{act}(k-1) + \dots \\ &\dots + (GB)^{-1} \left( \frac{\sigma(k) + (TD-1)\sigma(k-1)}{T} \right) \end{aligned} \quad (6.17)$$

where  $u_{act}(k-1)$  is the valve position read by the sensor at time  $k-1$ . Thus, the role of saturation function is naturally taken by the system itself.

Disturbance observer integrated control system is depicted in Fig. 6.3. Desired MAF and MAP values are interpolated from the pre-calibrated engine maps and appropriately saturated and filtered. Desired MAF values are limited with maximum possible flow via total flow calculation. Resultant references are then used in the feedback controller.

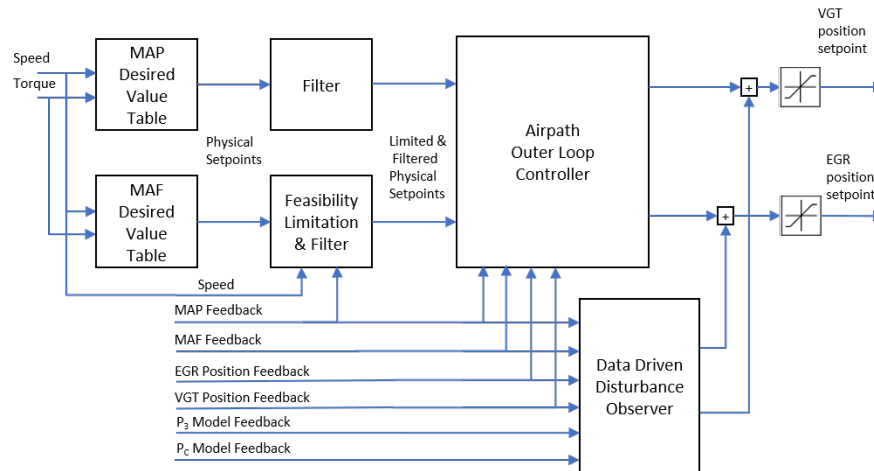


FIGURE 6.3: Overall Control Scheme with Data Driven Disturbance Observer, Airpath Outer Loop Controller (DTSMC) and Trajectory Generator

## 6.2 GPR Modeling Based Diesel Engine Airpath Robust Control

A calibratable and physical model free control approach is sought in our work. Singularity free and accurate inverse model for the airpath is known to be a hard problem; therefore a data driven inherently smooth modeling approach is favorable. On the other hand, mapping feedforward terms with respect to the physical states rather than operation points makes calibration procedure robust to the boundary condition variations such as backpressure. GPR can be seen as a gray-box modeling procedure since it is physically interpretable and contains prior information itself instead of a total abstraction. This nature of the model distinguishes from other modeling approaches from calibratability point of view.

### 6.2.1 GPR Feedforward Control

Mapping of the operation region of an engine in terms of speed and torque is possible in the engine development phase. Therefore, a priori information for the operation points and relevant states can be obtained. Mappings of the engine operation points (or fuel loops) are executed for steady state operation region.

Especially, emission modeling experiments cover the whole feasible operation zone. Since the steady state fuel loops, i.e. states for which  $\dot{x} = 0$ , are measurable with complete state and controlled values, the control effort which is required to conserve the states are also known. Thus, the feedforward control can be found by setting  $\dot{x} = 0$  as

$$0 = f(x) + b(x)u_{ff} \implies \hat{u}_{ff} = -\frac{\hat{f}(x)}{\hat{b}(x)} \quad (6.18)$$

Speed and inner torque based maps are commonly utilized in the automotive industry for the prediction of the feedforward term. This thesis proposes a GPR model based on physically related inputs  $P_x$ ,  $P_i$ ,  $W_{xi}$ . Inverse model for EGR line in [79], which is based on normal operation conditions, is given by (6.19).

$$Ar_{EGR} = \frac{W_{xi}\sqrt{RT_x}}{P_i[1 - (\frac{1 - \frac{P_i}{P_x}}{\Pi_{opt}} - 1)^2]} \quad (6.19)$$

In this equation of  $Ar_{EGR}$  shows that the area of the EGR valve, which is directly related to the EGR valve position ( $\theta_{EGR}$ ), is the output of the inverse actuator model. In order to achieve desired accuracy, introduction of additional parameters and related tuning effort are required. Details for this simplified physical modeling is given in [79]. VGT inverse model can be constructed based on energy flow from the turbine to the compressor. Utilizing steady state energy balance, the total efficiency for VGT based on vane position can be defined as

$$\eta_T(\theta_{VGT}) = \frac{P_c}{W_{xt}h_{xt}}T_x \quad (6.20)$$

An equation of compressor work can be rewritten in terms of efficiency as

$$\dot{P}_c = \frac{1}{\tau}(W_{xt}h_{xt}T_x\eta_T(\theta_{VGT}) - W_{ci}c_{air}(\frac{P_i}{P_a})^\mu) \quad (6.21)$$

The following input and output channels are selected based on the physical modeling presented above. Input channels for the inverse EGR line model are selected as  $P_i/P_x$ ,  $P_i$ ,  $W_{xi}$ . Inverse VGT model inputs are  $W_{ci}$ ,  $P_i$  and  $T_x$  respectively, and

its output is the VGT vane position,  $\theta_{VGT}$ . A space filling design of experiment (DoE) for the inputs is commonly used for GPR modeling. The test data is collected in the following steps. Transient engine mapping simulations are executed with a basic general engine controller by setting speed and desired torque to the grid points. First 10 seconds of the settling time is not used and average of the following 30 seconds are recorded. The test grid used for the design, which consists of 417 points of the engine operation region, is shown in Fig. 6.4.

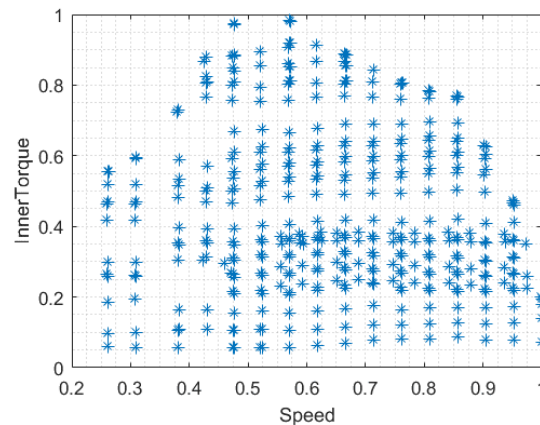


FIGURE 6.4: Engine Mapping Region

In order to model delayed boost characteristics of the turbocharger system, tests are repeated with 90% and 80% of the base calibration values as shown in Fig. 6.5.

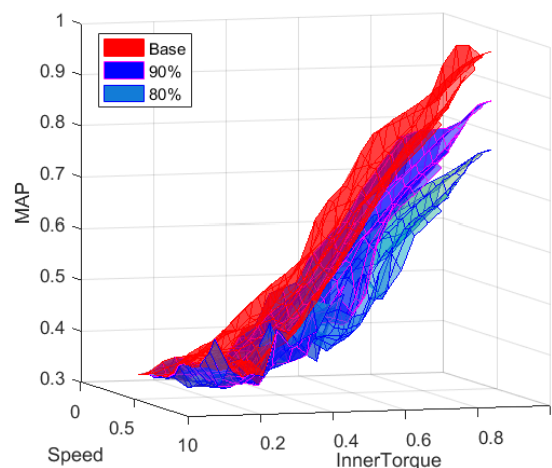


FIGURE 6.5: Three mapping boost values

In order to refine overlapping data, training points are selected via a bin logic. Input data space is divided into bins of equal intervals. Three values (i.e. minimum, maximum and median) of the each bin is selected as training samples. A sample bin for EGR model is depicted in Fig. 6.6.

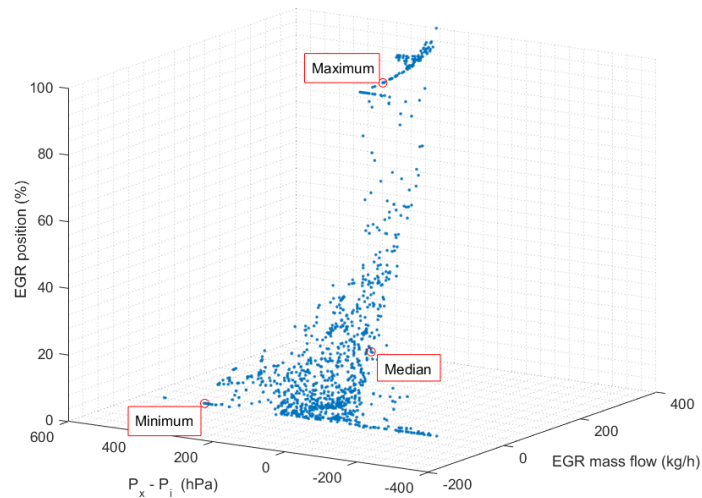


FIGURE 6.6: A sample training data selection bin

Total number of 179 training samples are utilized in training for VGT and 1252 points are used for validation. Due to increase calculation complexity of GPR quadratically with increasing number of training points, minimum number of training points is sought. However, due to lower fit values, EGR modeling required more training data (i.e. 312 training and 1164 validation) but resulted in a lower accuracy than the inverse VGT model. Model training is executed with *fitrgp* function of MATLAB. Exact GPR modeling method is used with squared exponential kernel configuration.

This feedforward controller is applied along with the discrete-time sliding mode controller (DTSMC) presented in Section 6.1.

## 6.2.2 GPR Feedback Control

Three feedback controllers based on control affine system given in (5.35) is explained in this section. A unique error term is defined for the subsequent control synthesis as

$$e_{GPR} \triangleq [(\hat{\theta}_{EGRdes} - \hat{\theta}_{EGRact}) \quad (\hat{\theta}_{VGTdes} - \hat{\theta}_{VGTact})]^T \quad (6.22)$$

Estimation of  $\hat{\theta}$  values requires a mapping from system outputs and states to the inputs. These models can be accepted as static inverse plant models and they are similar to the feedforward models presented in the previous section. Inverse models  $\hat{\theta}_{EGRdes}$ ,  $\hat{\theta}_{EGRact}$ ,  $\hat{\theta}_{VGTdes}$ ,  $\hat{\theta}_{VGTact}$  are estimated as

$$\hat{\theta}_{EGRdes} = G_{EGR}(P_i, P_x, T_x, \hat{W}_{xi-des}) \quad (6.23)$$

$$\hat{\theta}_{EGRact} = G_{EGR}(P_i, P_x, T_x, \hat{W}_{xi}) \quad (6.24)$$

$$\hat{\theta}_{VGTdes} = G_{VGT}(\hat{W}_{xt-des}, P_x, T_x, ) \quad (6.25)$$

$$\hat{\theta}_{VGTact} = G_{VGT}(\hat{W}_{xt}, P_x, T_x, ) \quad (6.26)$$

where  $G_{EGR}$  and  $G_{VGT}$  functions are GPR inverse models for EGR and turbine. Desired and actual EGR flows  $\hat{W}_{xi-des}$ ,  $\hat{W}_{xi}$  and desired and actual turbine flows  $\hat{W}_{xt-des}$ ,  $\hat{W}_{xt}$  are also estimated with the following inputs as

$$\hat{W}_{xi-des} = MAF_{des} - G_{Wie}(N, MAP, W_f) \quad (6.27)$$

$$\hat{W}_{xi} = MAF - G_{Wie}(N, MAP, W_f) \quad (6.28)$$

$$\hat{W}_{xt-des} = G_{Wie}(N, MAP_{des}, W_f) + W_f \quad (6.29)$$

$$\hat{W}_{xt} = G_{Wie}(N, MAP, W_f) + W_f \quad (6.30)$$

where MAF is the compressor inlet flow (i.e.  $W_{ci}$ ),  $\hat{W}_{ie} = G_{Wie}$  is the engine inlet total flow and  $W_f$  is the fuel flow.

### 6.2.2.1 GPR Based PI Control

Based on the error defined in (6.22) conventional PI controllers are proposed as

$$\theta_{EGRdes} = K_{pEGR}(\hat{\theta}_{EGRdes} - \hat{\theta}_{EGRact}) + K_{iEGR} \int (\hat{\theta}_{EGRdes} - \hat{\theta}_{EGRact}) dt \quad (6.31)$$

$$\theta_{VGTdes} = K_{pVGT}(\hat{\theta}_{VGTdes} - \hat{\theta}_{VGTact}) + K_{iVGT} \int (\hat{\theta}_{VGTdes} - \hat{\theta}_{VGTact}) dt \quad (6.32)$$

These controllers are compared with GPR based feedforward controllers on the WHTC simulation and results are presented in Chapter 7.

### 6.2.2.2 GPR Feedforward and Saturated Integral Control

Another application of GPR feedforward control presented in Section 6.2.1 is in  $P_{co}$  and MAP control via wastegate and throttle using the physical engine model published in [98]. This time, integral ( $I$ ) term is saturated with respect to the estimated feedforward standard deviations of the wastegate and the throttle ( $\sigma_{WG}$  and  $\sigma_{Thr}$ ).

$$\theta_{WGdes} = \hat{\theta}_{WGdes} + sat(K_{iWG} \int (P_{codes} - \hat{P}_{co}) dt) \quad (6.33)$$

$$\theta_{Thrdes} = \hat{\theta}_{Thrdes} + sat(K_{iThr} \int (MAP_{des} - MAP) dt) \quad (6.34)$$

where  $sat(\cdot)$  is defined such that the values inside the paranthesis are saturated with the upper limits of  $3\sigma_{WG}$ ,  $3\sigma_{Thr}$  and the lower limits of  $-3\sigma_{WG}$ ,  $-3\sigma_{Thr}$  for the wastegate and the throttle; respectively. Results of this controller are also shared in Chapter 7.

### 6.2.2.3 GPR Based Sliding Mode Control

Considering the system presented in the (5.35), sliding variable can be defined as

$$s(x) = S(x_d - x) \quad (6.35)$$

where  $x_d$  is the desired state vector and  $S$  is designed as

$$S = \begin{bmatrix} 0 & 0 & 0 & 0 & S_1 & 0 \\ 0 & 0 & 0 & 0 & 0 & S_2 \end{bmatrix} \quad (6.36)$$

where  $S_1 > 0$  and  $S_2 > 0$ . Assume that the control sensitivity matrix,  $B \in R^{6 \times 2}$ , is precisely known but the nonlinear part of the system,  $F \in R^6$ , is to be estimated. In light of (5.39), one can select  $S_1 = \tau_{EGR}$  and  $S_2 = \tau_{VGT}$ . With these choices,  $SB$  will be simply a  $2 \times 2$  identity matrix, i.e.  $SB = I$ . The sliding mode controller with equivalent control can be written as

$$\dot{s}(x) = 0 \implies \hat{u}_{eq} = (SB)^{-1}(S\dot{x}_d - S\hat{F}) \quad (6.37)$$

$$\implies u = (SB)^{-1}(S\dot{x}_d - S\hat{F}(x, d)) + K \text{sign}(S(x_d - x)) \quad (6.38)$$

where the sliding control gain is  $K > 0$ . Stability of the closed-loop system can be proven as follows. Selecting a positive definite Lyapunov function as  $V = \frac{1}{2}s(x)^T s(x)$ , its time derivative can be written as

$$\dot{V} = s(x)^T \dot{s}(x) \quad (6.39)$$

$$\dot{V} = s(x)^T S(\dot{x}_d - \dot{x}) = s(x)^T (S\dot{x}_d - S(F + Bu)) \quad (6.40)$$

Plugging (6.38) into (6.40) implies

$$\dot{V} = s(x)^T (S\hat{F} - SF) - SBK \text{sign}(s(x)) \quad (6.41)$$

Recalling  $SB = I_{2 \times 2}$  and  $K > 0$  is a scalar, (6.41) implies

$$\dot{V} = s(x)^T (S\hat{F} - SF) - Ks(x)^T \text{sign}(s(x)) \quad (6.42)$$

Using  $|a^T b| \leq \|a\| \|b\|$  (Cauchy-Schwarz inequality) and the fact that  $s(x)^T \text{sign}(s(x)) = \|s(x)\|$ , (6.42) can be rewritten as

$$\dot{V} \leq \|s(x)\| \|S(\hat{F} - F)\| - K\|s(x)\| \quad (6.43)$$

For a given bound on the estimation error,  $\|S(\hat{F} - F)\| < \delta$ , one obtains

$$\dot{V} \leq -(K - \delta)\|s(x)\| \quad (6.44)$$

Selecting  $K = \gamma + \delta$ ,  $\gamma > 0$ , it follows that

$$\dot{V} \leq -\gamma\|s(x)\| \quad (6.45)$$

Since  $\dot{V}$  is negative definite, the closed-loop system is globally asymptotically stable.

GPR based system models or equivalent control estimations create the following opportunities for the controller:

- If all the nonlinearities are estimated using GPR models, then online prediction of the estimation error bound ( $\hat{\delta}$ ) can be obtained directly. GPR models of the airpath components provide their variance estimates (e.g.  $\hat{\sigma}_F \in R^N$  for  $N$  components) as an output, and these values can be utilized for determining online values of the error bound (e.g.  $\hat{\delta} = 3\|\hat{\sigma}_F\|$ ). But this type of error bound estimation involves more than one GPR model, so variances will be accumulated.
- Alternatively, static part of the equivalent control ( $u_{eqs} = (SB)^{-1}(-SF)$ ) can be estimated with a GPR model. For the design presented above,  $SB = I$ , the estimation error bound can be rewritten as

$$\|(u_{eqs} - \hat{u}_{eqs})\| \leq \delta \quad (6.46)$$

so that standard deviation outputs of the GPR models ( $\hat{\sigma}_{u_{eqs}} \in R^2$ ) can be used for determining the error bound (e.g.  $\hat{\delta} = 3\|\hat{\sigma}_{u_{eqs}}\|$ ).

Accurate prediction of the error bound enables selection of just enough amplitude of the control gain  $K = \hat{\delta} + \gamma$ . Therefore actuator effort can be minimized.

# Chapter 7

## Results and Discussions

Proposed modeling and control approaches are trained and validated in various environments. Data driven disturbance observer based discrete time sliding mode control is implemented to the serial level controller and engine hardware. Part of the Gaussian process modeling is validated with real data. Gaussian process regression based modeling and control methods are implemented on the previously validated engine models. These models are based on simplified physical equations and they are calibrated with respect to a certain engine hardware in their original development. Details of the models, test environments and controller hardware are presented in the following subsections. Training, validation and controller performance results are given in detail after the preliminary information on the data sources.

### 7.1 Engine ECU Implementation

Model based software development is used in the implementation of the algorithms. Developed embedded control algorithms are implemented in two stages. First proof of concept is demonstrated with the prototype software tools. Specifically, in this study ETAS-Ehooks is used. All models are developed via MATLAB-Simulink using specialized libraries for the target environment. Functional by-pass is used

for implementation of new algorithms instead of existing ones. Final implementation of the models are done with software sharing interfaces between OTOSAN and BOSCH using related Simulink libraries and ETAS-ISOLAR toolchain. Developed software is integrated to serial level software; so the final implementation steps are the same as serial level software implementation process. So, the implemented algorithms are validated for resource consumption and feasibility aspects.

## 7.2 Engine Simulation Environments

Two types of engine models are used in this thesis. The first one is the OTOSAN in-house engine model which is developed for Hardware in the Loop (HIL) tests for the Ecotorq engines. The second one is the open-source engine model released by the Linkoping Vehicular System Laboratory. Both models are developed for heavy duty diesel engines. Latter one is validated on the Scania 13L diesel engines and the first one is validated on Ford-OTOSAN 12.7L diesel engines. Both models are mean value engine models (MVEM). A mean value model deals with average values of in cylinder events; therefore intake and exhaust pulsations or crank angle domain events are out of their scope.

### 7.2.1 OTOSAN Engine Model

This model is an extended form of the model presented in [32], [79]. Actuator dynamics and combustion modeling are the main differences of the OTOSAN engine model structure from the cited literature. Block diagram of the model is depicted in Fig. 7.1 and details of the functions and their training can be found in [80]. This model is first tuned for each component (i.e. turbine, compressor, valve...) and the overall engine model is then fitted to reference data. Model training required both transient and steady state measurements from the engine dynamometer tests.

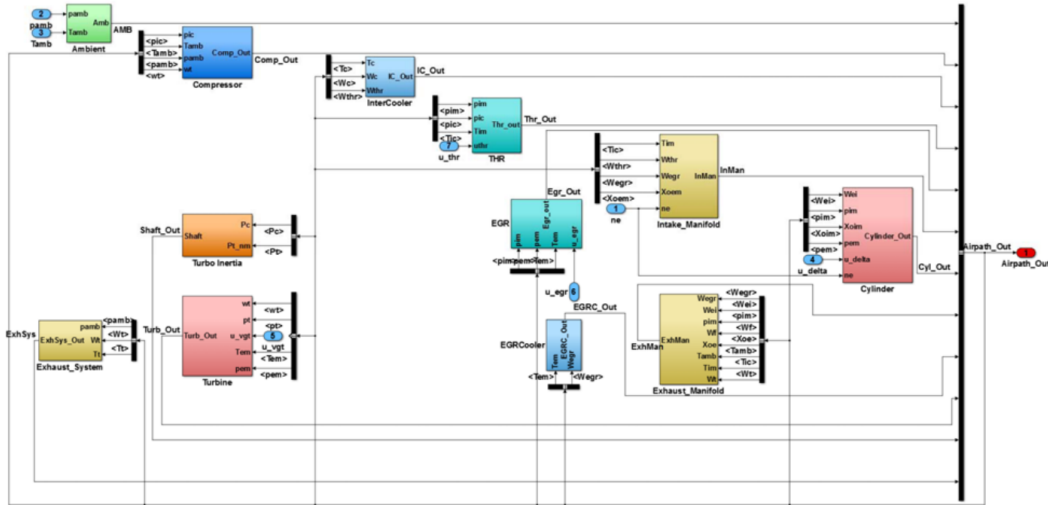


FIGURE 7.1: OTOSAN Engine Model Block Diagram

After this two step training, the error margin in terms of mean absolute relative error,  $\bar{e}_{rel}$  (similar to normalized mean squared error) is less than 10%. This model is used for engine control and modeling simulations with EGR and VGT hardware. Since parameters of the model and unpublished details are Ford-OTOSAN proprietary, the open source model which is described below is also used for further validation and publications.

## 7.2.2 Linkoping Engine Model

There are two open-source available diesel engine models in Linkoping vehicular systems laboratory website ([www.fs.isy.liu.se/Software/](http://www.fs.isy.liu.se/Software/)). Details of the original model are presented in [32], [79] and used for controller development studies. This first model is Simulink based simplified physical model and it is updated recently and validated with real engine data [98]. The latter model is generated with extensive data including simulation results from higher fidelity gas dynamics analysis tools, transient and steady real engine tests. It is used in this thesis and it is reported in [98] that the maximum of its output errors is  $\bar{e}_{rel} < 8\%$ . The model simulates a Scania 12.7 liter heavy-duty engine with throttle and waste-gate (WG) turbine. Typically this type of engines have MAP sensor, throttle and WG position sensor, and engine speed sensor. Turbine control hardware is different

from OTOSAN model. Hardware configuration flexibility claim of the proposed methods are demonstrated with application on both OTOSAN and Linkoping models.

### 7.3 Engine Testing

Ecotorq 12.7L is a heavy duty diesel engine developed by Ford-OTOSAN in Turkey for on road transportation and it was introduced in 2016. Its target vehicles are Ford Cargo and F-MAX. E6 variant of this engine has common-rail diesel injection system with maximum rail pressure capability of 250 Bar. Its airpath is composed of turbocharger with VGT, intercooler, throttle valve, cooled EGR as shown in Fig. 7.2. Its compression ratio is 17. This engine has power variants for 420-500 PS.

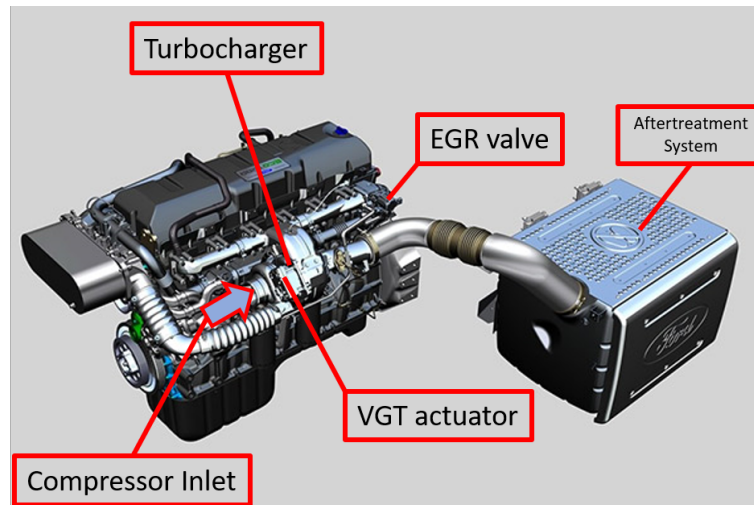


FIGURE 7.2: Ecotorq E6 engine and aftertreatment system

A dynamometer is a load measurement device in general. However, in automotive, this word is used for load simulation and measurement systems for vehicles or engines. Dynamometer data which are used in this thesis are taken from Ford-OTOSAN Golcuk test cells. Test cell is composed of all external instrumentations, environmental conditions control systems, data acquisition and load control assembly. Active dynamometers are used in this study and they are capable of delivering

both positive and negative torques. The engine dynamometer setup is depicted in Fig. 7.3. In order to simulate the vehicle behaviour, engine dynamometer creates resistance torque.

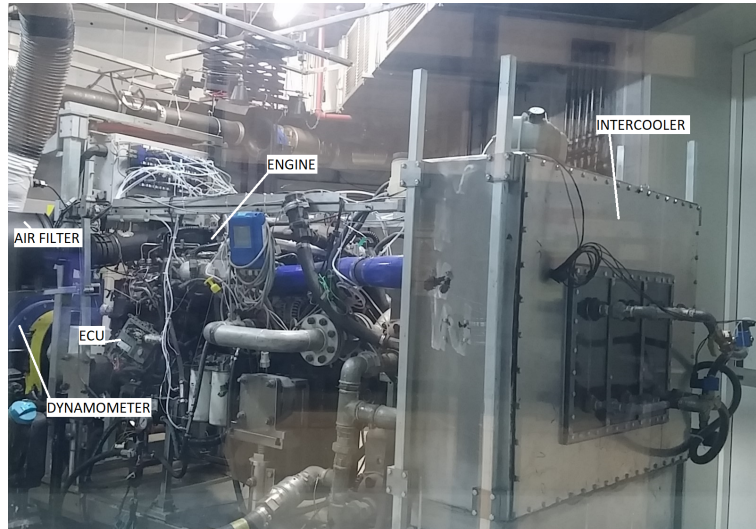


FIGURE 7.3: Test Setup

Heavy duty diesel engines are homologated with the standard test cycle WHTC on engine dynamometers. The test cycle is defined in terms of speed and torque trajectories. These two trajectories are controlled via test cell computer. AVL test cell control system is used for the experiments. Desired torque is controlled via engine accelerator pedal position and the dynamometer unit (electrical motor/generator) controls the desired speed.

## 7.4 Identification Results

Designed data driven disturbance observer requires identification of the airpath. System identification results based on simulation data and real engine dynamometer data are presented in this section.

### 7.4.1 OTOSAN Engine Model Implementation

Preliminary feasibility analysis is executed on OTOSAN engine model. This is done for only MAF to EGR channel. The inputs-output scheme used for identification is depicted in Fig. 7.4. For the specific model used in the study, all inputs

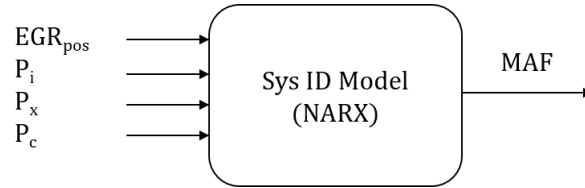


FIGURE 7.4: EGR Model inputs and output

have 5 past values and no output term is added to regressors for both linear and nonlinear part. 5 sigmoid units are used for modeling nonlinear dynamics. Model training best fit value is 82% and validation on the WHTC cycle is 70% as shown in Fig. 7.5.

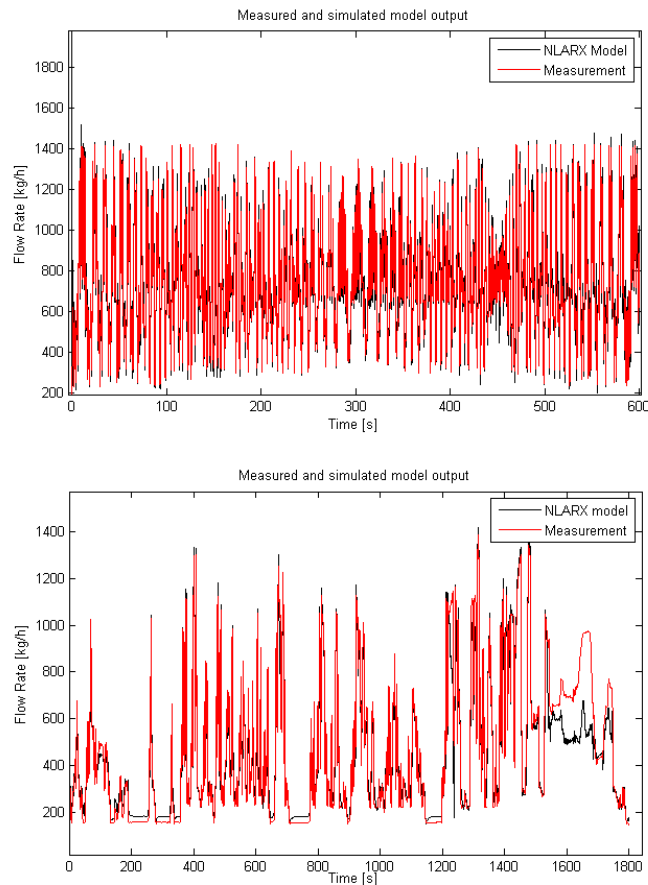


FIGURE 7.5: Training (Top) and Validation (Bottom) Results

## 7.4.2 Real Engine Implementation

Chirp signals are used for training both MAF and MAP channels. Model orders and delays are chosen as  $n_a = 0$  for both channels,  $n_b$  is [5 5 5 5] for MAF and [5 5 1] for MAP, and  $n_k = [1 1 1]$  for both channels. Training fit value of MAF channel is 81%, and measured and modelled signals are shown in Fig. 7.6.

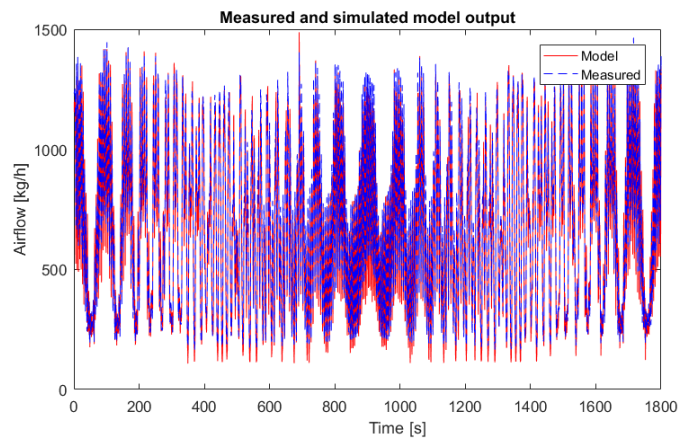


FIGURE 7.6: MAF training test overall

Validation of the models are done with the WHTC test. Best fit value of 80% is achieved in the validation test. Signal traces are depicted in Fig. 7.7.

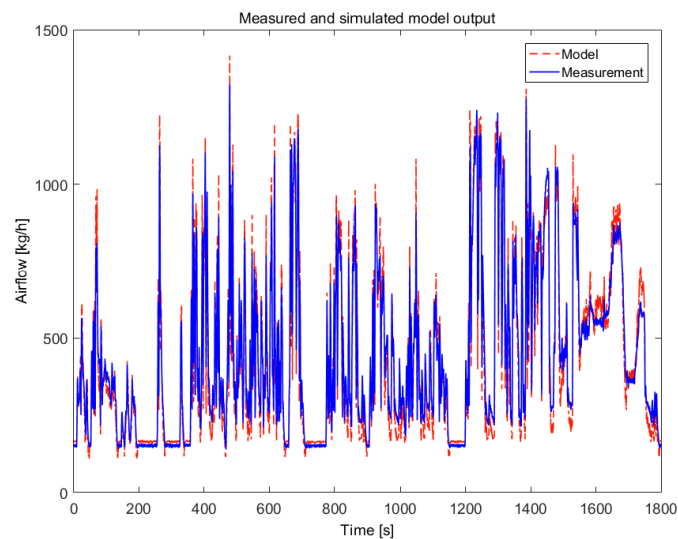


FIGURE 7.7: MAF validation test overall

Similar to the MAF channel, the same tests are used for MAP modeling and training fit accuracy of 78% is attained. Model and measurement signals are depicted in Fig. 7.8. Contrary to the MAF model, intermittent peaks are observed in this model.

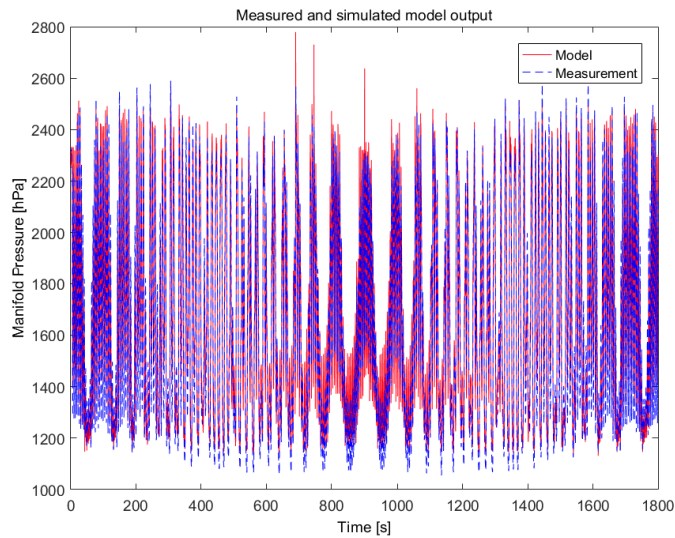


FIGURE 7.8: MAP training test overall

WHTC fit of the MAP model is 77%; but as can be seen from Fig. 7.9, model response is not as aggressive as in the training test. This difference is expected to be a result of the excitation of a singular mode in the training set which includes wide combination of input amplitudes.

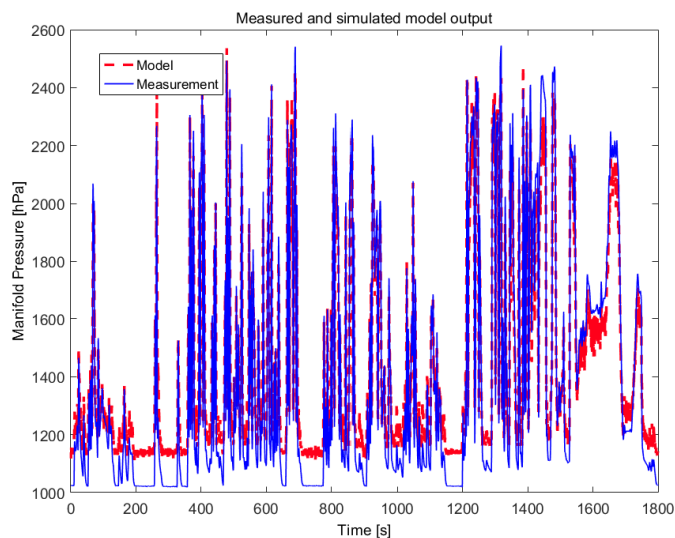


FIGURE 7.9: MAP validation test overall

Linear and nonlinear parts of the identification models are examined first and inverse model results are shared afterwards. Proposed disturbance observer utilizes only the linear part of the models; therefore representation capability of the linear part is an important factor on DOB performance. Linear and nonlinear parts are depicted in Figs. 7.10 and 7.11 for a selected interval (from 760 sec to 860 sec) of 1800 seconds WHTC.

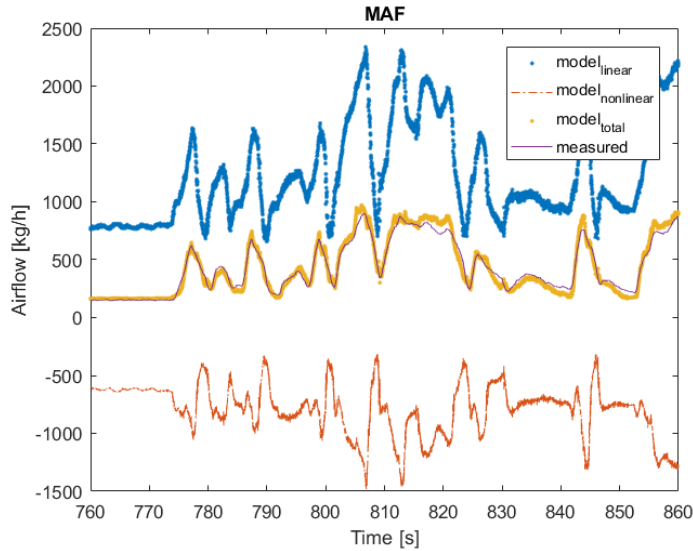


FIGURE 7.10: MAF model contributions

A 100 seconds transient section is selected for the representation of the linear and nonlinear dynamics. Significant nonlinear contributions are evident from these figures. Variations of linear and nonlinear model outputs are compared for MAF and MAP channels. This calculation indicates that MAF has higher nonlinearity with this modeling approach (i.e.  $var(MAF_{nonlinear})/var(MAF_{linear}) = 0.20$ ) whereas  $var(MAP_{nonlinear})/var(MAP_{linear}) = 0.16$  ).

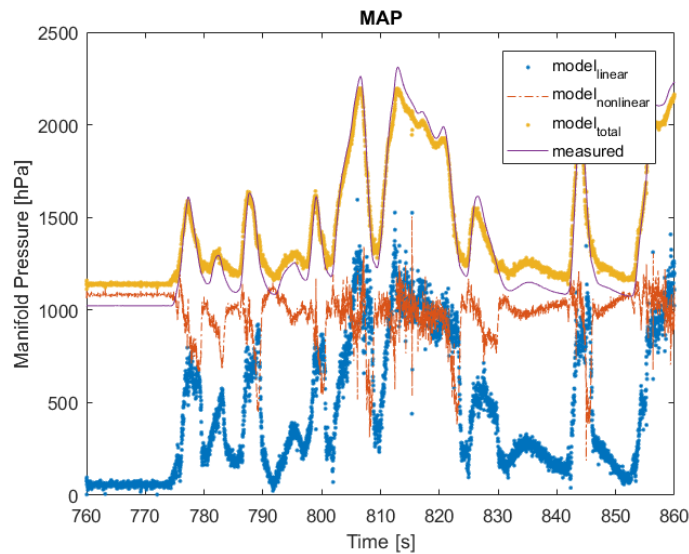


FIGURE 7.11: MAP model contributions

Inverse linear models are compared with the current commercial feedforward structures. Commercial software utilizes a speed torque table based feedforward values for VGT and a simplified physical model based feedforward for EGR. Proposed linear inverse VGT model output, commercial feedforward values and the proposed controlled valve position are presented in Fig. 7.12. Same information is depicted in Fig. 7.13 for VGT channel. Model based feedforward for the EGR channel is very close to the control signal. But inverse model has a similar dynamic with a slowly varying offset. VGT inverse model is more responsive to the trajectory changes with respect to the legacy feedforward term.

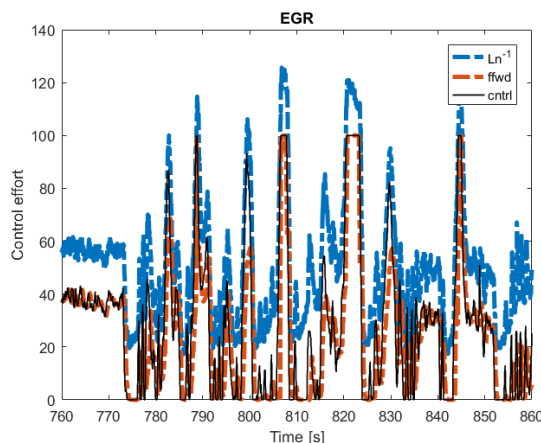


FIGURE 7.12: Feedforward and inverse model comparison for EGR

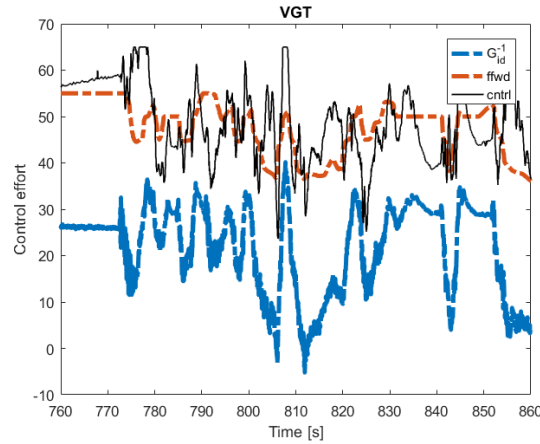


FIGURE 7.13: Feedforward and inverse model comparison for VGT

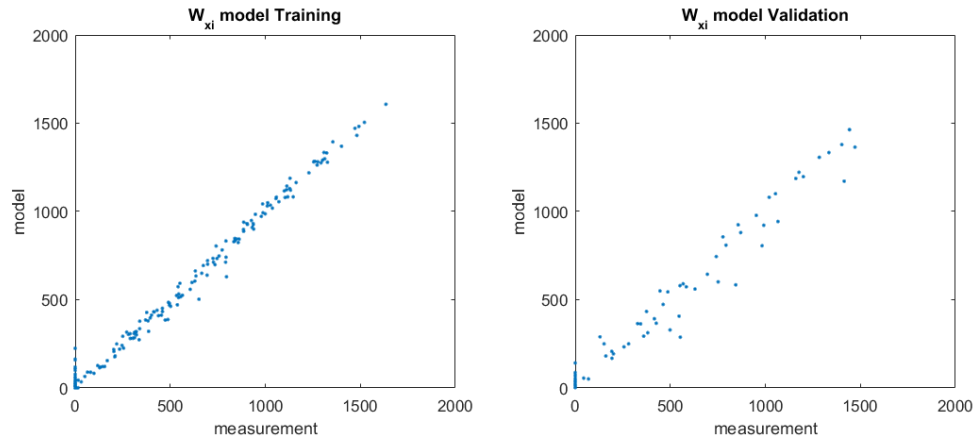
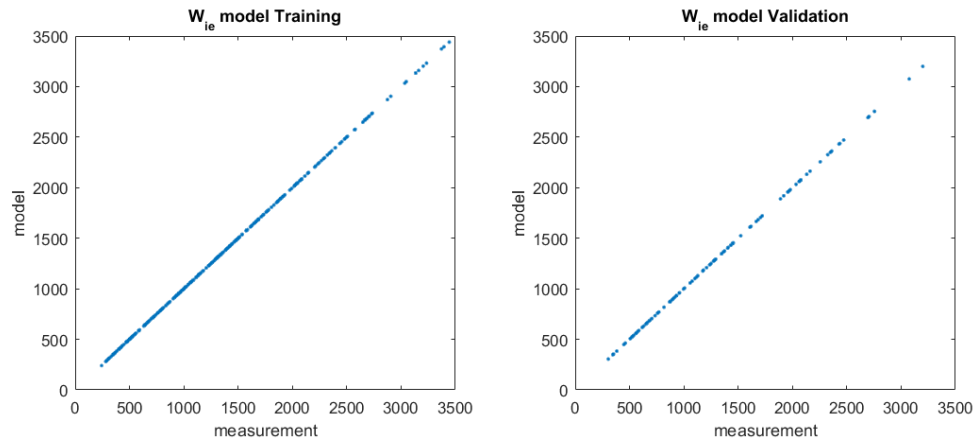
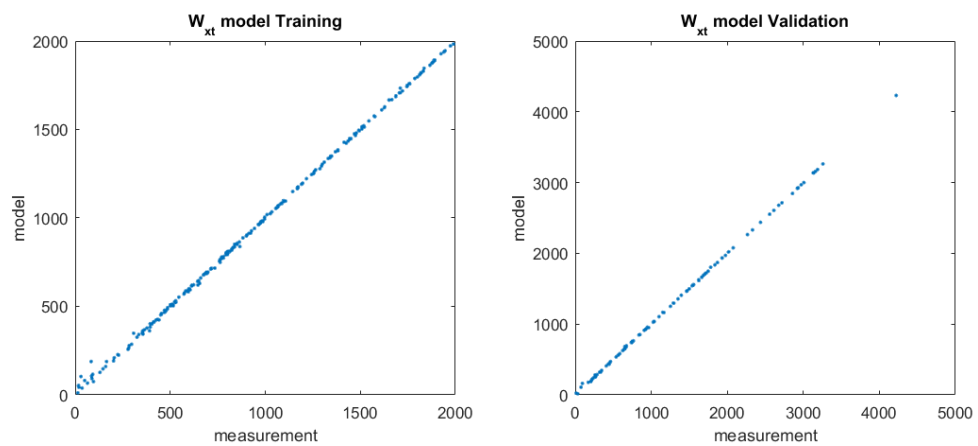
## 7.5 GPR Modeling Results

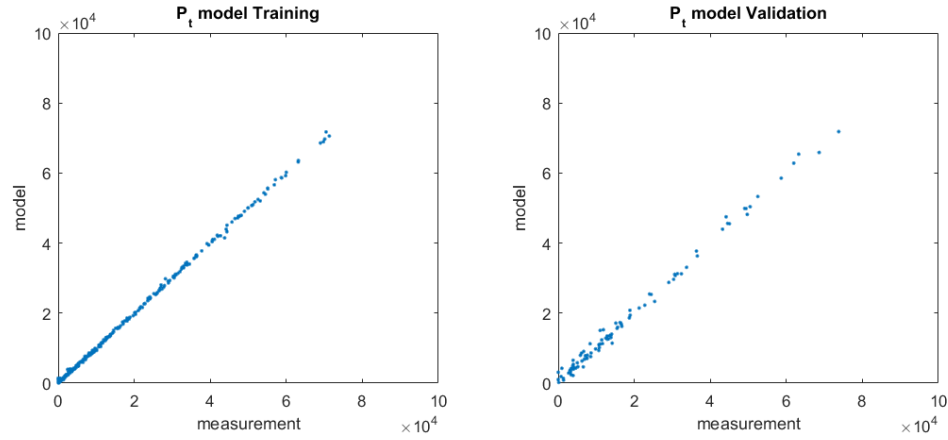
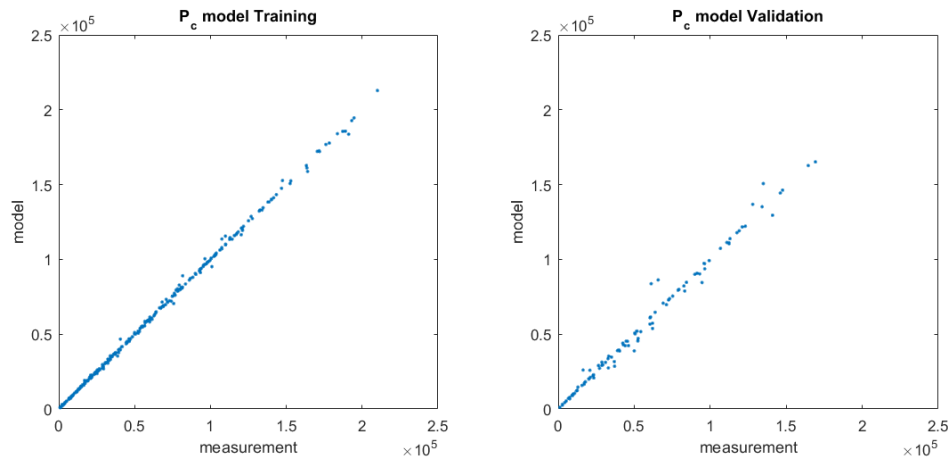
Results of the airpath component modeling and feedforward control studies are presented in this section. The same modeling methodologies described before are applied to the different environments (i.e. OTOSAN Model, Linkoping Model and Real Engine). The following subsections are organized with respect to the environment and the model type.

### 7.5.1 OTOSAN Engine Model

#### 7.5.1.1 Airpath Components

Selected airpath model has 5 main parts namely, compressor, turbine, engine cylinders, EGR line and turbine inlet nozzle. Outputs of these subassemblies are represented with  $P_c, P_t, W_{ie}, W_{xi}, W_{xt}$ . For each component, a Latin-hypercube space-filling experiment is designed in the feasible input limits, and DoE is designed with the minimum number of data points that satisfies  $R^2 > 0.95$  on the validation data set. Created space-filling data set is shared as 2/3 for training and 1/3 for validation. For each model, validation plots are presented in Fig. 7.14 to Fig. 7.18. Their corresponding  $R^2$  values are provided under the plots.

FIGURE 7.14:  $W_{xi}$  validation plot  $R^2 = 0.95$ FIGURE 7.15:  $W_{ie}$  validation plot  $R^2 = 0.97$ FIGURE 7.16:  $W_{xt}$  validation plot  $R^2 = 0.98$

FIGURE 7.17:  $P_t$  validation plot  $R^2 = 0.99$ FIGURE 7.18:  $P_c$  validation plot  $R^2 = 0.98$ 

All models are obtained with the number of points less than 800. Gaussian process (GP) models with these number of elements can be embedded into modern engine control units such as Bosch MD-1 generation.

### 7.5.1.2 Feedforward

Total number of 179 training samples are selected for VGT and 1252 points are left for validation. EGR modeling required more training data (i.e. 312 samples for training and 1164 samples for validation) yet resulted in lower accuracy than the VGT inverse model. Model training is done with fitrgp function in MATLAB. Validation results for VGT and EGR valve position estimations are depicted in Fig. 7.19 and Fig. 7.20, respectively.

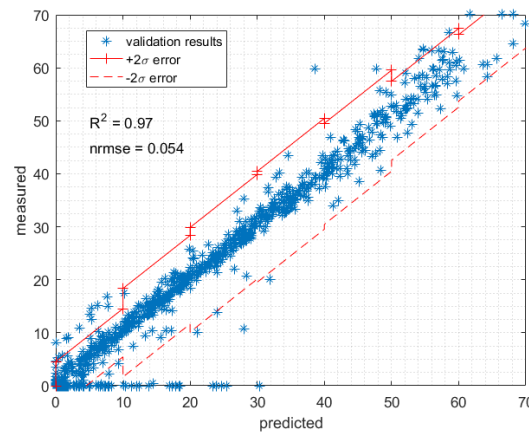


FIGURE 7.19: Validation Fit Results for VGT with 95% validation confidence regions

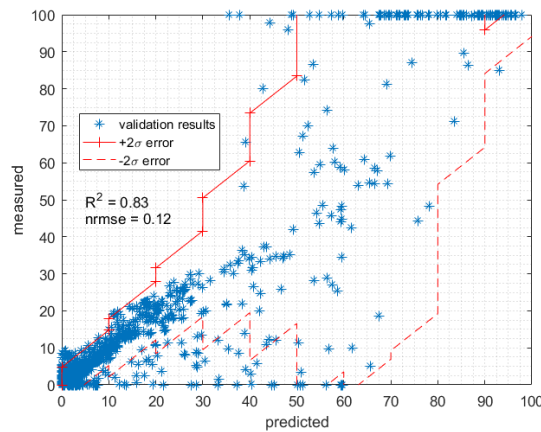


FIGURE 7.20: Validation Fit Results for EGR with 95% validation confidence regions

Although less training samples are used for VGT inverse model fitting (feedforward for MAP control), its validation accuracy is higher than EGR inverse model (feedforward for MAF control). Since our covariance function assumes smoothness on the EGR, accuracy is suffered from the singular behavior of the inverse plant when pressure difference is near zero as shown in Figure 7.21.

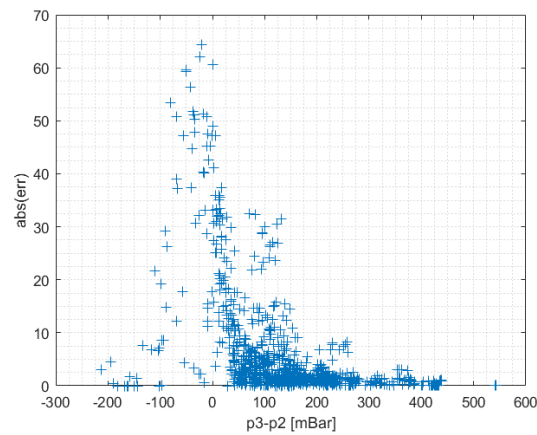


FIGURE 7.21: EGR Model Error vs. Pressure Difference on the EGR Line

## 7.5.2 Linkoping Engine Model

The latest Linkoping engine model (LiEM) is based on a no EGR waste-gate and throttle engine. Without EGR line, airpath simplifies in a great deal and this is also observed in the following model accuracies. In this modeling study, 1000 point Lattice hypercube type DoE is used for model inputs. This type of engine experiments are implemented during engine development process for emissions modeling; so using this data for control can be accepted as virtually free. Some of the input combinations resulted in infeasible results and they are filtered. Different training and validation sets are selected for respective models. A sample implementation of 496 point DoE is depicted in Fig. 7.22.

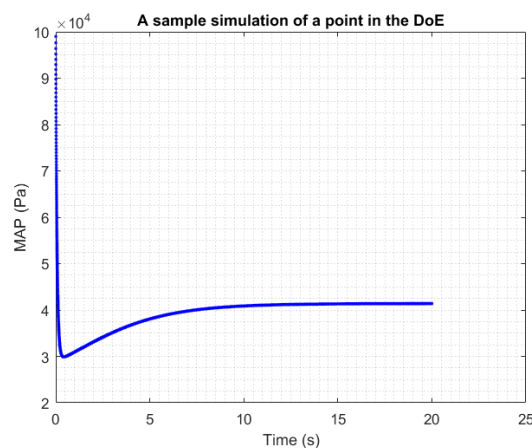


FIGURE 7.22: Manifold absolute pressure vs. time simulation result with LiEM

For each simulation of DoE test points, 20 seconds is waited and the last value is taken for steady state modeling. For this model 10 second is generally enough for settling of the output states with  $1ms$  sampling time.

### 7.5.2.1 Airpath Components

MAF, throttle flow, compressor power, manifold absolute pressure (MAP) are modelled for control development on LiEM. Different inputs and training data size are utilized for these models. Each are presented in the following. Since LiEM assumes constant intake manifold temperature, mass air flow (MAF) through the cylinder is modelled with engine speed and manifold pressure inputs. Engine flow modeling results are depicted in Fig. 7.23.

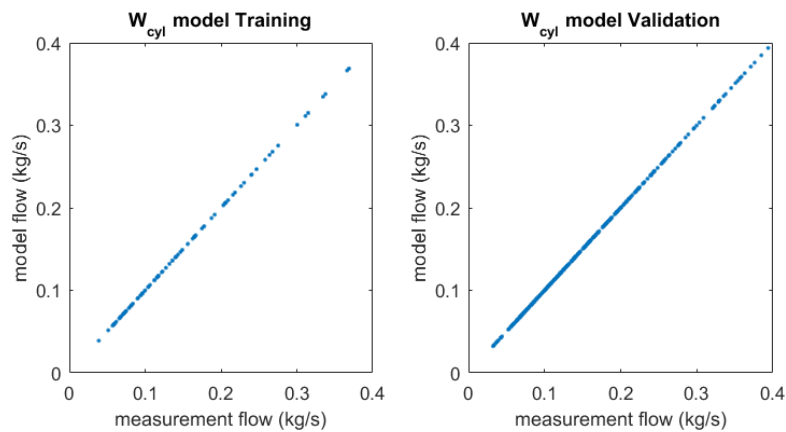


FIGURE 7.23: MAF modeling results

Engine cylinder flow is modelled with 99 points and validated on remaining 397 points. Since the models for this flow are generally accurate, a non-EGR engine does not utilize MAF sensors. Both of the training and validation  $R^2 \approx 1$ , and their *nrmse* values are 0.0002 and 0.0003, respectively. Mass flow through the throttle valve is modelled with its upstream and downstream pressure and valve position inputs. Training set consists of 99 points and the rest are left for validation. Training and validation results are depicted in Fig. 7.24 and their *nrmse* values are 0.006 and 0.023, respectively.

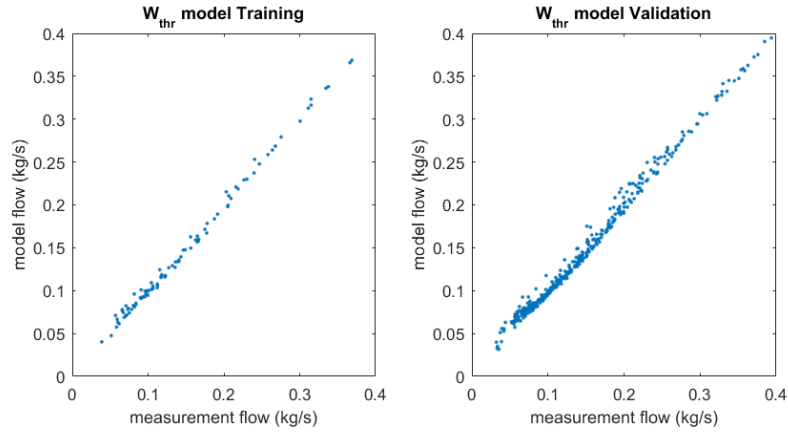


FIGURE 7.24: Throttle flow modeling results

Similarly, compressor power is modelled with 99 training points and its inputs are MAP, throttle position and engine speed. Results are plotted in Fig. 7.25 and its *nrmse* values for training and validation are 0.007 and 0.027, respectively.

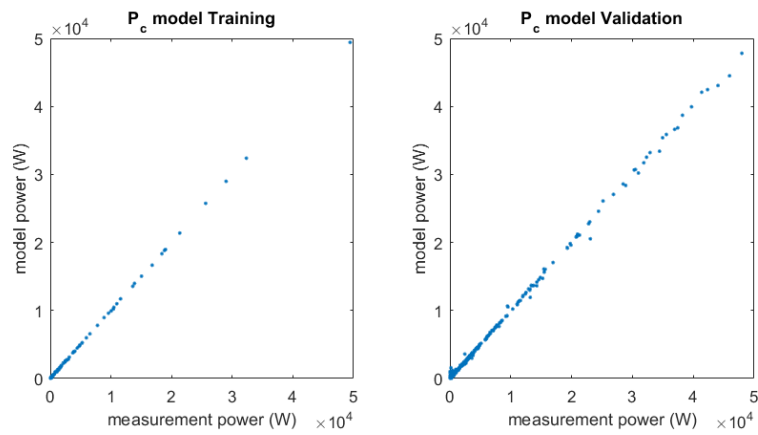


FIGURE 7.25: Compressor power modeling results

Manifold absolute pressure, which is also measurable via its sensor, is modelled with 99 training points and its inputs are fuel quantity, throttle position, WG position, and engine speed.

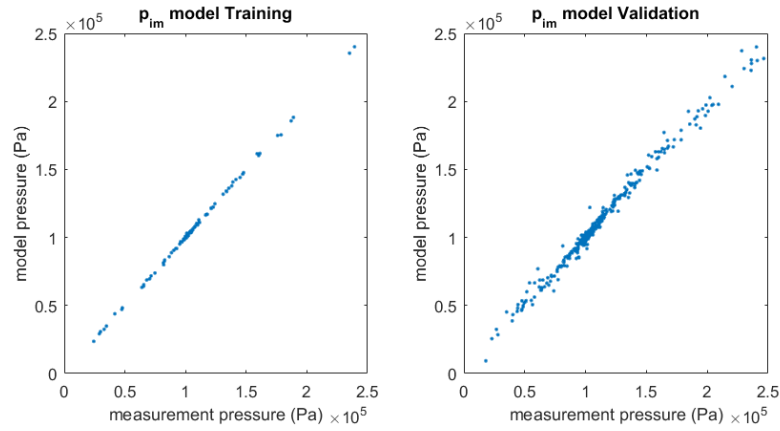


FIGURE 7.26: MAP modeling results

The results are depicted in Fig. 7.26 and their *nrmse* values are 0.024 in training and 0.037 in validation. Compressor outlet pressure or throttle inlet pressure is modelled with throttle position, MAP and MAF inputs. Training data has 99 points and results are depicted in Fig. 7.27. Training and validation *nrmse* values are 0.001 and 0.004.

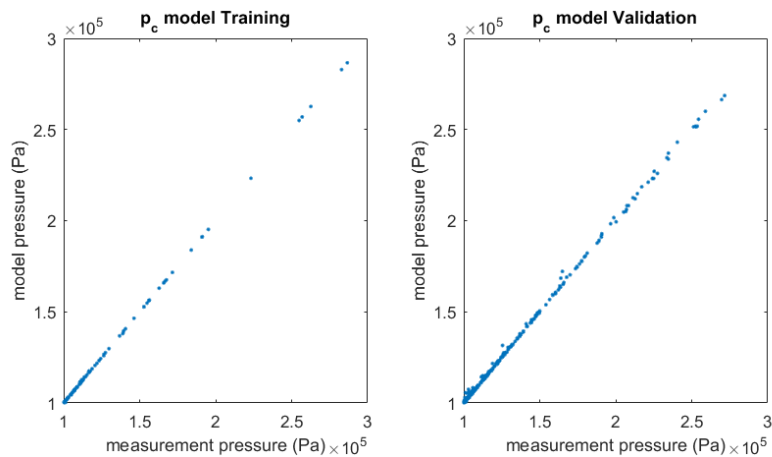


FIGURE 7.27: Compressor outlet pressure modeling results

Exhaust manifold temperature is required for feedforward modeling for LiEM implementation. It is modelled using MAP, MAF, injected fuel quantity inputs, and 245 points are used for the training set.

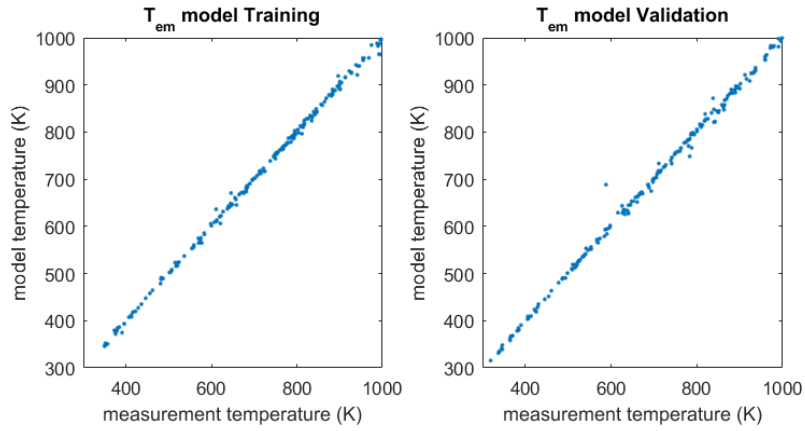


FIGURE 7.28: Exhaust manifold temperature modeling results

Exhaust manifold temperature training and validation results are depicted in Fig. 7.28. The *nrmse* error metrics are 0.006 for training and 0.009 for validation.

### 7.5.2.2 Feedforward

Similar to component models, waste-gate and throttle feedforward are estimated with GPR models using the same data set. Throttle inverse model is built with WG position, compressor outlet pressure, fuel injection quantity and engine speed inputs. Training set included 295 points and its results and validation variance estimation are depicted in Fig. 7.29.

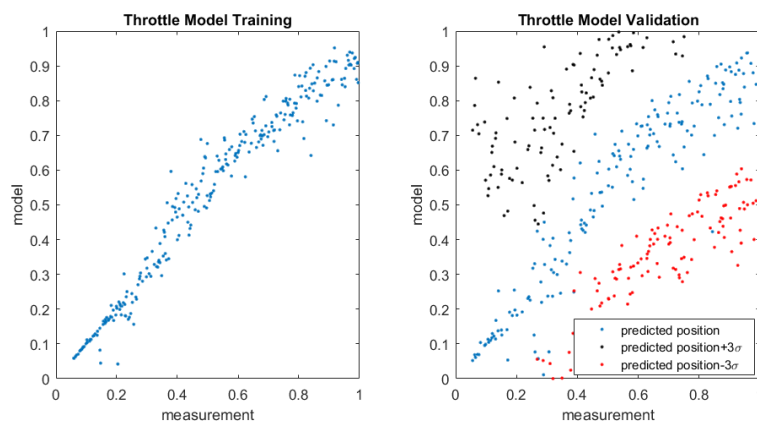


FIGURE 7.29: Inverse throttle model results

Throttle model training and validation *nrmse* values are 0.092 and 0.139, respectively.

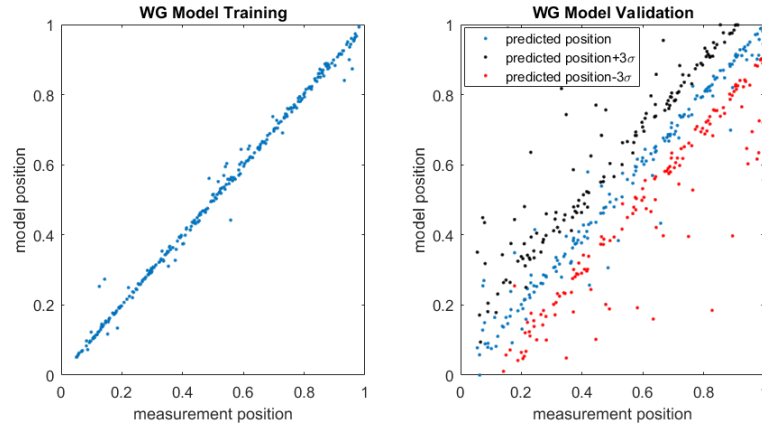


FIGURE 7.30: Inverse WG model results

Inverse waste-gate model is constructed with throttle position, MAP, fuel injection quantity and engine speed inputs. Similar to the throttle, training set included 295 points and its results and validation variance estimation are illustrated in Fig. 7.30. WG model training and validation *nrmse* values are 0.017 and 0.043, respectively.

## 7.6 Disturbance Observer Based Control Results

### 7.6.1 OTOSAN Engine Model Implementation

Controller performance evaluation is done via acceleration pedal position steps (load step). MAF setpoints are interpolated from desired value maps and they are limited with maximum possible flow to create feasible setpoints. In this maneuver, good tracking behaviour is achieved when there is no external disturbance (Fig. 7.31) . External disturbances in the form of sinusoidal and pulse waveforms are then applied to the EGR valve position and the system is simulated. Applied disturbances and their estimated values by DOB are presented in Figs. 7.32 and 7.33. DOB output may include any real plant behaviour that can not be captured by the nominal inverse plant. It should be noted that only disturbances that are in the bandwidth of the low-pass filter can reliably be estimated. It can be observed from these figures that while sinusoidal disturbance waveform is preserved with

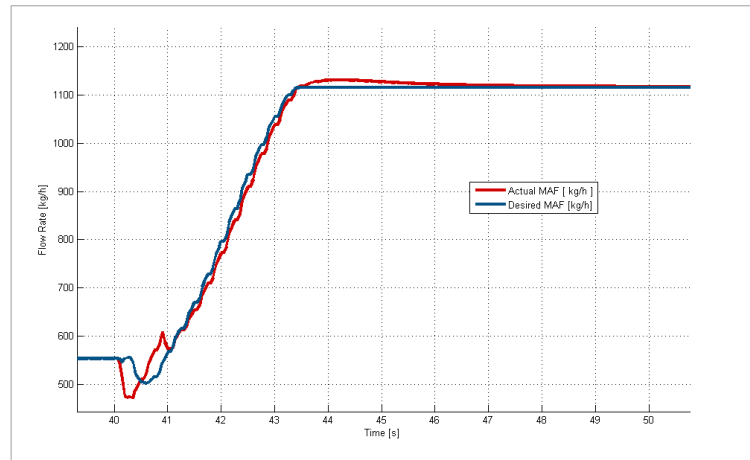


FIGURE 7.31: MAF control result for 20% to 80% load step test

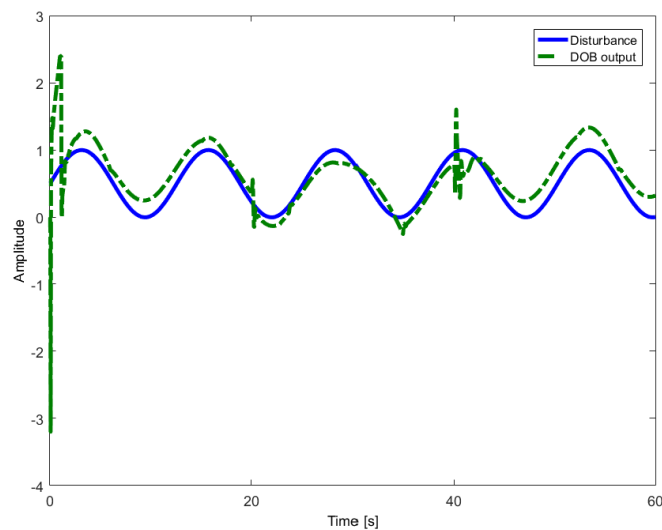


FIGURE 7.32: Sinusoidal disturbance vs. DOB output

only a slight phase shift in the estimation, pulse disturbance is estimated with some significant deterioration in the waveform. Disturbance observer effect in the closed-loop control under sinusoidal disturbance can be seen by comparing results without DOB (Fig. 7.34) and with DOB (Fig. 7.35). Similar to the previous results, DOB improves overshoot and undershoots as can be seen from the difference of the results depicted in Fig. 7.36 and Fig. 7.37. However, for both type of disturbances simulation results provided in Figs. 7.34-7.37 show that using DOB improves the performance of the system.

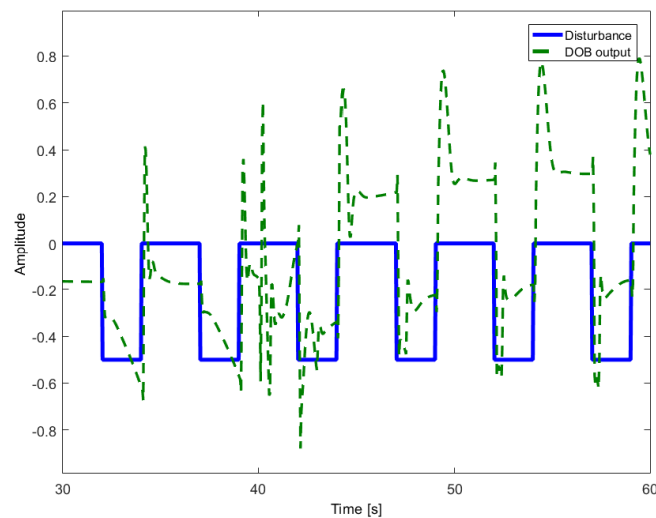


FIGURE 7.33: Pulse array disturbance vs. DOB output

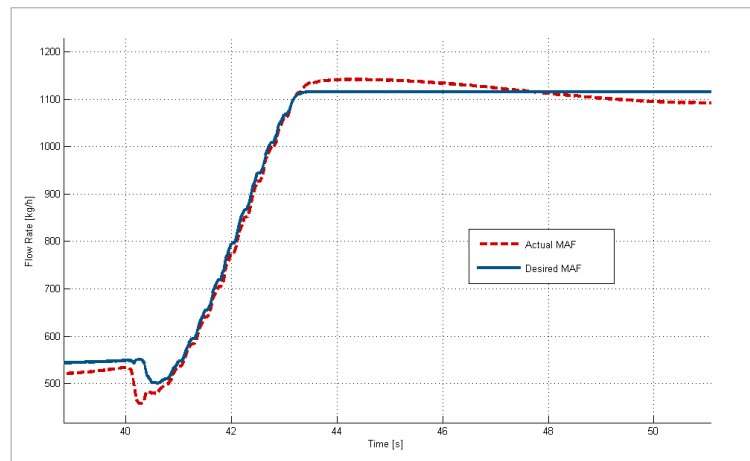


FIGURE 7.34: The step test - sinusoidal disturbance and DOB inactive

## 7.6.2 Real Engine Implementation

Current Ecotorq engine is Eu6 certified and uses a well tuned controller. In order to show performance of the proposed control system, the same speed&torque profile cycle was run back to back in the same engine. Since it is hard to visualize all of the 30 minutes cycle, a 100 sec dynamic part is shown throughout the thesis. Overall performance metrics will be shared at the end of the section.

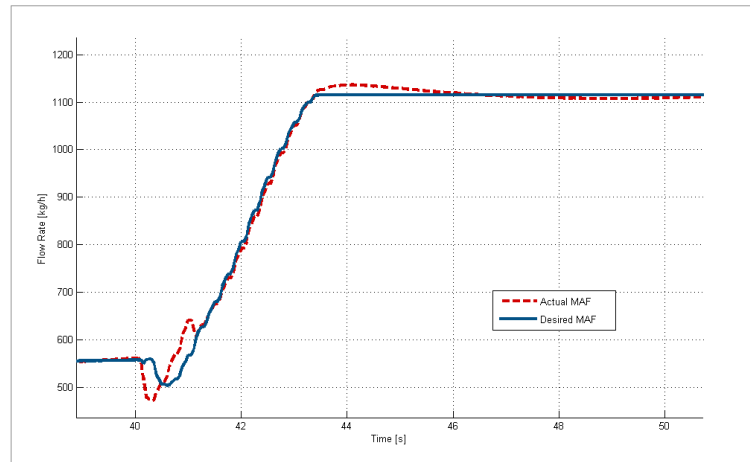


FIGURE 7.35: The step test - sinusoidal disturbance and DOB active

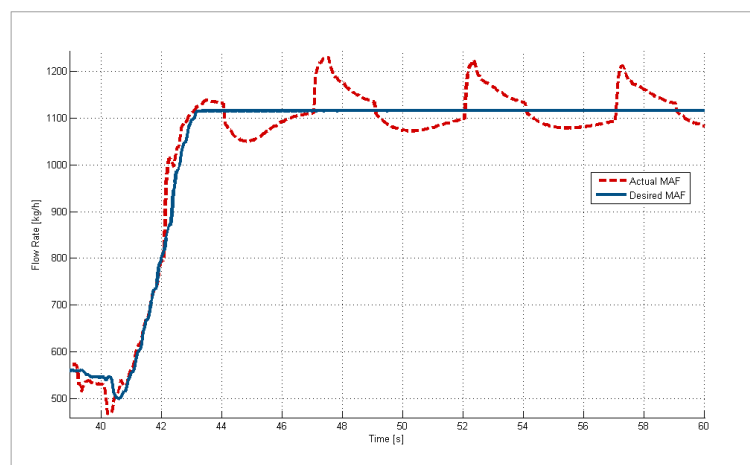


FIGURE 7.36: The step test - pulse disturbance and DOB inactive

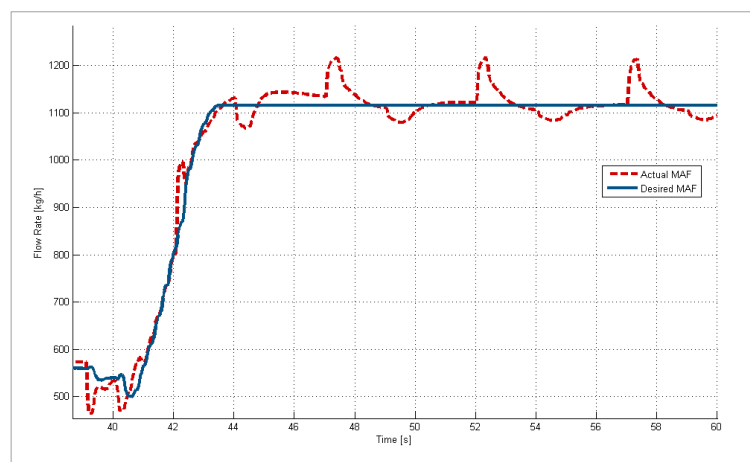


FIGURE 7.37: The step test - pulse disturbance and DOB active

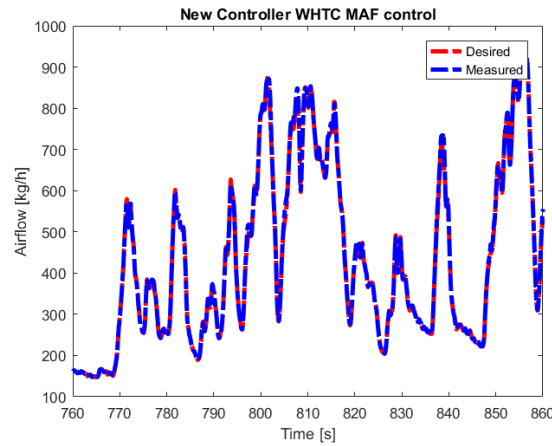


FIGURE 7.38: Proposed MAF controller performance on WHTC

MAF tracking results for the proposed controller is given in Fig. 7.38. Since maximum available airflow is limited with the boost pressure, desired trajectories are not exactly the same with the reference test shown in Fig. 7.39. It is seen from the new controller results in Fig. 7.38 that sharp trajectory changes are followed with the increased performance of the proposed controller with respect to the commercial one.

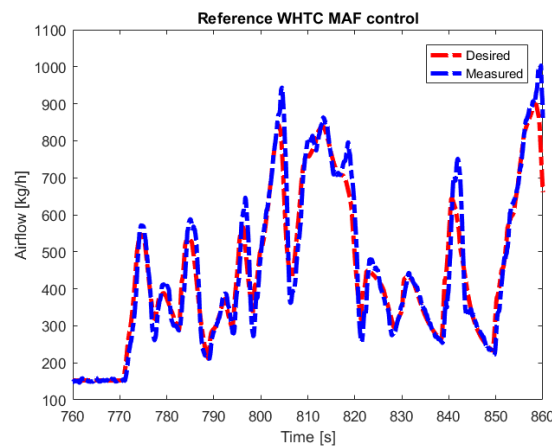


FIGURE 7.39: Commercial MAF controller performance on WHTC

MAF and MAP controls are closely coupled. The sudden changes in the MAF trajectory in Fig. 7.38 is related with MAP control in Fig. 7.40. Proposed control scheme has more aggressive control behaviour with respect to the commercial one. Since MAP is related with the maximum value of the desired MAF value, new

MAP controller helps MAF control to have higher setpoint values and more sudden changes with respect to the commercial control results depicted in Fig. 7.41.

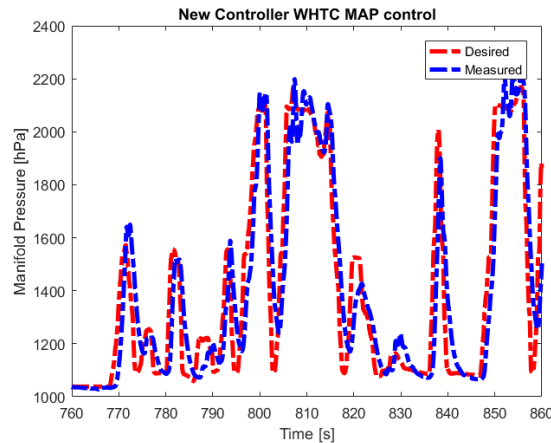


FIGURE 7.40: Proposed MAP controller performance on WHTC

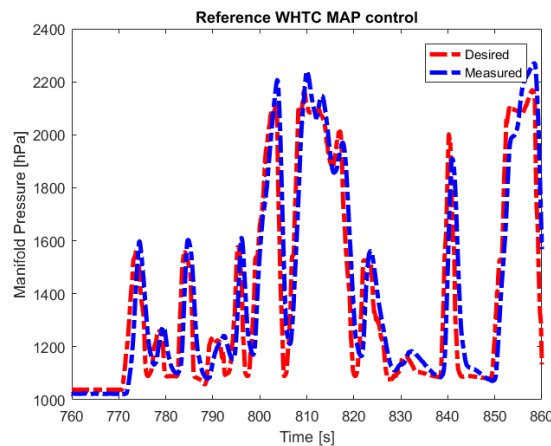


FIGURE 7.41: Commercial MAP controller performance on WHTC

MAF control is achieved with EGR position manipulation. EGR valve inlet pressure is a function of VGT position. On the other hand, VGT flow is strongly correlated with MAF and therefore it is the result of EGR position. So these valves create disturbances for each other. Traditional control structures choose to slow down one of the controllers and use significantly faster control in the other channel. Proposed DOB scheme allows us to use fast valve actions in each channel without deterioration in the other channel. EGR valve positions in Fig. 7.42 show significant more action with respect to the commercial controller valve position demands in Fig. 7.43.

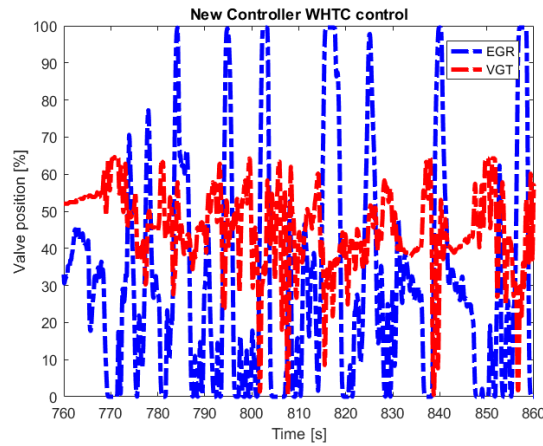


FIGURE 7.42: Proposed controller for EGR valve actuation on WHTC

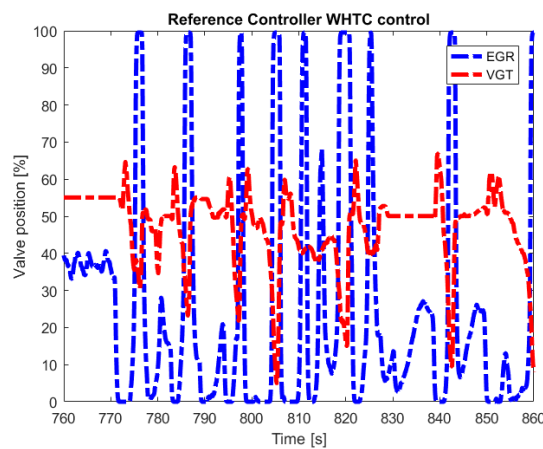


FIGURE 7.43: Commercial controller for EGR valve actuation on WHTC

Figures 7.38-7.43 describe control details for a selected interval of the WHTC. Overall performances are compared with the original map values. These two controllers use the same control setpoint maps but dynamic adaptations are unique. So in order to make a fair comparison, the difference between table values and the sensor readings are defined as the errors. The overall performances for the whole cycle are compared in Table 7.1 where Prop. and Com. denote proposed and commercial controllers. Proposed controllers provide better tracking performance in all metrics. MAP channel performances are close but the proposed controller requires less control effort. However, higher tracking performance of the MAF controller requires more control effort.

TABLE 7.1: MAF &amp; MAP Control Performance Metrics

Metric	Prop.	Com.	Prop.	Com.
	MAF	MAF	MAP	MAP
nRMS Error	0.046	0.056	0.034	0.053
Max Absolute Error	346	343	668	801
RMS Control Effort	41.9	29.8	45.4	45.7
Max Control Effort	99.5	99.5	65.2	69.6

## 7.7 GPR Based Control Results and Discussions

All GPR based control simulations are done on OTOSAN and Linkoping engine models. GPR feedforward with discrete time sliding mode control results are presented first.

### 7.7.1 GPR Feedforward with Discrete Time Sliding Mode Control

Reference conventional controllers for the airpath benchmark are PID controllers for both EGR and VGT with a look-up table based feedforward. Conventional controller (look-up table based feedforward plus PID) performance on the WHTC cycle is presented in Figs. 7.44-7.46.

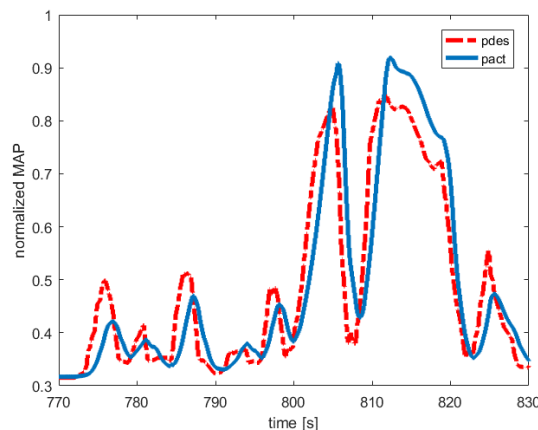


FIGURE 7.44: MAP tracking with look-up FF + PID on a WHTC section

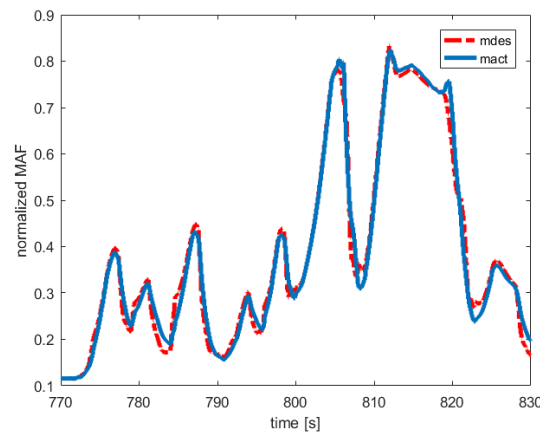


FIGURE 7.45: MAF tracking with look-up FF + PID on a WHTC section

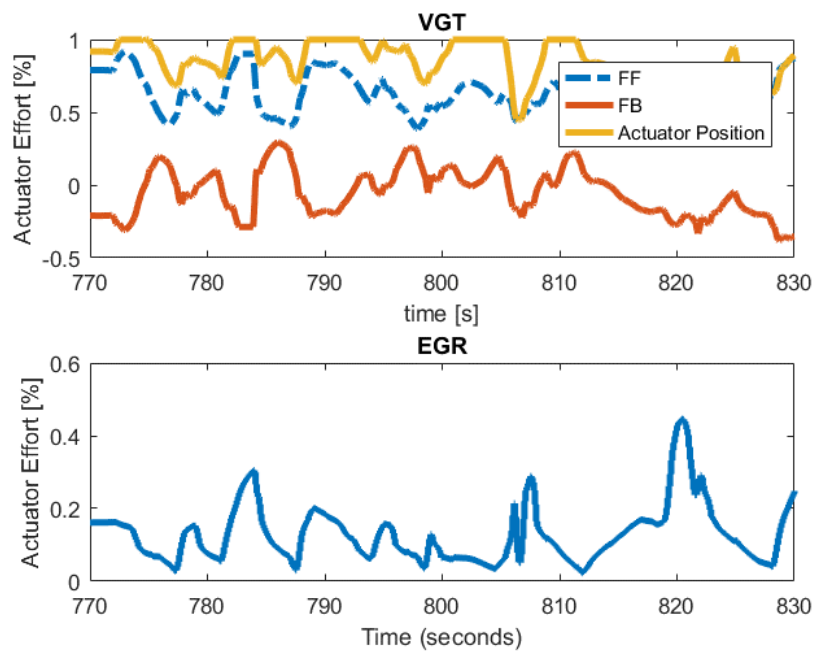


FIGURE 7.46: Actuator efforts with look-up FF + PID on a WHTC section

Performance of the GPR feedforward plus DTSMC controller on the WHTC cycle is presented in Figs. 7.47-7.49. Thanks to the accurate estimation of GPR feedforward model, better tracking results are observed as in Fig. 7.47 and it requires less control effort than the feedback as depicted in Fig. 7.49.

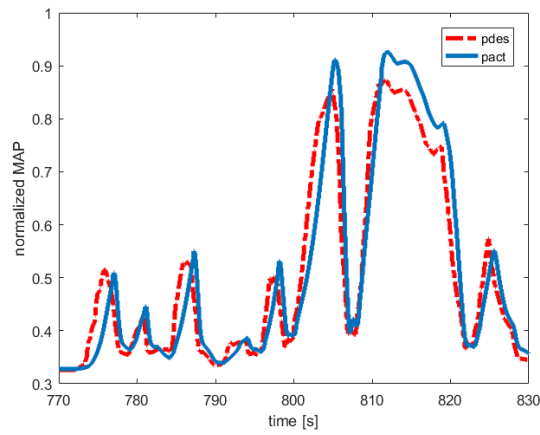


FIGURE 7.47: MAP tracking with GPR FF + DTSMC on a WHTC section

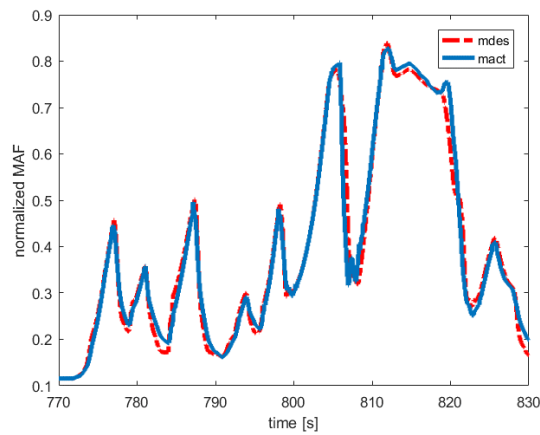


FIGURE 7.48: MAF tracking with GPR FF + DTSMC on a WHTC section

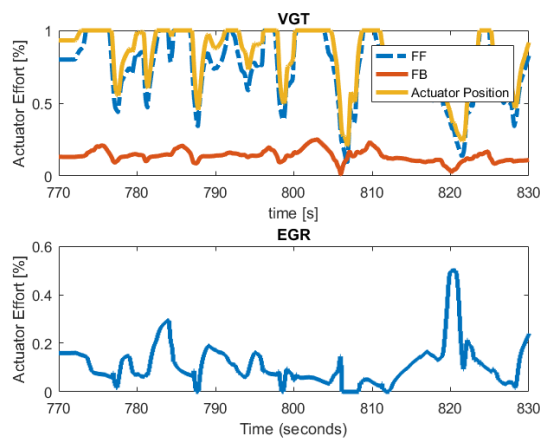


FIGURE 7.49: Actuator efforts with GPR FF + DTSMC on a WHTC section

Overall reference tracking errors of the controllers are evaluated using various metrics on WHTC test cycle which has a duration of 1800 seconds. The performance metrics are presented in Table 7.2.

TABLE 7.2: MAF & MAP Control Performance Metrics

Metric	PID+FF MAF	GPR-FF +DTSMC MAF	PID+FF MAP	GPR-FF +DTSMC MAP
nRMS Error	0.045	0.041	0.080	0.061
Max Absolute Error	478	478	1290	1277
RMS Control Effort	23	18	83	80
Max Control Effort	100	100	100	100

The MAF performance of the conventional approach is significantly less in best fit metric although *nrmse* indicates less significant difference. This difference between the metrics is caused by a few error peaks of the PID controller results in certain intervals of the cycle. Such behavior significantly affects soot formation, thus, SMC controller is superior for airpath control in terms of soot. MAP control performance results show more clear separation in all types of metrics. GPR feedforward achieves this result with limited feedback controller contribution.

### 7.7.2 GPR PI Control

This controller is tested with the same setpoints and the simulation model in the previous subsection. In comparison to the performance depicted in Fig. 7.47, GPR PI control result shown in Fig. 7.50 is superior in terms of MAP tracking error. On the other hand MAF responses in Fig. 7.50 are similar with the response depicted in Fig. 7.48, and VGT actuator positions are more aggressive in Fig. 7.50.

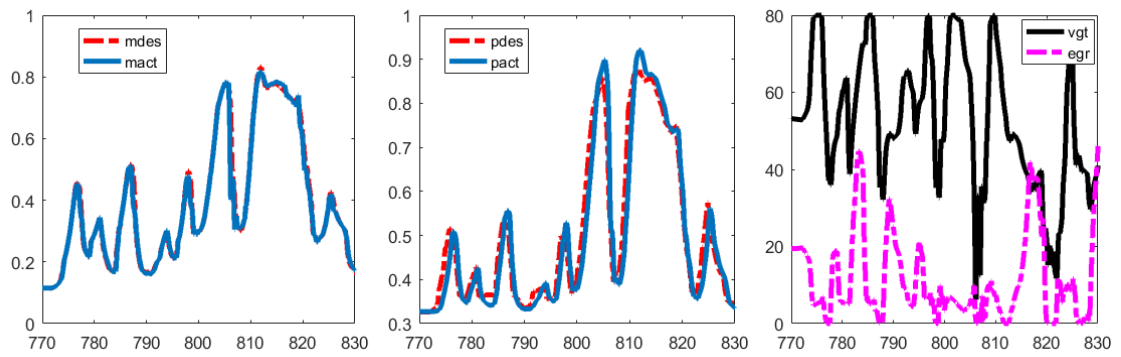


FIGURE 7.50: MAF (left), MAP (middle) tracking and actuator positions (right) at a selected transient section of WHTC

The downside of this controller is its steady state error around certain idle points as depicted in Fig. 7.51. This may require an additional adaptation logic on the desired and actual position model.

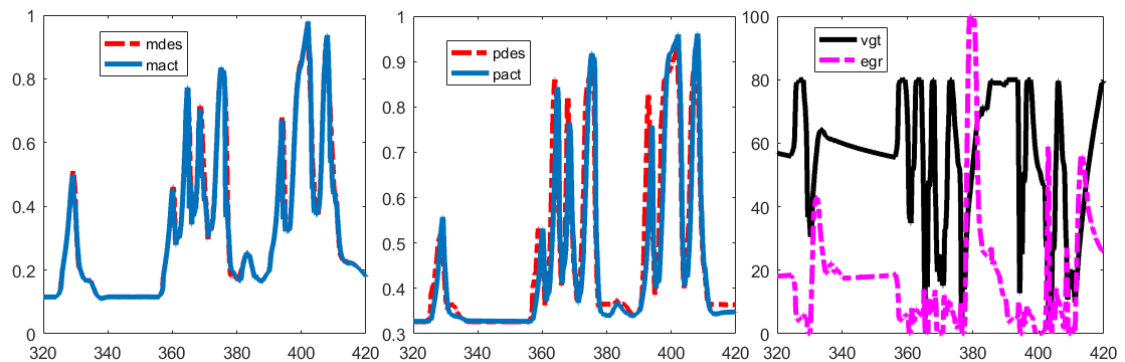


FIGURE 7.51: MAF (left), MAP (middle) tracking and actuator positions (right) at another selected transient section of WHTC

In the overall performance metrics, GPR PI has better performance in all categories as presented in the Table 7.3.

TABLE 7.3: MAF &amp; MAP Control Performance Metrics for GPR-PI and GPR-FF +DTSMC

Metric	GPR-PI	GPR-FF +DTSMC	GPR-PI	GPR-FF +DTSMC
	MAF	MAF	MAP	MAP
nRMS Error	0.041	0.017	0.061	0.040
Max Absolute Error	478	478	1277	1120
RMS Control Effort	18	21	80	79
Max Control Effort	100	100	100	100

### 7.7.3 GPR-FF Saturated Integral Control

GPR feedforward (GPR-FF) saturated integral control is implemented on LiEM model. Compressor outlet pressure ( $p_c$ ) and MAP is controlled with throttle and waste-gate. It is assumed that MAP sensor is available but there is no compressor outlet pressure sensor. Very good responses are obtained with GPR-FF and variance saturated I term application. Its step test accuracy is presented in Fig. 7.52. As can be seen from the figure, variance saturation of I term is very effective against overshoots. Steady state error of MAP in the second step is caused by the error in  $P_{co}$  and since there is no compressor outlet sensor in the assumption, this error is in the acceptable range.

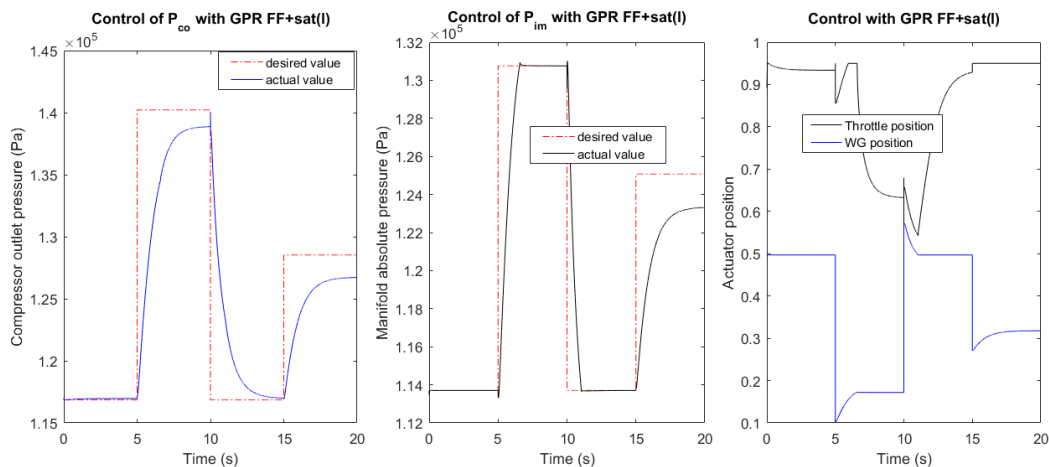


FIGURE 7.52: Compressor outlet pressure and MAP step responses of GPR FF+sat(I)

### 7.7.4 GPR Based Sliding Mode Control

Same tests are conducted with the GPR based SMC for throttle and wastegate control. Although better steady state overall error is achieved severe chatter is observed as seen in Fig. 7.53.

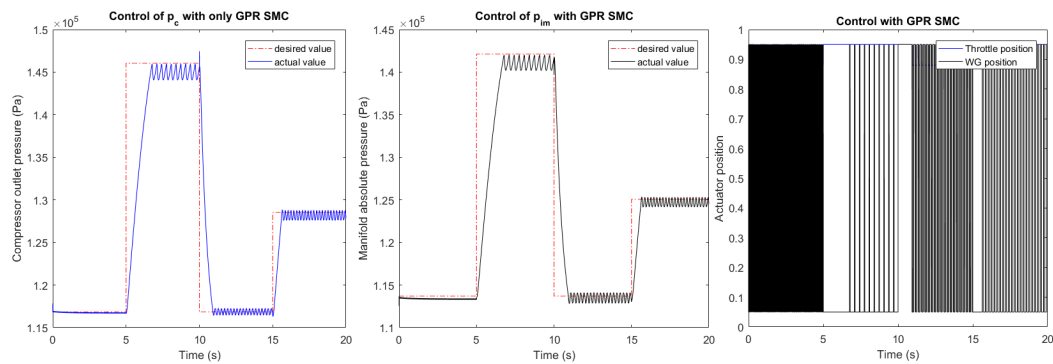


FIGURE 7.53: Compressor outlet pressure and MAP step responses of GPR based SMC

The chatter can be alleviated using boundary layer techniques with the expense of steady state error as depicted in Fig. 7.54.

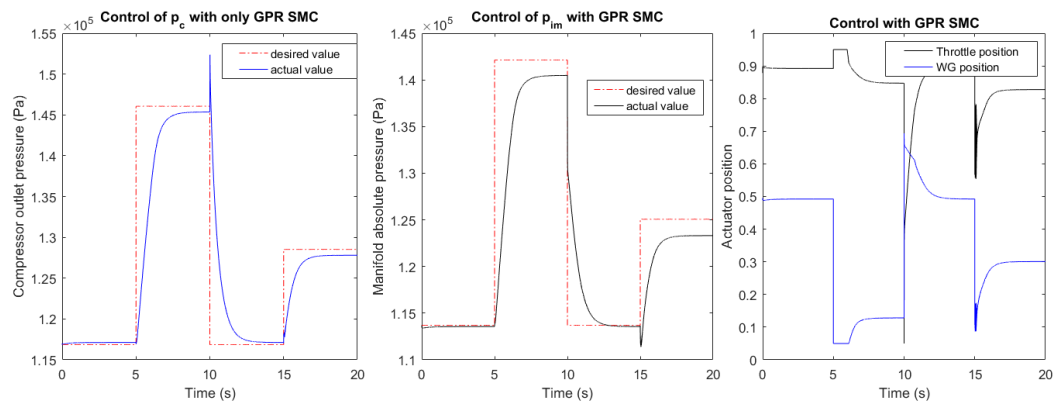


FIGURE 7.54: Compressor outlet pressure and MAP step responses of GPR based SMC

The steady state errors can be diminished with online training of GPR algorithm but it is infeasible for the next generation ECU implementation.

# Chapter 8

## Conclusions

This thesis presents two different solution approaches for flexible and robust control of the diesel engine airpath. Data driven disturbance observer and discrete time sliding mode controller is proposed for available electronic control units. Gaussian process regression based modeling and control approaches are studied for next generation engine control units.

The proposed disturbance observer is based on dynamic identification of the airpath. The experiment is designed for real engine tests. Same identification process is first applied on the physical engine model and than to the real engine at dynamometer test cell. Dynamometer experiments are conducted at Ford OTOSAN Gölcük Test Cells. Identified models have training and validation fit accuracies around 80% and 70% respectively on reference physical models. However, training and validation fit values for the real engine test results are more consistent. Real engine fit results for MAF channel for training and validation tests are 81% and 80%, respectively. MAP channel training accuracy is 78% and validation fit reaches to 77%. This difference between model and real engine is due to simplifications in the physical engines. It is encouraging that the data driven model has higher consistency in real engine implementation. These models are used for the design of data driven disturbance observer. Data driven disturbance observer is first evaluated with engine model simulations and periodic input disturbances. Simulations demonstrated tracking performance improvement under simulated disturbances.

After verification on the simulation models, same control architecture is applied to Ecotorq 13L engine for EGR and VGT control. Controller application is done via standard commercial software toolchain and a serial level code is generated. The standard commercial controller and the proposed controller co-existed in the test software and activated via calibratable switches. Therefore feasibility of the application is proven. Back to back WHTC tests are conducted with proposed DOB assisted controller and commercial controller. Since disturbance observer is an active disturbance control device, its output is compared with physical model based controller feedforward values and similar waveforms are observed. Tracking performances of the proposed and commercial controllers are compared with their overall WHTC error metrics. Tracking error, *nrmse*, is improved by 2% for MAF and by 1% for MAP for overall WHTC.

Feedforward control values are modelled with an easy to implement engine mapping based experiment design on the physical model. This type of experiment design resulted in high validation accuracy for VGT 95% but lower accuracy for EGR 83%. The reason behind this validation performance deterioration is found as low pressure difference on the EGR line. VGT feedforward model is utilized with DTSMC and tested on the physical engine model. Simulation results indicated that feedforward model resulted in a smooth valve actuation and superior tracking performance with respect to the conventional PID control. It is also noted that GPR feedforward control contribution is dominant over feedback control contribution along the WHTC simulation. Apart from feedforward control, airpath components are modelled with GPR method on physical model with steady state and dynamic test data. GPR validation and training fit  $R^2$  values are higher than 95% on the physical model data. A data driven modeling approach will give the required flexibility for the engine manufacturer or the control software developer to shorten development and validation time for new engine configurations by using prevalidated building blocks for new hardware layouts. Using these models, two types of closed-loop controllers are designed. GPR based closed-loop control is compared with GPR feedforward control and significant improvement is observed.

*nrmse* value is improved by 1% for MAF and by 4% for MAP for the overall WHTC.

Finally, data-driven models and respective controllers are designed and validated which are flexible and robust thanks to the disturbance observer and GPR feed-forward terms.

As a future direction, online adaption of models and validation of online adapted controllers can be studied. Electric assisted airpath hardware and model applications are also important. Designed architecture can be easily adapted to those type of implementations.

# Bibliography

- [1] J. Heywood, *Internal Combustion Engine Fundamentals*. McGraw-Hill Book Co., 2000.
- [2] “<https://www.truck.man.eu/de/en/man-world/man-stories/one-invention-still-shapes-our-world-268034.html>.”
- [3] “[https://www.iarc.fr/wp-content/uploads/2018/07/pr213\\_e.pdf](https://www.iarc.fr/wp-content/uploads/2018/07/pr213_e.pdf).”
- [4] Alamir, M. A framework for monitoring control updating period in real-time NMPC schemes. In *Lecture notes in control and information sciences* (pp. 433445). Berlin Heidelberg: Springer.
- [5] G. T. Kalghatgi, The outlook for fuels for internal combustion engines, *Int. J. Engine Res.*, vol. 15, no. 4, pp. 383398, 2014.
- [6] S. A. Ali and N. Langlois, Sliding mode control for diesel engine air path subject to matched and unmatched disturbances using extended state observer, *Math. Probl. Eng.*, vol. 2013, pp. 1013, 2013.
- [7] A. Amstutz and L. K. Del Re, EGO Sensor Based Robust Output Control, *IEEE Trans. Control Syst. Technol.*, vol. 3, no. 1, pp. 3948, 1995.
- [8] J. Chauvin, G. Corde, and N. Petit, Transient control of a diesel engine airpath, *Proc. Am. Control Conf.*, pp. 43944400, 2007.
- [9] H. Berggren and M. Melin, UKF and EKF with time dependent measurement and model uncertainties for state estimation in heavy duty diesel engines .2011 Linkping thesis

- 
- [10] J. Chauvin, G. Corde, N. Petit, and P. Rouchon, Motion planning for experimental airpath control of a diesel homogeneous charge-compression ignition engine, *Control Eng. Pract.*, vol. 16, no. 9, pp. 10811091, 2008.
- [11] C. Criens, Air-Path Control of Clean Diesel Engines:for disturbance rejection on NOx , PM and fuel efficien, no. x. 2013.
- [12] H. J. Ferreau, P. Ortner, P. Langthaler, L. Del Re, and M. Diehl, Predictive control of a real-world Diesel engine using an extended online active set strategy, *Annu. Rev. Control*, vol. 31, no. 2, pp. 293301, 2007.
- [13] S. Formentin, S. M. Savaresi, and L. Del Re, Non-iterative direct data-driven controller tuning for multivariable systems: theory and application, *IET Control Theory Appl.*, vol. 6, no. 9, p. 1250, 2012.
- [14] M. Huang, Robust Rate-Based Model Predictive Control of Diesel Engine Air Path, pp. 15051510, 2014.
- [15] M. Jankovic and I. Kolmanovsky, Robust nonlinear controller for turbocharged diesel engines, *Am. Control Conf.*, pp. 13891394, 1998.
- [16] M. Jung and K. Glover, Calibratable linear parameter-varying control of a turbocharged diesel engine, *IEEE Trans. Control Syst. Technol.*, vol. 14, no. 1, pp. 4562, 2006.
- [17] M. Jung, K. Glover, and U. Christen, Comparison of uncertainty parameterisations for  $H_{\infty}$  robust control of turbocharged diesel engines, *Control Eng. Pract.*, vol. 13, no. 1, pp. 1525, 2005.
- [18] T. Maruyama, T. Shimura, A. Ejiri, Y. Ikai, and K. Shimotani, Model Predictive Control Applied to a Diesel Engine Air-Path System with Dead Time, no. 2, pp. 26282633, 2011.
- [19] A. Murilo, M. Alamir, and D. Alberer, A General NMPC Framework for a Diesel Engine Air Path, *Int. J. Control*, no. June 2015, pp. 121, 2014.

- 
- [20] M. J. Van Nieuwstadt, I. V. Kolmanovsky, P. E. Moraal, a. Stefanopoulou, and M. Jankovic, EGR-VGT control schemes: experimental comparison for a high-speed diesel engine, *Control Syst. IEEE*, vol. 20, no. 3, 2000.
- [21] R. Omran, R. Younes, and J. C. Champoussin, Optimal Control of a Variable Geometry Turbocharged Diesel Engine Using Neural Networks: Applications on the ETC Test Cycle, *IEEE Trans. Control Syst. Technol.*, vol. 17, no. 2, pp. 380393, 2009.
- [22] P. Ortner and L. del Re, Predictive Control of a Diesel Engine Air Path, *Control Syst. Technol. IEEE Trans.*, vol. 15, no. 3, pp. 449456, 2007.
- [23] I. Park, S. Hong, and M. Sunwoo, Robust Air-to-Fuel Ratio and Boost Pressure Controller Design for the EGR and VGT Systems Using Quantitative Feedback Theory, vol. 22, no. 6, pp. 22182231, 2014.
- [24] A. Plianos and R. K. Stobart, Nonlinear airpath control of modern diesel powertrains: a fuzzy systems approach, *Int. J. Syst. Sci.*, vol. 42, no. 2, pp. 263275, 2011.
- [25] G. Stefanopoulou, I. Kolmanovsky, and J. S. Freudenberg, Control of variable geometry turbocharged diesel engines for reduced emissions, *Proc. 1998 Am. Control Conf. ACC IEEE Cat No98CH36207*, vol. 3, no. 4, pp. 733745, 2000.
- [26] G. Stewart and F. Borrelli, A model predictive control framework for industrial turbodiesel engine control, 2008 47th IEEE Conf. Decis. Control, pp. 57045711, 2008.
- [27] G. Stewart, F. Borrelli, J. Pekar, D. Germann, D. Pachner, and D. Kihás, Toward a systematic design for turbocharged engine control, *Lect. Notes Control Inf. Sci.*, vol. 402, pp. 211230, 2010.
- [28] D. Q. Mayne, M. M. Seron, and S. V. Rakovi, Robust model predictive control of constrained linear systems with bounded disturbances, *Automatica*, vol. 41, no. 2, pp. 219224, 2005.

- 
- [29] D. Upadhyay, *Multivariable Control Design for Intake Flow Regulation of a Diesel*, 2002.
- [30] V. I. Utkin, H.-C. Chang, I. Kolmanovsky, and J. a Cook, Sliding Mode Control, in *American Control Conference (ACC)*, 2000, 2000, no. June, pp. 584588.
- [31] J. Wahlstrom and L. Eriksson, Output selection and its implications for MPC of EGR and VGT in diesel engines, *IEEE Trans. Control Syst. Technol.*, vol. 21, no. 3, pp. 932940, 2013.
- [32] J. Wahlstrm, L. Eriksson, and L. Nielsen, EGR-VGT control and tuning for pumping work minimization and emission control, *IEEE Trans. Control Syst. Technol.*, vol. 18, no. 4, pp. 9931003, 2010.
- [33] J. Wang, Hybrid robust air-path control for diesel engines operating conventional and low temperature combustion modes, *IEEE Trans. Control Syst. Technol.*, vol. 16, no. 6, pp. 11381151, 2008.
- [34] P. Andersson, *Comparison of two Exhaust Manifold Pressure Estimation Methods*, 2001.
- [35] C. Bergstrm and G. Hckerdal, *Model Based Diagnosis of the Intake Manifold Pressure on a Diesel Engine*, 2009.
- [36] F. Castillo, E. Witrant, L. Dugard, and R. Sas, *Exhaust Manifold Pressure Estimation Diesel Equipped with a VGT Turbocharger*, 2013.
- [37] E. Hockerdal, *Model Error Compensation in ODE and DAE Estimators Thesis - Linkoping Univ.*, 2011.
- [38] E. Hockerdal, E. Frisk, and L. Eriksson, Observer design and model augmentation for bias compensation with a truck engine application, *Control Eng. Pract.*, vol. 17, no. 3, pp. 408417, 2009.
- [39] A. Jerhammar, *Gas flow observer for a Scania Diesel Engine with VGT and EGR*, 2006.

- [40] I. Kolmanovsky, Issues in modelling and control of intake flow in variable geometry turbocharged engines, Proc. 18th IFIP Conf. Syst. Model. Optim., pp. 436445, 1997.
- [41] O. Leufvn, Compressor Modeling for Control of Automotive Two Stage Turbochargers, no. 1463. 2010.
- [42] A. G. Stefanopoulou, O. F. Storset, and R. Smith, Pressure and temperature-based adaptive observer of air charge for turbocharged diesel engines, Int. J. Robust Nonlinear Control, vol. 14, no. 6, pp. 543560, 2004.
- [43] S. Stockar, Model-Order Reduction for Nonlinear Distributed Parameter Systems with Application to Internal Combustion Engine Modeling and Simulation, 2013.
- [44] J. Ritzn, Modelling and Fixed Step Simulation of a Turbo Charged Diesel Engine, M.Sc. thesis Linkping
- [45] I. Stamati D. Telen and F. L. E. Van Derlinden, Optimal experiment design for calibrating an airpath model of a Diesel engine, pp. 16, 2012.
- [46] F. Tschanz, a. Amstutz, C. H. Onder, and L. Guzzella, Control of diesel engines using NO<sub>x</sub>-emission feedback, Int. J. Engine Res., no. May 2012, 2012.
- [47] X. Wei, L. del Re, and L. Liu, Air path identification of diesel engines by LPV techniques for gain scheduled control, Math. Comput. Model. Dyn. Syst., vol. 14, no. 6, pp. 495513, 2008.
- [48] X. Wei and L. del Re, Gain Scheduled  $H_\infty$  Control for Air Path Systems of Diesel Engines Using LPV Techniques, IEEE Trans. Control Syst. Technol. 15 (2007), pp. 406415.
- [49] J. Wahlstrom and L. Eriksson, Modelling diesel engines with a variable-geometry turbocharger and exhaust gas recirculation by optimization of model parameters for capturing non-linear system dynamics, Proc. Inst. Mech. Eng. Part D J. Automob. Eng., vol. 225, no. 7, pp. 960986, 2011.

- [50] R. C. Grande, G. Chowdhary, and J. P. How, Nonparametric adaptive control using Gaussian processes with online hyperparameter estimation, Proc. IEEE Conf. Decis. Control, pp. 861867, 2013.
- [51] R. C. Grande, Computationally Efficient Gaussian Process Change-point Detection and Regression, M.Sc. Thesis 2014.
- [52] T. Boz, M. Unel, V. Aran, M. Yilmaz, C. Gurel, C. Bayburtlu, K. Koprubasi, Diesel Engine NOx Emission Modeling with Airpath Input Channels, 41st Annual Conference of the IEEE Industrial Electronics Society (IECON 2015), Yokohama, November 9-12, 2015.
- [53] V. Aran, M. Unel, Feedforward Mapping for Engine Control, 42nd Annual Conference of the IEEE Industrial Electronics Society (IECON 2016), Florence, Italy, October 24-27, 2016.
- [54] Ljung, L. System Identification: Theory for the User, Prentice Hall, 1999.
- [55] Goodwin G. and Payne R., Dynamic system identification : experiment design and data analysis, New York : Academic Press, 1977.
- [56] "<http://dsc.ijs.si/jus.kocijan/GPdyn/>"
- [57] Chen T., On kernel design for regularized LTI system identification. Automatica, Volume 90, Pages 109122, 2018.
- [58] M. Raissi, P. Perdikaris, G. Karniadakis. Numerical Gaussian Processes for Time-Dependent and Nonlinear Partial Differential Equations. SIAM Journal on Scientific Computing, Volume 40, Pages A172-A198, 2018.
- [59] Jackson R., Jump M., Green P., Towards Gaussian Process Models of Complex Rotorcraft Dynamics., 74th Annual Forum and Technology Display; The Future of Vertical Flight, Phoenix, Arizona, USA, 15 May 2018
- [60] Lang M., Kleinstueber M., Hirche S., Gaussian process for 6-DoF rigid motions. Autonomous Robots, Volume 42, Pages 11511167, 2018.
- [61] ETAS-ASCMO, <https://www.etas.com/en/products/ascmo.php>

- 
- [62] Sbarbaro, D. and Murray-Smith, R. Self-tuning control of nonlinear systems using gaussian process prior models. *Lecture Notes in Computer Science* 3355:pp. 140-157. 2005
- [63] Beckers T., Umlauf J., Hirche S., Stable Model-based Control with Gaussian Process Regression for Robot Manipulators, *IFAC-PapersOnLine* Volume 50, Issue 1, July 2017
- [64] Hewing L., Liniger A., Melanie Zeilinger N., Cautious NMPC with Gaussian Process Dynamics for Autonomous Miniature Race Cars. *European Control Conference (ECC 2018)*, 2018.
- [65] Steven, H., Development of a worldwide harmonised heavy-duty engine emissions test cycle, *Technical Report*, United Nations, 2001.
- [66] Shihua Li, Jun Yang, Wen-Hua Chen, Xisong Chen-Disturbance Observer-Based Control Methods and Applications, *CRC Press*, 2014).
- [67] Ohishi, K., Ohnishi, K., and Miyachi, K., Torque-Speed Regulation of dc Motor Based on Load Torque Estimation, *Proc. IEEJ IPEC-TOKYO*, 2, pp. 1209-1216. 1983
- [68] W. H. Chen, J. Yang, L. Guo and S. Li, Disturbance-Observer-Based Control and Related Methods An Overview, in *IEEE Transactions on Industrial Electronics*, vol. 63, no. 2, pp. 1083-1095, Feb. 2016.
- [69] Q.-C. Zhong, A. Kuperman, and R.K. Stobart, Design of UDE based controllers from their two-degree-of-freedom nature, *Int. J. Robust Nonlinear Control*, vol. 17, no. 21, pp. 1994-2008, 2011.
- [70] Aran V., Unel M., Gaussian process regression feedforward controller for diesel engine airpath, *International Journal of Automotive Technology*, vol. 19, no. 4, pp. 635-642, Aug 2018.
- [71] Aran V. and Unel M. Feedforward mapping for engine control, *IECON Proc. (Industrial Electron. Conf.)*, pp. 154159, 2016

- [72] Jankovic M. and Kolmanovsky I. (1998), Robust nonlinear controller for turbocharged diesel engines, *Am. Control Conf.* , pp. 1389-1394, 1998.
- [73] Rasmussen C. E. and Williams C. , *Gaussian Processes for Machine Learning*, the MIT Press online version. 2006
- [74] Bischoff B., Nguyen-Tuong D., Koller T., Markert H., and Knoll A. , Learning throttle valve control using policy search, *Lect. Notes Comput. Sci. (including Subser. Lect. Notes Artif. Intell. Lect. Notes Bioinformatics)*, vol. 8188 LNAI, no. PART 1, pp. 4964, 2013.
- [75] Tietze N. , *Model-based Calibration of Engine Control Units Using Gaussian Process Regression*, Ph.D. Thesis, Vom Fachbereich Elektrotechnik und Informationstechnik der Technischen Universität Darmstadt 2015
- [76] <http://www.turbos.bwauto.com/en/aftermarket/airwerksDimensionalReference.aspx>
- [77] SAE Supercharger Testing Standard J1723 1995-08-01
- [78] *Introduction to Turbomachinery*, D. Japikse, N. C. Baines, Oxford University Press, 1997.
- [79] J. Wahlstrom and L. Eriksson, Modelling diesel engines with a variable-geometry turbocharger and exhaust gas recirculation by optimization of model parameters for capturing non-linear system dynamics, *Proc. Inst. Mech. Eng. Part D J. Automob. Eng.*, vol. 225, no. 7, pp. 960-986, 2011.
- [80] Unver B., Koyuncuoglu Y., Gokasan M., and Bogosyan S. (2016) Modeling and validation of turbocharged diesel engine airpath and combustion systems, *Int. J. Automot. Technol.*, Vol. 17, No. 1, pp. 133-144 2016.
- [81] Y.-Y. Wang and I. Haskara, Exhaust pressure estimation and its application to variable geometry turbine and wastegate diagnostics, *Am. Control Conf. (ACC)*, 2010, pp. 27, 2010.

- 
- [82] T. Zeng, D. Upadhyay, H. Sun, and G. G. Zhu, Physics-based turbine power models for a Variable Geometry Turbocharger, Proc. Am. Control Conf. (ACC), vol. 2016 July, pp. 5099–5104, 2016.
- [83] J. W. Chapman, T. M. Lavalle, J. S. Litt, Practical Techniques for Modeling Gas Turbine Engine Performance, 52nd AIAA/SAE/ASEE Joint Propulsion Conference 2016
- [84] Heywood, John B., Internal Combustion Engine Fundamentals, McGraw-Hill New York, 1988.
- [85] Carlson, P., Flow Through a Throttle Body A Comparative Study of Heat Transfer, Wall Surface Roughness and Discharge Coefficient, M.Sc. Thesis, Dept. of Electrical Engineering Linkoping University, Linkoping, Sweden, 2005.
- [86] M. Jankovic and I. Kolmanovsky, Robust nonlinear controller for turbocharged diesel engines, Am. Control Conf., pp. 13891394, 1998.
- [87] M. Jung and K. Glover, Calibratable linear parameter-varying control of a turbocharged diesel engine, IEEE Trans. Control Syst. Technol., vol. 14, no. 1, pp. 4562, 2006.
- [88] P. Ortner and L. del Re, Predictive Control of a Diesel Engine Air Path, Control Syst. Technol. IEEE Trans., vol. 15, no. 3, pp. 449456, 2007.
- [89] J. Chauvin, G. Corde, N. Petit, and P. Rouchon, Motion planning for experimental airpath control of a diesel homogeneous charge-compression ignition engine, Control Eng. Pract., vol. 16, no. 9, pp. 10811091, 2008.
- [90] J. Wahlstrom and L. Eriksson, Output selection and its implications for MPC of EGR and VGT in diesel engines, IEEE Trans. Control Syst. Technol., vol. 21, no. 3, pp. 932940, 2013.
- [91] Assibey-Bonsu, W.. The basic tenets of evaluating the Mineral Resource assets of mining companies, as observed through Professor Daniel Krige’s pioneering work over half a century. J. S. Afr. Inst. Min. Metall., Johannesburg , v. 116, n. 7, p. 635-643, July 2016

- 
- [92] Rasmussen C. E. and Williams C. , Gaussian Processes for Machine Learning, the MIT Press online version, 2016.
- [93] Bischoff B., Nguyen-Tuong D., Koller T., Markert H., and Knoll A., Learning throttle valve control using policy search, *Lect. Notes Comput. Sci. (including Subser. Lect. Notes Artif. Intell. Lect. Notes Bioinformatics)*, vol. 8188 LNAI, no. Part 1, pp. 4964, 2013
- [94] Tietze N., Model-based Calibration of Engine Control Units Using Gaussian Process Regression, Ph.D. Thesis, Vom Fachbereich Elektrotechnik und Informationstechnik der Technischen Universität Darmstadt. 2015
- [95] S. Khan, A. Sabanovic and A. O. Nergiz, Scaled Bilateral Teleoperation Using Discrete-Time Sliding-Mode Controller, in *IEEE Transactions on Industrial Electronics*, vol. 56, no. 9, pp. 3609-3618, Sept. 2009.
- [96] Schreiter J., Nguyen-Tuong D., and Toussaint M. Efficient sparsification for Gaussian process regression, *Neurocomputing*, vol. 192, pp. 2937, 2016.
- [97] B. Unver, Y. Koyuncuoglu, M. Gokasan, and S. Bogosyan, Modeling and validation of turbocharged diesel engine airpath and combustion systems, *Int. J. Automot. Technol.*, vol. 17, no. 1, pp. 1334, Feb. 2016.
- [98] K. Ekberg, V. Leek, and L. Eriksson, Validation of an Open-Source Mean-Value Heavy-Duty Diesel Engine Model, *Proc. 59th Conf. Simulation Model. (SIMS 59)*, 26-28 Sept. 2018, Oslo Metrop. Univ. Norw., vol. 153, no. September, pp. 290296, 2018.